

Reconstructing a Dilution Refrigerator for use in Low Energy Nuclear Experiments

Matthew John Roberts

Howell, New Jersey

Bachelor of Science Physics

The College of William and Mary, 2015

A Dissertation presented to the Graduate Faculty of the
University of Virginia in Candidacy for the Degree of Doctor
of Philosophy



Physics

University of Virginia

United States

August 2023

Abstract

The High Intensity Gamma Source Frozen Spin Target, or HIFROST, is a system designed to cool and polarize target material for nuclear experiments. This system will be used in experiments at the Triangle Universities Nuclear Laboratory (TUNL) in Durham, North Carolina. At the center of this system is a dilution refrigerator, a machine that uses a series of pumps and the quantum properties of two stable isotopes of helium to achieve temperatures below 100 mK. Preparations for polarized target experiments were put on hold when an inoperable leak in our dilution refrigerator was discovered in November of 2017.

Since then, we have dedicated our time to designing, fabricating, and assembling a new dilution unit for the refrigerator. This process has been met with unfortunate setbacks in the form of welding mishaps, design errors, and the Covid-19 pandemic. Although these setbacks were frustrating, they were also educational. Using the SolidWorks software to make the design, we were able to fully explore the process of making a dilution refrigerator and gain a wealth of knowledge in translating the ideal image we see from our perspective as physicists, into the real world scenario of engineering and machining.

In addition to the refrigerator, we also worked on systems that were directly and indirectly related, such as installing a new waveguide, configuring a new residual gas analyzer, and setting up our electronics rack. This dissertation will discuss what has been done, how we did it, and what we still need to do.

Acknowledgements

My predecessor Ryan Duve once told me that the experience a grad student has can be measured by the number of things they have broken over the years. Those words have helped fight off imposter syndrome for years, and allowed me to be grateful for those who have helped me over the years.

My advisor, Blaine Norum, as well as Don Crabb and Dustin Keller were my own personal treasure trove of knowledge and experience that I have had the unique privilege of being able to access whenever I needed them. They have taught me more about polarized targets and dilution refrigerators than I could have ever gotten from reading about them in books. By allowing me to learn about them at my own pace, I was able to absorb all of the necessary knowledge without becoming overwhelmed.

Whenever we needed something fabricated for use in the lab, we had the irreplaceable skill and expertise of David Wimer, Will Fariss, and Josh Ocheltree to help us. Their skill at taking crude drawings and turning them into actual instruments and flanges is surpassed only by their patience. It was easy to get lost in how we wanted a piece to function, but they were always sure to point out in how something would not be able to be machined or welded so that we were aware of the physical limitations of the real world. We would have not gotten as far as we did if it was not for their attention to detail.

While we were focused on getting our experiment running, the Physics staff worked tirelessly to ensure that we could send off equipment to be repaired, our computers were running smoothly, and we could purchase and receive whatever we needed in a prompt and orderly manner. On top of being good at their jobs, they are genuinely fantastic people and I am blessed to have them working with us.

When the Covid-19 pandemic hit, we were forced to delay our project and find a new place to do our welding. Thankfully, we were able to use the talents of the machinists at Jefferson Lab through the kind offer of Chris Keith. Mark Hoegerl was the answer to our prayers and we are eternally grateful. Chris and Mark saved our skins on multiple occasions, and we cannot thank them enough for fitting us into their packed schedules even with the Covid restrictions in place.

Finally, I would like to acknowledge two of the people that guided me on the path that got me here in the first place. First, my mother Elayne worked tirelessly to nurture my interests and talents in math, physics, and whatever else caught my eye at the time, regardless of whether they would pan out or not. Second, my very first physics teacher Dr. Arundhati Prencipe who saw my potential, and did her best to make sure I did not slack off in class too much to grow as a budding physicist. Both of these women helped shape me into the person I am today, and I am better off not only academically, but also as a human being thanks to their influence.

Contents

1	Theory	1
1.1	GDH Sum Rule	1
	Derivation	1
	Understanding the Discrepancy	4
1.2	Target Polarization	8
	Boltzmann Representations for Polarization	8
	Dynamic Nuclear Polarization	10
	Doping Target Material	11
	Nuclear Magnetic Resonance	14
	Frozen Spin Target	15
1.3	Evaporation and Dilution Refrigerators	16
	Evaporation Refrigerators	16
	Dilution Refrigerators	17
2	Experiment	19
3	Our Dilution Refrigerator	22
3.1	History and Overview of the System	22
3.2	Cooldowns	27
3.3	Goals and Design	30
3.4	First Version	33
	Indium Adapter Ring	33
	Vacuum Layer Can	34
	The Still	35
	Heat Exchanger	35
	Sleeve	36
3.5	Second Version	36
	Vacuum Layer Can	36
	The Still	37
	Sleeve	39
4	Construction	39
4.1	Fabrication and Welding	39
4.2	The ^3He Line	44
	Soldering on Stainless Steel	46
4.3	Electrical Connections	47
	Electrical Feedthroughs	47
	The Electronics	54

	External Connections	56
4.4	Sealing up the assembly	61
	The Problem	63
4.5	Diagnosing the Problem	67
4.6	Third Version	69
5	Other Systems	71
5.1	The Residual Gas Analyzer	71
5.2	Simulations	74
	Phase 1: Setting up the cooldown simulation	75
	Phase 2: The Exchange Gas	76
	Gas Movement	78
	Heat Exchanger Analysis	78
5.3	The DAQ	80
5.4	The Stepper Motor	82
6	Notable Cooldowns	84
6.1	December 9th, 2016	84
6.2	November 7th, 2017	85
6.3	February 25th, 2019	86
6.4	July 2nd, 2019	87
6.5	February 12th, 2022	89
7	Conclusions	90

1 Theory

1.1 GDH Sum Rule

Derivation

The GDH Integrand is a sum rule that relates experimentally measured cross-sections to the anomalous magnetic moment of the target particle. There are a total of three different methods used to derive the GDH Integrand, but we will focus on only one approach for now: The dispersion theoretic derivation. This approach was used independently by Gerasimov in Russia as well as Drell and Hearn in the United States. This method relies on the following principles [1]:

- Lorentz Invariance
- Gauge Invariance
- Crossing Symmetry
- Rotational Invariance
- Causality
- Unitarity

It is important to note that these principles also serve as the foundations of quantum mechanics and relativity. Thus, testing the GDH Sum Rule also doubles as a check to those fundamental areas of physics. The derivation begins with Compton scattering off a spin 1/2 object. The two polarizabilities between the incoming and outgoing photon, as well as the target before and after the scattering, give us a total of 16 different helicity amplitudes to think about. However, through the use of C, P, and T invariance, the number of amplitudes is reduced to six. Of those six remaining, only two contribute when angular momentum conservation is used in the forward direction. We can then use the gauge condition $\mathcal{A}^0 = 0$ to set the time-component of the photon field to zero. This allows us to make Compton Scattering symmetric under the exchange of incoming and outgoing photons, also known as Crossing Symmetry. This gives our Compton amplitude the following property:

$$F(\vec{k}_1, \vec{\epsilon}_1, \vec{\epsilon}_2) = F^*(-\vec{k}_2, \vec{\epsilon}_2^*, \vec{\epsilon}_1^*) \quad (1)$$

We know from the Superposition Principle that F has to be linear in both $\vec{\epsilon}_1$ and $\vec{\epsilon}_2$. Then, when restricting our case to forward scattering and staying in the rest frame of the target, the Compton amplitude can be written as

$$\begin{aligned} F = & \left\langle \chi_2^\dagger \left| \sum_{i=1}^5 f_i K_i \right| \chi_1 \right\rangle = \\ & \langle \chi_2^\dagger | f_1(\vec{\epsilon}_2^* \cdot \vec{\epsilon}_1) + f_2 i \vec{\sigma}(\vec{\epsilon}_2^* \times \vec{\epsilon}_1) + \\ & f_3(\vec{\epsilon}_2^* \cdot \vec{k})(\vec{\epsilon}_1 \cdot \vec{k}) + f_4 i \vec{\sigma}[\vec{\epsilon}_2^*(\vec{\epsilon}_1 \cdot \vec{k}) - \vec{\epsilon}_1(\vec{\epsilon}_2^* \cdot \vec{k})] + \\ & f_5 i \vec{\sigma}[(\vec{\epsilon}_2^* \times \vec{k})(\vec{\epsilon}_1 \cdot \vec{k}) - (\vec{\epsilon}_1 \times \vec{k})(\vec{\epsilon}_2^* \cdot \vec{k})] | \chi_1 \rangle \end{aligned} \quad (2)$$

where $\vec{\sigma}$ is the Pauli Spin Matrix vector, $\chi_1(\chi_2)$ is the initial (final) spinor of the target, and f_i are scalar functions. This expression can be simplified since $\vec{\epsilon} \cdot \vec{k} = 0$ for real photons, leaving only the f_1 and f_2 terms in the equation. Assuming the photon is traveling along the z-axis, the polarization vectors for left-handed and right-handed photons are:

$$\vec{\epsilon}_L = \frac{1}{\sqrt{2}}(\vec{\epsilon}_x - i\vec{\epsilon}_y) \quad \vec{\epsilon}_R = \frac{-1}{\sqrt{2}}(\vec{\epsilon}_x + i\vec{\epsilon}_y) \quad (3)$$

When these vectors are plugged in for $\vec{\epsilon}_1$ and $\vec{\epsilon}_2$, we find that the dot product in the f_1 term simplifies to 1 when $\vec{\epsilon}_1 = \vec{\epsilon}_2$, and zero otherwise. Likewise, the cross product in the f_2 term simplifies to $\pm\vec{\epsilon}_z$ when $\vec{\epsilon}_1$ and $\vec{\epsilon}_2$ are equal, and to zero when they are not. With this information, we can find the Compton Amplitude for every spin configuration which, due to the simplifying done earlier, are the cases where the photon and target polarizations are parallel and anti-parallel to each other in the target's rest frame. These cases are represented as linear combinations of the scalar functions:

$$f_P = f_1 - f_2 \quad f_A = f_1 + f_2 \quad (4)$$

To derive the explicit formulas for f_1 and f_2 , we have to use a different method. The form of the forward scattering amplitude has properties that we can take advantage of. When we use causality, we can relate the scattered wave to the incident one:

$$\psi_f(z, t) = \int_{-\infty}^{\infty} dt' K(z' - z, t' - t) \psi_i(z', t') \quad (5)$$

where K is a function that goes to zero when $z' - z > t' - t$. We can change this formula into a function dependent on energy by using a Fourier transform. When we set $z = 0$, we can use contour integration to evaluate the integral in the upper half of the complex plane. We can then apply Cauchy's integral formula to transform this integral:

$$f(\nu) = \frac{1}{2\pi i} \oint_C d\nu' \frac{f(\nu')}{\nu' - \nu} \quad (6)$$

which we can simplify into a regular integral with bounds:

$$f(\nu) = \frac{\mathcal{P}}{i\pi} \int_{-\infty}^{\infty} \frac{f(\nu')}{\nu' - \nu} \quad (7)$$

and \mathcal{P} is the Cauchy principal value. When we look back at the property of our Compton amplitude, we can rewrite the integral, and when we isolate the real part, we get the Kramers-Kronig dispersion relation:

$$Re f(\nu) = \frac{2}{\pi} \mathcal{P} \int_0^{\infty} d\nu' \nu' \frac{Im f(\nu')}{\nu'^2 - \nu^2} \quad (8)$$

Since our targets are nucleons, we have to consider the modified Dirac equation for nucleons:

$$(\gamma^\mu (i\partial_\nu - eA_\nu) - \frac{\kappa\mu_N}{2} \sigma_{\mu\nu} F^{\mu\nu} - m_N) \psi = 0 \quad (9)$$

Here, κ is the anomalous magnetic moment of the target particle. Using the Dirac equation and the general Compton Amplitude, we can find the forward Compton scattering amplitude to be:

$$f(\nu) = -\frac{\alpha}{m}\vec{\epsilon}_2^* \cdot \vec{\epsilon}_1 - \frac{\alpha}{2m^2}\kappa^2\nu i\vec{\sigma} \cdot (\vec{\epsilon}_2^* \times \vec{\epsilon}_1) \quad (10)$$

Next, we consider the optical theorem. The optical theorem relates the forward scattering amplitude to the total cross-section, which we can then use with the Kramers-Kronig dispersion relation to get:

$$\begin{aligned} \text{Im}f_1(\nu) &= \frac{\nu}{8\pi}[\sigma_A(\nu) + \sigma_P(\nu)] \\ \text{Im}f_2(\nu) &= \frac{\nu}{8\pi}[\sigma_A(\nu) - \sigma_P(\nu)] \end{aligned} \quad (11)$$

Before we combine the results into a low energy expansion, it is important to note that $f_1(\nu)$ is even and $f_2(\nu)$ is odd. Due to crossing symmetry, all odd terms go to zero, so instead we consider the function $\frac{f_2(\nu)}{\nu}$:

$$\begin{aligned} f_1(\nu) &= -\frac{\alpha}{m} + (\alpha_E + \beta_M)\nu^2 + \mathcal{O}(\nu^4) \\ \frac{f_2(\nu)}{\nu} &= -\frac{\alpha}{2m^2}\kappa^2 + \gamma_0\nu^2 + \mathcal{O}(\nu^4) \end{aligned} \quad (12)$$

As we can see, these amplitudes also give us insight into the electric and magnetic dipole polarizabilities α_E and β_M , as well as the forward spin polarizability γ_0 . Now that we have these equations, we can combine them with the Kramers-Kronig dispersion relation from earlier and write the low energy expansion in terms of a Taylor series:

$$\begin{aligned} \text{Re}f_1(\nu) &= \frac{1}{2\pi^2} \sum_{n=0}^{\infty} \int_0^{\infty} d\nu' (\sigma_A(\nu') + \sigma_P(\nu')) \left(\frac{\nu}{\nu'}\right)^{2n} \\ \text{Re}\frac{f_2(\nu)}{\nu} &= \frac{1}{4\pi^2} \sum_{n=0}^{\infty} \int_0^{\infty} \frac{d\nu'}{\nu'} (\sigma_A(\nu') - \sigma_P(\nu')) \left(\frac{\nu}{\nu'}\right)^{2n} \end{aligned} \quad (13)$$

From here, we can focus on individual terms. When we match terms from the Taylor series to the low energy expansion, we get the following sum rules:

$$\begin{aligned} \alpha_E + \beta_M &= \frac{1}{2\pi^2} \int_0^{\infty} \frac{\sigma_A(\nu') + \sigma_P(\nu')}{\nu'^2} d\nu' \\ \frac{\alpha\kappa^2}{2m^2} &= \frac{1}{4\pi^2} \int_0^{\infty} \frac{\sigma_P(\nu') - \sigma_A(\nu')}{\nu'} d\nu' \\ \gamma_0 &= -\frac{1}{4\pi^2} \int_0^{\infty} \frac{\sigma_P(\nu') - \sigma_A(\nu')}{\nu'^3} d\nu' \end{aligned} \quad (14)$$

The first equation is known as Baldin's sum rule, and the second is the GDH sum rule. While this was derived with a spin-1/2 target in mind, it is possible to prove

its validity for targets with higher spin values, such as for the deuteron. The general GDH sum rule [2] is given by:

$$\int_{\nu_{Th}}^{\infty} \frac{\sigma_P - \sigma_A}{\nu} d\nu = \frac{4S\pi^2\alpha\kappa^2}{m^2} \quad (15)$$

where ν_{Th} is the threshold energy for the first inelastic channel (photodisintegration in the case of the deuteron), σ_P is the parallel cross-section, σ_A is the anti-parallel cross-section, S is the spin of the target, α is the fine structure constant, κ is the anomalous magnetic moment, and m is the mass of the target particle.

Understanding the Discrepancy

In 2006, the GDH Integrand was tested at the Laser Electron Gamma Source (LEGS) at Brookhaven for the neutron and proton at photon energies below 400 MeV. In the case of the neutron, since it decays after 15 minutes, they instead used the deuteron as their target. At that time, the GDH Integrand for the proton was known and was in agreement with theory from previous work at MAMI and ELSA. They used that information along with their measurements and the knowledge of the structure of the deuteron to derive a pseudo-experimental value for the neutron. The main method for finding this value was to look at the connections between the inelastic channels:

$$\frac{p(\gamma, \pi^+)}{d(\gamma, \pi^+)} \rightarrow \frac{n(\gamma, \pi^-)}{d(\gamma, \pi^-)} \quad (16)$$

However, the measured GDH integrand value showed a 10% discrepancy with theory. After verifying that the data were valid, researchers suspected their understanding of the deuteron from current nuclear theory must be incomplete and decided to look closer at the GDH Integrand. For the deuteron, one can expand the GDH integral into three smaller integrals over three different ranges:

$$\int_{\nu_0}^{\infty} \frac{\sigma_P - \sigma_A}{\nu} d\nu = \int_{\nu_0}^{\nu_\pi} \frac{\sigma_P - \sigma_A}{\nu} d\nu + \int_{\nu_\pi}^{\nu_{MAX}} \frac{\sigma_P - \sigma_A}{\nu} d\nu + \int_{\nu_{MAX}}^{\infty} \frac{\sigma_P - \sigma_A}{\nu} d\nu \quad (17)$$

From the photodisintegration threshold (ν_0) to pion threshold (ν_π), from pion threshold to the maximum photon energy (ν_{MAX}), and from the maximum photon energy to infinity. Three possible explanations for this discrepancy are:

- The GDH Sum rule is flawed

However, since the GDH sum rule is derived from well-established principles like quantum mechanics and Lorentz invariance, that possibility is highly unlikely.

- There is some contribution in the high energy range

As for this possibility, since the contribution to the anomalous magnetic moment goes like $\frac{1}{\nu}$ in the integral and the effect of spin decreases at high energies, it cannot explain the ten percent discrepancy observed.

- There is some contribution in the low energy range

Therefore, the most probable cause lies in the low energy regime, meaning there is something wrong with the extraction of the neutron integrand from the deuteron measurements that would be reflected in measurements on the deuteron below pion threshold.

One encouraging source we have on the origin of the discrepancy comes from the work of Fil'kov *et al.*[3]. In their work, Fil'kov observed narrow structures in the missing mass spectrum of the final state in the $pd \rightarrow ppX$ reaction (see the top graph in the figure below). It was suggested by Fil'kov that this phenomenon should also be present in the reaction $\gamma d \rightarrow \pi^+ X$, data for which were been collected by the LEGS collaboration. These data showed good agreement with Fil'kov's data, but were not enough to confirm it.

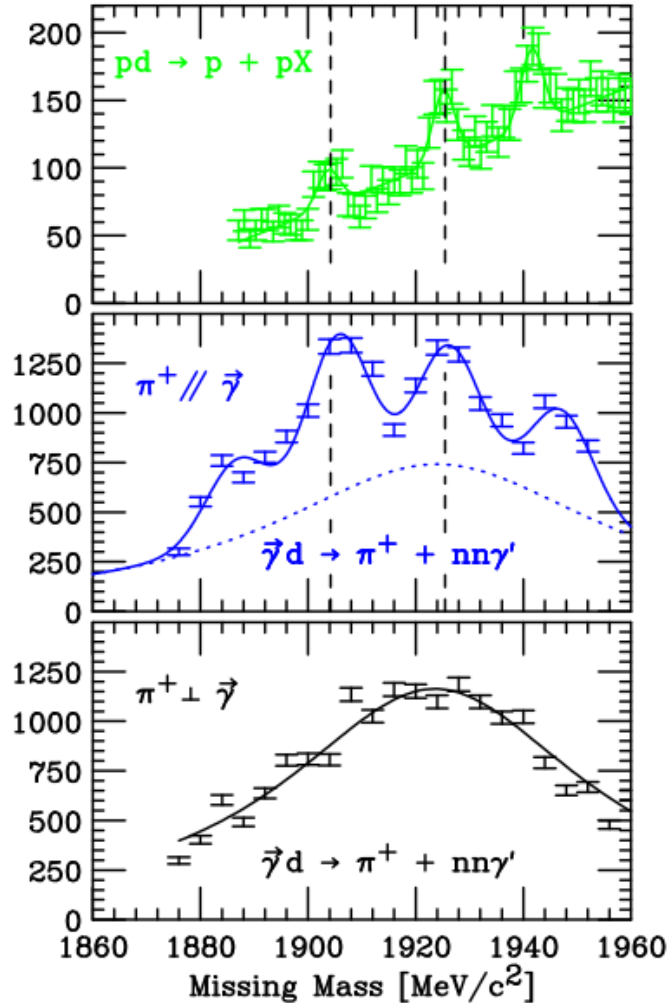


Figure 1: Comparing Fil'kov's (top)[3] results with the results from LEGS[4] (middle and bottom). As we can see, the two peaks indicated by the dashed lines line up very nicely between the two sets of data.

To look for this reaction, a final state required a coincidence between a charged pion, a neutron (implying a π^+ was produced), and an emitted photon (to eliminate the large number of $d(\gamma, \pi^+)nn$ events). We can see that the LEGS data have been split into two different categories based on the trajectory of the emitted π^+ ; parallel and perpendicular to the plane of the incident photon's polarization. When the reaction occurs, the detectors pick up a neutron, a π^+ , and a photon. Looking at the middle and bottom graphs in Figure 1, what normally creates a peak in this region is pion bremsstrahlung. Pion bremsstrahlung occurs when a pion is created in the target nuclei and is accelerated by the strong force. It results in a broad peak and, since it is predominantly a magnetic transition, has more of a contribution when the π^+ is emitted in the perpendicular direction. What was not expected was the appearance of the narrower peaks in the middle graph. The expected spectrum in the middle graph is depicted by the dashed line in Figure 1. Normally, the broad peaks produced from pion bremsstrahlung are to be expected, and the ratio between the peaks is taken to be compared with theory, but in the parallel case we see something extra has manifested with the pion bremsstrahlung. Since these peaks are present when the π^+ is parallel to the polarization of the incident photon, that suggests that they are electric transitions. Thus, in the parallel case, the data show evidence that some unknown particle, which we will call D^* , is created in an intermediate step in this inelastic channel. In the $d(\gamma, \pi^+) D^*$ reaction, it seems to decay from resonance to resonance until the unknown particle decays into two neutrons and a photon. But the more interesting observation is what happens when you take note of the location of the peaks in relation to the others. Using the middle graph as the reference, as well as the fact that two neutrons have a mass of approximately 1.878 GeV, the peaks are located around:

Table 1: Peaks near Photodisintegration threshold

Peak Number	Peak Location	Distance from Previous Peak
1	1.887 GeV	9 MeV
2	1.906 GeV	19 MeV
3	1.926 GeV	20 MeV
4	1.947 GeV	21 MeV

Starting from the masses of two neutrons, our first state is about 10 MeV away, with each subsequent state about 20 MeV. From basic quantum mechanics, we know that these energy differences closely resemble the spectrum from a harmonic oscillator, $E = (n + 1/2)\hbar\omega$ where $\hbar\omega$ is equal to 20 MeV here. While these two sets of data seem to agree with Fil'kov's hypothesis, further analysis into the LEGS data was inconclusive due to most of the data being accidentally deleted when the LEGS facility was closed. While these two sets of data seem to agree, it is important to note that an attempt to duplicate Fil'kov's results was made by Tamii *et al.*[5], but their data showed no evidence of a peak.

In their experiment, they scattered protons off deuterons and were detecting two

outgoing protons. These reactions were being interpreted as:

$$pd \rightarrow p'D^* \rightarrow p'p''n\gamma \quad (18)$$

with the D^* as a single intermediate state. The detection of the first proton defined the missing mass of D^* . The momentum of the second proton constrained the possible values of the $n\gamma$ kinematics. But what was not considered was the possibility of a lower energy state than Fil'kov's D^* . We will refer to Fil'kov's D^* as D_2^* and the first peak in the LEGS data as D_1^* . When the D_2^* state is produced, it would most likely decay to the next lowest energy peak, D_1^* , emitting a photon. The D_1^* would then decay into a proton, a neutron, and a second photon. The existence of this unrecognized two-step process makes the identification of the event highly improbable.

Another set of data that supports our hypothesis, that of Khrykin *et al.* [7]. They were explicitly looking for narrow dibaryon peaks below the pion production threshold in proton scattering experiments. They were looking at the reaction $pp \rightarrow \gamma\gamma X$ and got the results shown in Figure 2: They observed a narrow peak at about 24 MeV,

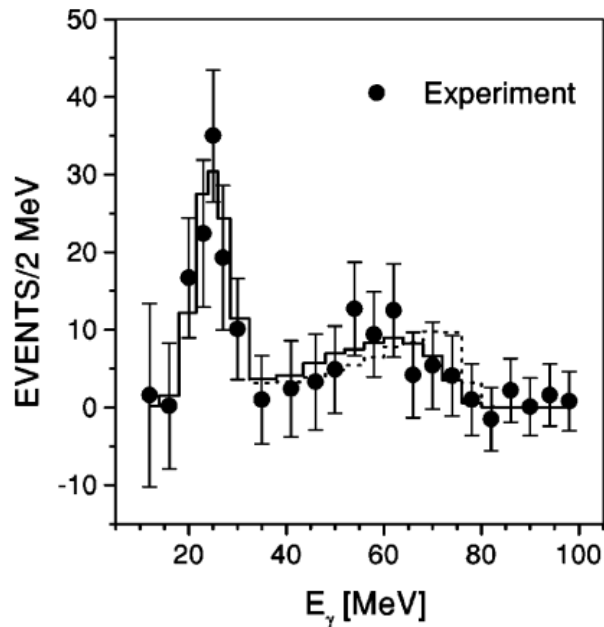


Figure 2: Spectrum of observed photon energies from $p(p, \gamma\gamma)$ [7]

with a width of approximately 8 MeV, which was the resolution of their detectors. The peak at 24 MeV suggests that the dibaryon emits photons of that energy when decaying state to state. These data also correspond to what they referred to as the d_1^* , with a mass of $1956 \pm 6 \text{ MeV}$, which is close to the mass of peak number four in Table 1. It might be slightly different, but that is most likely due to Khrykin having a dibaryon made of a pp pair as opposed to the nn pairs observed at LEGS. Evidence suggests that these dibaryons are compact, and when the dibaryon is composed of a pn or nn pair, it does not affect it. But when a pp pair is used, the Coulomb repulsion

makes it more energetic, leading to larger gaps between energy levels. However, they were not convinced that this was enough to definitively prove the existence of these dibaryons and called for a more in-depth study of this reaction to carefully measure the $pp\gamma\gamma$ reaction and extract the properties of the dibaryon.

Another experiment that favors the existence of the dibaryon comes from the data from Nath *et al.* who were measuring the differential polarization of photo-neutrons off of deuterium. Significantly, their data started to diverge from theoretical models.

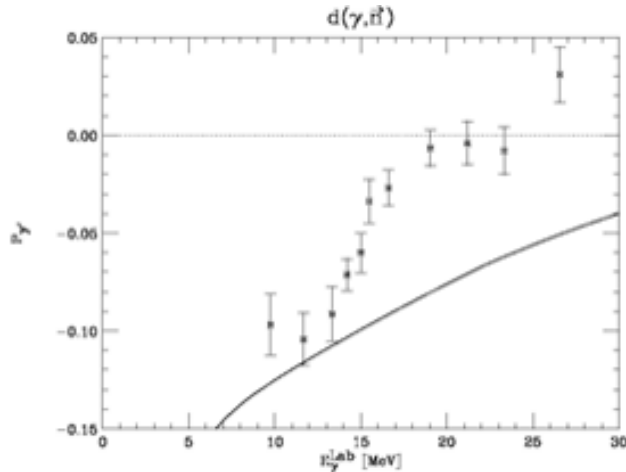


Figure 3: Neutron Polarization as a function of Photon Energy[8], with Arenhovel’s calculation (solid line) for comparison

In their conclusions, Nath *et al.* claimed this disagreement with theory seemed to “indicate that the contributions from the E1 amplitude may not be known exactly” [8]. When looking back at the LEGS data, in the middle graph of Figure 1, which is mostly electric (E1) events, we get our peaks. We can not say for certain whether Nath *et al.* ever considered something like our D_1^* particle, but they were confident enough in their data to state that they thought something beyond what was known at the time was happening there. When comparing to the best current theoretical model[9], we can see an abrupt discontinuity at around 12 MeV. A photon at 12 MeV in the lab frame striking a deuteron target, just so happens to be approximately equal to $2 * M_N + 9MeV$ in rest energy, the “ground state” of our theoretical D^* particle.

1.2 Target Polarization

Boltzmann Representations for Polarization

To sufficiently test the GDH Integrand, a polarized target is essential. While a high magnetic field and a low temperature generated by the dilution refrigerator is necessary, they are not the only things needed to achieve a polarization high enough to run the experiment. To understand why, we will use a spin 1/2 target as a simple example. In this target, there are N spin 1/2 particles with an equal probability of

being spin up or spin down. In the case of spin 1/2 particles, we can express the polarization as:

$$\frac{N_{\uparrow} - N_{\downarrow}}{N} \quad (19)$$

Here, $N = N_{\uparrow} + N_{\downarrow}$ and $N_{\uparrow}(N_{\downarrow})$ is the number of particles in the spin up (down) state. Since the polarization depends only on the number of particles in each state, it does not matter which particles are spin up or down. Therefore, there can be multiple configurations for a polarization value. This means that the probability our system has a certain polarization value is directly proportional to how many ways the system can be arranged to have that value. With this information, we can use the statistical mechanical definition of entropy, $S = k_B \ln \Omega$, where k_B is the Boltzmann constant, and Ω is the number of possible combinations for a system to be in a specific state. We can then use the Boltzmann distribution to express the probability of the system having a specific value of spins in the up (down) state:

$$\frac{N_{\uparrow}}{N_{\downarrow}} = \frac{\ln \Omega_{\uparrow}}{\ln \Omega_{\downarrow}} = \frac{e^{-E_{\uparrow}/k_B T}}{e^{-E_{\downarrow}/k_B T}} \quad (20)$$

Here, $E_{\uparrow}(E_{\downarrow})$ is the energy of the particle in the spin up (down) state, which can be rewritten as $E = \mu B$, where μ is the magnetic moment and B is the external magnetic field. We can then use this information to rewrite our definition of the polarization:

$$\frac{N_{\uparrow}}{N_{\uparrow} + N_{\downarrow}} - \frac{N_{\downarrow}}{N_{\uparrow} + N_{\downarrow}} = \frac{1}{1 + e^{-2\mu B/k_B T}} - \frac{1}{1 + e^{2\mu B/k_B T}} = \tanh\left(\frac{\mu B}{k_B T}\right) \quad (21)$$

With this simplification, we can use the magnetic moment of the proton ($1.4 \cdot 10^{-26} \text{ J/T}$) for μ , 5 Tesla for B , and 25 mK for T , which is on the lower end of possible temperatures able to be reached in a dilution refrigerator. With these values, it corresponds to a polarization of about 21.2%. While this does seem significant, this polarization value is nowhere near the desired value for a polarized target experiment. If we use a temperature closer to where a typical dilution refrigerator operates, 100 mK, the polarization value drops to 5.38%. If we want to know how a spin-1 target fares, we must first change our polarization equation. There are three different spin states for a spin-1 particle with mass, and define the polarization as:

$$P_{S=1} = \frac{N_{\uparrow} - N_{\downarrow}}{N_{\uparrow} + N_0 + N_{\downarrow}} \quad (22)$$

Here, N_0 is the number of particles in the spin-0 state. While this does change our polarization equation, we can still use the Boltzmann distribution for the population ratios to rewrite the equation in terms of μ , B , k_B , and T (albeit with a different value for μ). We divide the polarization equation by N_0 , and we get our new polarization equation:

$$\begin{aligned} P_{S=1} &= \frac{e^{\mu B/k_B T} - e^{-\mu B/k_B T}}{e^{\mu B/k_B T} + 1 + e^{-\mu B/k_B T}} = \frac{2\sinh(\frac{\mu B}{k_B T})}{2\cosh(\frac{\mu B}{k_B T}) + 1} = \\ &= \frac{4\sinh(\frac{\mu B}{2k_B T})\cosh(\frac{\mu B}{2k_B T})}{4\sinh(\frac{\mu B}{2k_B T})\cosh(\frac{\mu B}{2k_B T})\tanh(\frac{\mu B}{2k_B T}) + 3} = \frac{4\tanh(\frac{\mu B}{2k_B T})}{\tanh^2(\frac{\mu B}{2k_B T}) + 3} \end{aligned} \quad (23)$$

When we use the previous values for B and T, as well as the measured value for the deuteron’s magnetic moment, we obtain a polarization value of just 1%. In the case of an optimally running dilution refrigerator, that polarization only goes up to about 4% at 25mK. In addition to polarization, spin-1 target particles also have another orientation known as tensor polarization, or alignment, which is defined as:

$$\frac{N_{\uparrow} + N_{\downarrow} - 2N_0}{N_{\uparrow} + N_0 + N_{\downarrow}} \quad (24)$$

If we use the Boltzmann distribution to rewrite this equation, we can rewrite the equation for alignment as:

$$\frac{4\tanh^2\left(\frac{\mu B}{2k_B T}\right)}{\tanh^2\left(\frac{\mu B}{2k_B T}\right) + 3} \quad (25)$$

When our values for the magnetic field and magnetic moment are used, we get $8.2 \times 10^{-3}\%$ at 100 mK and 0.13% at 25 mK. Given this information, it is clear that we need another method to achieve a higher polarization and alignment. Fortunately, Dynamic Nuclear Polarization (DNP) allows us to achieve those higher values.

Dynamic Nuclear Polarization

The basic principle behind DNP is to use photons to “swap” the spin alignments of the orbiting electrons with the nuclei at their core. Unlike their nucleon counterparts, electrons are very easy to polarize, which we can see using the polarization formula for spin-1/2 particles. When we plug in the value for the electron magnetic moment into the formula (-9.284×10^{-24} J/T) we get a polarization value of almost 100% at 100mK. As for how we would transfer the polarization to the nucleus, we will use the explanation provided by Borghini[10]. Borghini begins by using the most simple system: an electron with a spin-1/2 nucleus. When placed in a magnetic field, these particles can be excited into the higher energy spin state when struck with a photon at a specific energy, $\hbar\omega_{e(N)}$, where $\omega_{e(N)}$ is the Larmor frequency for the electron (nucleon). This frequency is dependent on the strength of the magnetic field and is determined by the equation:

$$\omega = \frac{g\mu B}{\hbar} \quad (26)$$

This equation comes from the Zeeman effect, where g is the g-factor, and μ is the magnetic moment. The particle has a probability, W, of undergoing this transition, as well as probability W_L , which corresponds to spin-lattice relaxation. Borghini references four different types of spin flips, which he categorizes into two different categories: allowed and forbidden. Allowed transitions refer to electrons flipping their spins, while forbidden transitions involve the simultaneous flips of both the nucleus and the electron(s). For simplicity, we will discuss only the transitions Borghini refers to as Type 1 and Type 3. In the case of Type 3 transitions, there are two sub-types where the nucleus can either flip with the electron, or swap the spins. All three of these transitions occur when struck with a photon with frequency ω_e for Type 1, $\omega_e \pm \omega_N$ for the Type 3 sub-types. Since we have different frequencies for the Type 3

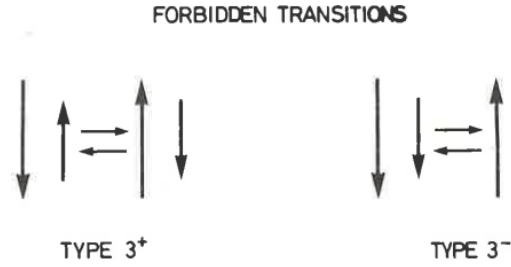


Figure 4: Borghini’s Type-3 transitions; The larger arrow represents the electron’s spin, and the smaller arrow is for the nuclear spin

sub-types, that means we have control over how we flip the nuclear spins. Once those transitions occur, the electron’s spin will quickly reorient itself back into the more energetically favorable spin state. Due to this rate of electron spin relaxation being much higher than the nuclear spin flip, which is also higher than the spin relaxation rate, polarization can accumulate in the nuclear target.

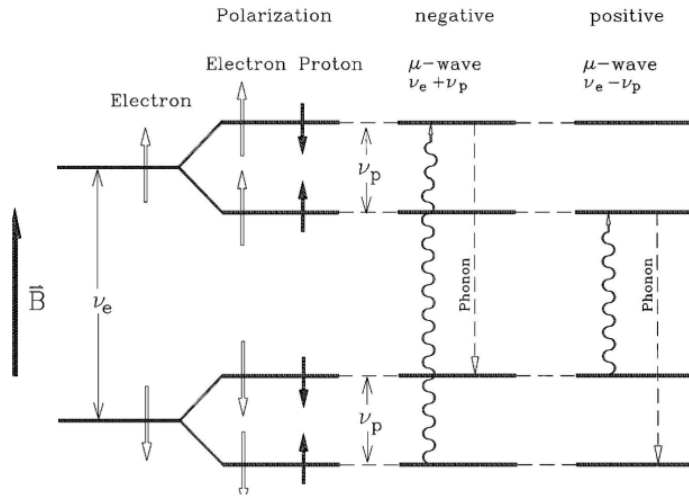


Figure 5: A visual aid for the Zeeman splitting in the spin states; The clear arrow represents the electron’s spin, and the solid arrow is for the nuclear spin[11]

Doping Target Material

Since the polarization of nuclear targets is dependent on electrons, it is a common practice to dope target materials. These electron dopants can be chemicals added to the target material, or introduced via irradiation. The most common target materials used today are ammonia (NH_3) doped via irradiation, and butanol which is doped chemically. Both materials’ popularity are due to their high radiation resistance, meaning they lose very little polarization after being bombarded with radiation.

Ammonia, in particular, has a much higher resistance to radiation than most target materials, with its characteristic flux being at least an order of magnitude higher than butanol. They also have higher max polarizations, with ammonia reaching polarizations of 97% and -100% , and butanol reaching $\pm 93\%$. Their deuterated counterparts can achieve deuteron polarizations of 49% and -53% for ammonia, and $\pm 50\%$ for butanol. Ammonia target beads are made by feeding gas through liquid nitrogen. The frozen pellets of ammonia are then collected into small plastic bottles and stored in dewars filled with liquid nitrogen. These dewars have six slots for specialized metal holders that can contain around three or four plastic bottles of target material each.

(a) Storage Dewars



(b) The metal holders that keep the ammonia in the liquid nitrogen bath



When the dewars are not being used in experiments or being irradiated, they are refilled on a weekly basis. When it is time to irradiate the target material, they are transported to a facility with an electron beam. Once inside, the task of getting the beads into the beamline can begin. First, a small plastic tub is filled with liquid nitrogen. The plastic bottles are then transferred from their dewars into the bath. Using insulated gloves, tongs, and a funnel, the contents of the bottle are poured into a small cylindrical container. The walls of this container are made of a wire mesh to allow the incoming electrons to pass through. This container is then placed into a specialized dewar filled with liquid argon. This dewar has a window for the electron beam. The wire mesh container is attached to an apparatus that serves as the “lid” of the specialized dewar and holds the container with the target material in between the two windows on the walls of the dewar. In the picture below, the target material container would be attached to the right angle bent part in the left part of the picture, and the round base on the right is the “lid”.



Figure 7: The metal apparatus used to hold target material in the beamline.

The axis of the cylindrical container is perpendicular to the windows, to maximize the amount of material being irradiated. Depending on the beam intensity, will be finished in about 15-60 minutes. Once the beam is off, and the area checked for lingering radiation, the target material can be retrieved and inspected. If properly irradiated, the ammonia should be purple in color. The target beads are then returned to their plastic bottles, and placed back in their storage dewars. This process is then repeated until there is no more material to irradiate or beamtime to use. It is important to note that there is a minimum beam intensity needed to properly dope the sample. Even if the sample is left in the beam for hours at a time, there will be little, if any, doping in the target material if the beam intensity is not high enough. Butanol is often doped with EHBA, a synthetic form of the chromium radical Cr(V). For deuterated butanol, the deuterated variant of EHBA, EDDBA is used instead. The dopant is mixed into a solution with the target material, and frozen with liquid nitrogen. The target beads should ideally be around 1.5mm in diameter, and that it usually achieved by dripping the liquid solution through a wire mesh. Butanol has a slightly lower polarizability than ammonia, but has the advantage of having a lower polarized background. This is due to the larger quadrupole moment of the ^{14}N atom, a spin-1 nucleus, which is an order of magnitude higher than the deuteron's moment, making it difficult to get an accurate measurement of the deuteron's polarization. This can be rectified by using ammonia with ^{15}N , which is spin-1/2, but is harder to get since ^{14}N is much more abundant. Another obstacle to using ND_3 as a deuteron target material is the added difficulty in preparing it. Crabb and Meyer [11] state that this comes mostly from the temperature at which it is prepared. They define two different methods for preparation, known as the high temperature and low temperature irradiation. The high temperature method was described above using liquid nitrogen and liquid argon to keep the target beads solid. Low temperature irradiation occurs at 1K, and is produced during the experiment it is planned to be used. In their experience, they have found that deuteron polarizations of at least 30% can only be produced with a low-temperature irradiation. In their findings, Crabb and Meyer state the optimal electron flux for the irradiation of ND_3 to be between $4 \times 10^{14} e^- / \text{cm}^2$ and $1 \times 10^{16} e^- / \text{cm}^2$. Plus, unlike ammonia, butanol is doped chemically, making it easier to prepare since there is no need for an electron laser. Once

the target is sufficiently doped, the microwaves are added, and the target is polarized, the next step is to be able to measure the polarization. This is done through Nuclear Magnetic Resonance (NMR).

Nuclear Magnetic Resonance

NMR occurs when nuclei are held in a strong, constant magnetic field and a weaker, oscillating magnetic field perpendicular to it. If that field is oscillating at a specific frequency, the nuclei will either absorb or emit energy. That frequency is known as the Larmor frequency, and it describes the rate at which a nuclei with spin precesses about its axis in a magnetic field. The Larmor frequency is dependent on the strength of the holding field and the species of the nuclei. This absorption/emission produces a measurable electromagnetic signal, and corresponds to the nuclei undergoing Rabi oscillations. This signal is typically measured with a series LRC circuit known as a Q-meter. The Q-meter measures the resonance as a change in induction, and is related to the magnetic susceptibility of the system. The magnetic susceptibility can be written as:

$$\chi(\omega) = \chi'(\omega) - i\chi''(\omega) \quad (27)$$

Here, χ' is the dispersive part and χ'' is the absorptive part. Here, χ'' is the part of interest, because the polarization of the target sample is directly proportional to the integral of the absorptive susceptibility over all frequencies. When the Q-meter starts up, it cycles through the frequencies that are lower, to those well above the Larmor frequency of the target material. Getting the NMR signal is a complex process that involves using a phase-sensitive detector (PSD in the Q-meter diagram below) to “select” the real part of the voltage, and subtracting off the Q-curve from the signal. The Q-curve is obtained by adjusting the strength of the holding field so that the Larmor frequency of the spin species of interest is far outside the frequency sweep of the Q-meter. The process continues with a calibration for the polarization value. This is done by running the Q-meter on a sample with a known polarization value.

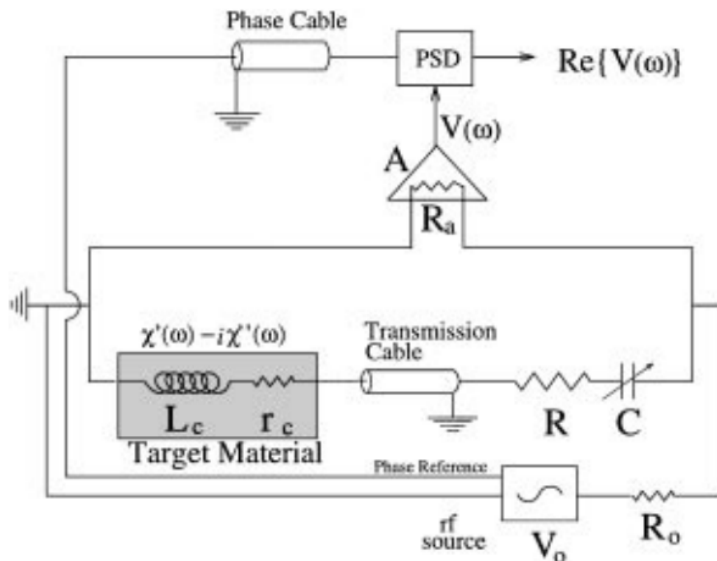


Figure 8: Q-meter schematic[11]

This polarization value is typically calculated for the sample at a known temperature typically around 1 or 2K, and a known magnetic field. Given that this calibration is without the perturbation of DNP, the polarization is calculated using the expressions derived in Section 1.2. The calculated polarization and the signal from the calibration is then used with the signal from the DNP-enhanced polarized material to deduce the actual polarization of the DNP-enhanced material.

Frozen Spin Target

Given that one of the factors limiting the polarization of a target nuclei is the nuclear relaxation time, it is important to know what that is in our system. One of the biggest factors determining this relaxation time is temperature. If the target is not cold enough, the polarized material must have a constant bombardment of microwaves to maintain it. This does not prevent experiments from being run, and some experiments have been performed using this continuous-DNP method. However, due to the dimensions of the magnet needed to maintain the holding field in this setup, the angles at which particles emitted during an experiment are extremely limited. The continuous-DNP method is usually reserved for experiments with higher intensity beams and are cooled with evaporation refrigerators. But, if a larger kinematic range and/or lower intensity beam is needed, this is an incompatible method. The solution to this problem is to drastically increase the nuclear spin relaxation time, so that the large coils of the holding field are no longer necessary. This is the main philosophy of a Frozen Spin Target. A Frozen Spin Target requires colder temperatures than what is possible from an evaporation refrigerator, and instead uses a dilution refrigerator. ^4He evaporation refrigerators typically have a minimum temperature of around 1K, which corresponds to a nuclear relaxation time on the order of minutes. ^3He evaporation refrigerators perform slightly better, with minimum temperatures

closer to 0.5K. However, that it is not enough to improve the relaxation time. Dilution refrigerators can achieve temperatures as low as 25mK, which correspond to a relaxation time on the order of days. Since the goal is to remove the holding magnet with a minimal loss of polarization, once the optimal polarization is reached, the microwave bombardment ends, and the dilution refrigerator “freezes” the spin. The holding field is typically on the order of 2.5T, and after the microwaves are turned off, the temperature in the refrigerator is lowered to around 50mK. As the holding field is turned off, a magnet on the inside of the refrigerator is turned on. This internal magnet is not as strong, and the field it produces acts as a guide to keep the nuclear spins oriented and reduce the amount of polarization degradation. Once the holding field magnet is completely off, it is moved from the area, and the detector array can take its place.

1.3 Evaporation and Dilution Refrigerators

Evaporation Refrigerators

Since they are necessary to run polarized target experiments, it is necessary to discuss the workings of evaporation and dilution refrigerators. Evaporation refrigerators have two main types, ^4He and ^3He , named for the variety of cryogenic liquid circulating in the system. The theory behind an evaporation refrigerator is fairly straightforward. The cryogenic liquid enters a bath and is pumped on by a pump stack. The liquid travels from the helium supply through a tube with sufficient impedance. This impedance expands the liquid as it approaches the evaporation bath, causing it to lose heat and have a lower temperature when it arrives. Pobell[12] gives a general equation on the impedance needed for proper function in an evaporation refrigerator:

$$Z = \frac{\Delta P}{\dot{V}\eta} \quad (28)$$

Here, Z is the impedance, ΔP is the change in pressure from the source to the bath, \dot{V} is the volume flow rate, and η is the viscosity. This impedance is important, since the right value will prevent the 1K bath from emptying out, while also making the 1K temperature minimum possible. As the helium sits in the bath at its boiling point, the individual atoms are either sitting in the bath in liquid form, or hovering above it as a vapor. The atoms forming the helium vapor are more energetic than their liquid counterparts. When the pumps remove the vapor, the average temperature of the bath is lowered. This process continues until the vapor pressure reaches its minimum. For ^4He , this typically occurs around 1K. ^3He evaporation refrigerators can reach 0.5K, but due to the rarity and cost of ^3He , makes it less appealing to use than its more common counterpart. Due to this concern, as well as the fact that the boiling point is lower than ^4He , ^3He evaporation refrigerators are built with ^4He evaporators as pre-coolers designed to liquefy gaseous ^3He . The ^3He baths at the core of these refrigerators are pumped on, similar to their ^4He counterparts, but are typically recirculated through the system to be cooled again.

Dilution Refrigerators

The next type of refrigerator to be discussed is the dilution refrigerator. While evaporation refrigerators function due to the latent heat of evaporation by pumping on a bath of liquid helium, a dilution refrigerator relies on the latent heat of mixing between the two different isotopes of helium. Referring to the figure below, ^4He starts to become a superfluid around 2K. Depending on the temperature and the percentage of ^3He , the mixture can be either be superfluid, or regular liquid.

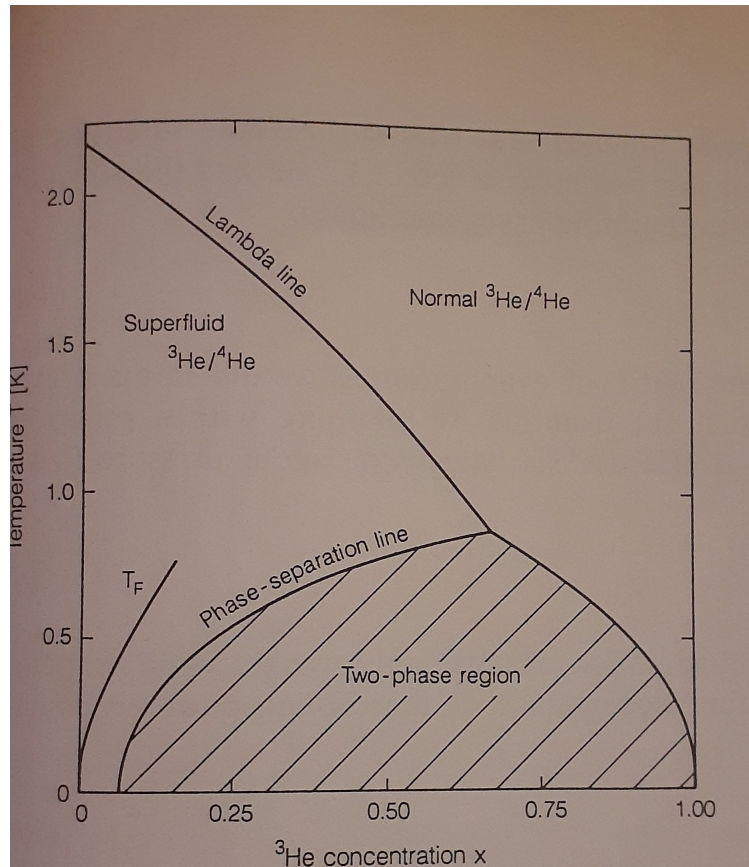


Figure 9: State of Liquid Helium Mixture as a function of ^3He concentration and temperature[12]

The boundary between these two phases is known as the Lambda line, and as we can see, below 1K is where it starts to diverge. The bottom region is a forbidden region, and we start to see the helium mixture split into a ^3He rich liquid phase sitting atop a mostly ^4He superfluid phase. The key to the function of the dilution refrigerator can be found in the lower left corner of this graph. As we can see, as the temperature approaches absolute zero, the ^3He concentration in the superfluid phase does not drop to zero, and instead approaches 6.5%. This comes from the quantum properties of ^3He and ^4He as fermions and bosons, respectively. Once cold enough, ^3He atoms have a stronger binding energy with ^4He , and cross the phase boundary into the dilute ^4He superfluid, expending some energy in the process. As more and

more ^3He atoms cross the phase boundary, they occupy more and more energy states according to the Pauli Exclusion Principle until the binding energy of the dilute phase matches that of the ^3He liquid. While this is the operating principle, there are steps that need to happen before any of this occur. Dilution is one of the last things to happen during the operation of a dilution refrigerator, and since it is an involved and complex process, practice runs, or “cooldowns” must occur to perfect the process. A cooldown begins when a dewar of liquid helium is inserted into the refrigerator.

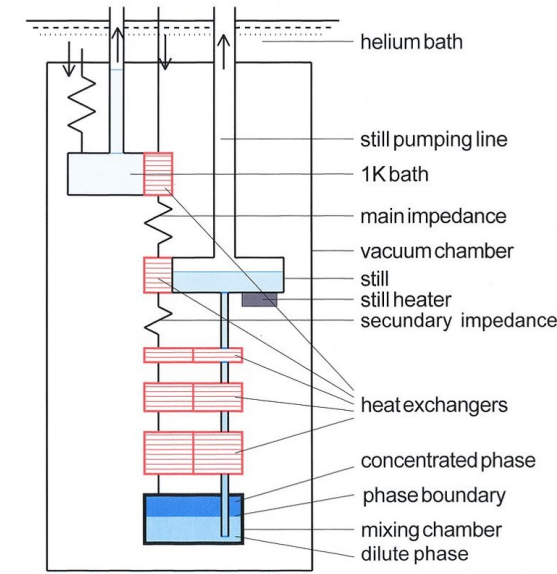


Figure 10: Schematic of a Basic Dilution Refrigerator [13]

This dewar is pressurized by room temperature ^4He gas, and is forced from the dewar into the refrigerator from a liquid transfer line. Liquid ^4He is introduced into the refrigerator where it enters the evaporator. Once the bath is cooled to 1K, circulated ^3He is cooled by this liquid helium bath, and then cooled further by the liquid inside the still. After leaving the still, the circulated He-3 enters the final heat exchanger, where it is cooled again by the helium mixture leaving the target chamber. When it does enter the target chamber, the dilution process described previously occurs, reaching temperatures in the low millikelvin range. The dilute phase then leaves the target chamber, cooling the incoming ^3He as it does until it reaches the still. The still is being constantly pumped on, removing the vapor that evaporates. This vapor is mostly ^3He , and gets recirculated to repeat the process. When everything works, we take detailed notes of everything we do and record various temperature and pressure measurements over a long period of time, to replicate that process in the future. When things go wrong, we go over our notes to see if we did something wrong, or diagnose the problem and fix it before the next cooldown. While the dilution refrigerator is running, we would run the polarization process.

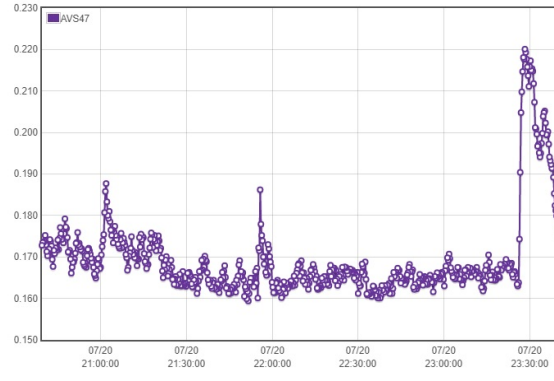


Figure 11: Target Chamber temperature from a successful cooldown

2 Experiment

For the experiment, the plan is to test the low energy region from threshold up to the pion threshold. In theory, the only contribution should be the photo-disintegration or $d(\vec{\gamma}, n)p$ channel. Specifically, we will be probing deuteron targets with photons with energies between 8-16 MeV. The target used will be composed of deuterated butanol. Due to the presence of carbon and oxygen in the target material, the upper limit of 16 MeV was chosen to eliminate the need to filter out neutrons ejected from those atoms. The lower limit of 8 MeV was chosen due to the need for having a scintillating target in order to be able to detect neutrons from nuclear events of interest at lower energies. These targets were not initially available at the time the proposal was written. Three specific energies for the beam have been chosen to run; 8, 12, and 16 MeV. To understand some of the decision making on these energies, we need to take a look at a calculation performed by H.Arenhovel *et al.*[9] on the cross-section differences for the deuteron at low energies.

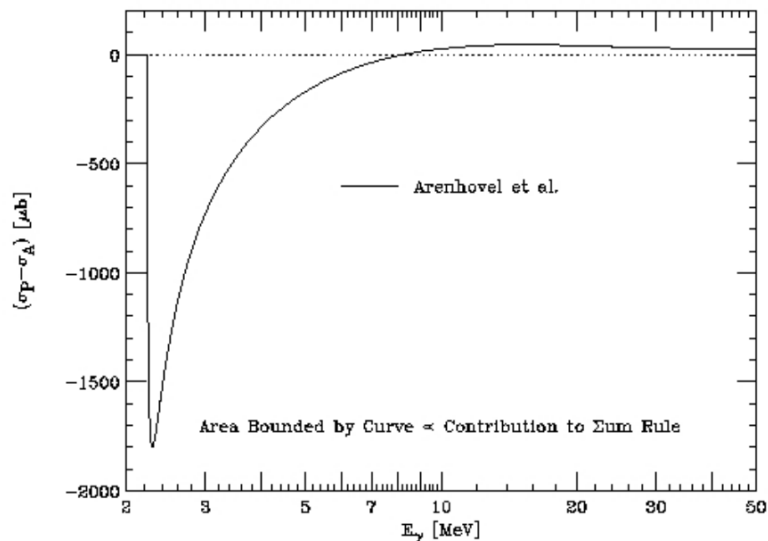


Figure 12: Calculated Deuteron cross-section difference as a function of photon energy

The value starts off at a high negative value, until it crosses the x-axis around 8 MeV, meaning the asymmetry between σ_P and σ_A should be zero. The asymmetry here is defined as $A = \frac{\sigma_A - \sigma_P}{\sigma_P + \sigma_A}$ [6]. If any non-zero value is measured for the asymmetry at 8 MeV, it can give us an idea on the magnitude of the discrepancy. Conversely, at 16 MeV, the asymmetry is at its highest value within our selected range. It also has the advantage of having data from previous experiments to compare to. As for 12 MeV, that value is in the middle of the region where the largest discrepancies between theory and experiment were found. By having in-depth measurements in this range, we can adequately examine the nature of the discrepancy and determine the cause. It is also important to note that the forward spin polarizability, γ_0 , can also be found with this set up, albeit with some minor changes. γ_0 can be defined as:

$$\gamma_0 = \frac{S}{2\pi^2} \int_{\nu_0}^{\infty} \frac{\sigma_P - \sigma_A}{\nu^3} d\nu \quad (29)$$

Due to the stronger ν dependence, higher energy contributions matter even less for γ_0 , so much so that data collected for the first part of the experiment would make a negligible contribution. The data for this part of the experiment will be measured with a maximum photon energy of 6 MeV. Thus, there will be a need for a scintillating target. This experiment will take place at TUNL in Durham, North Carolina. Since we want a photon beam, the electron beam will be configured to collide with photons, making a beam of backscattered photons. The electron beam is usually run with two bunches of electrons in the ring. The bunches are usually around 1.2 mA, which corresponds to about 7.5×10^{15} electrons per second. The electron beam has a pulse about every 179 ns. The photons are created through the use of an undulator in the path of the electrons. The undulator contains a region of alternating magnetic fields, which causes the electrons to oscillate, and in the process, radiate photons. The photons travel until they hit a mirror and are reflected back in such a way that

they return to the undulator at the same time as the electron bunch. The photons will also be polarized by the electron beam, giving either left-handed or right handed circular polarization. References [14] and [15] estimate the photon flux to be between $1 - 5 \times 10^8/sec$.

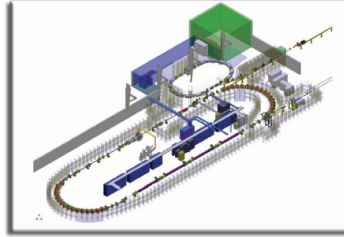


Figure 13: The accelerator at DFEL [16]

Downstream from the laser, we have our detector system, known as the Blowfish. It contains 88 liquid scintillator detectors set up at various angles to catch as many neutrons escaping as possible. There are eight “arms” with 11 detectors each, that cover polar scattering angles (θ) between 22.5° and 157.5° . The arms uniformly spaced to cover the azimuthal angle ϕ .

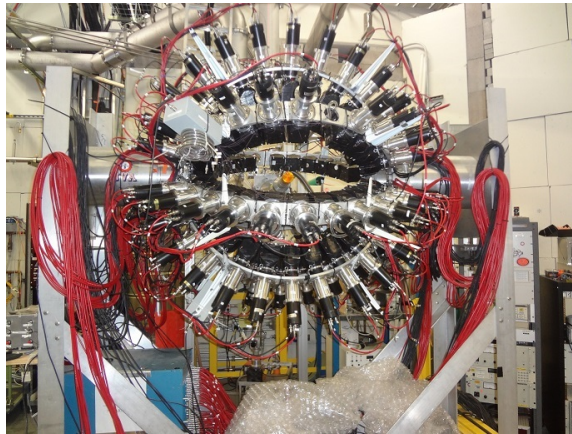


Figure 14: The Blowfish detector

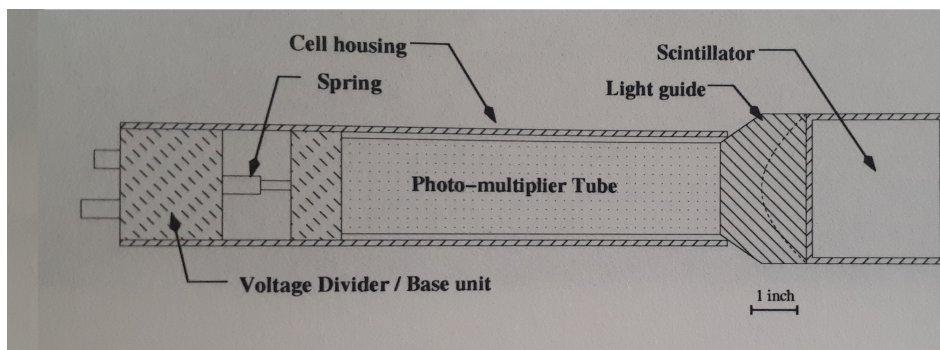


Figure 15: Diagram of one of the Blowfish cells from Brad Sawatsky’s dissertation [17]

A single cell from the Blowfish is shown in Figure 15. The cell consists of a lucite “box” filled with the liquid scintillator BC-505 attached to a photo-multiplier tube. BC-505 was chosen due its excellent neutral particle identification abilities at lower energies. The box is optically coupled to the photo-multiplier using a light guide. When the detector is put together, the lucite box is treated with a high-reflectivity coating and wrapped in aluminum foil. A final layer of black plastic sheeting is added to complete the assembly. The aluminum foil helps minimize light losses from the scintillator, while the black plastic functions as a protective layer to keep out unwanted outside light. We keep the dilution refrigerator at UVA to run cooldowns with it. The main purposes of these cooldowns are to make sure the refrigerator is in working order, optimize our $^3\text{He}/^4\text{He}$ ratio, and to help everyone involved master the procedure for the actual experimental run.

3 Our Dilution Refrigerator

3.1 History and Overview of the System

Our dilution refrigerator was originally built in the 1970s by Tapio Niinikoski[18] for pion experiments at CERN. It was later sent to the Helmholtz Institute in Geesthacht, Germany where it was modified into a supercooled ^4He refrigerator to be used in neutron experiments. It came into our possession in 2012, when we removed the modifications to the best of our ability to use it as a dilution refrigerator once again.

Figure 16: Side view of the Dilution Refrigerator from its first use at CERN[18]

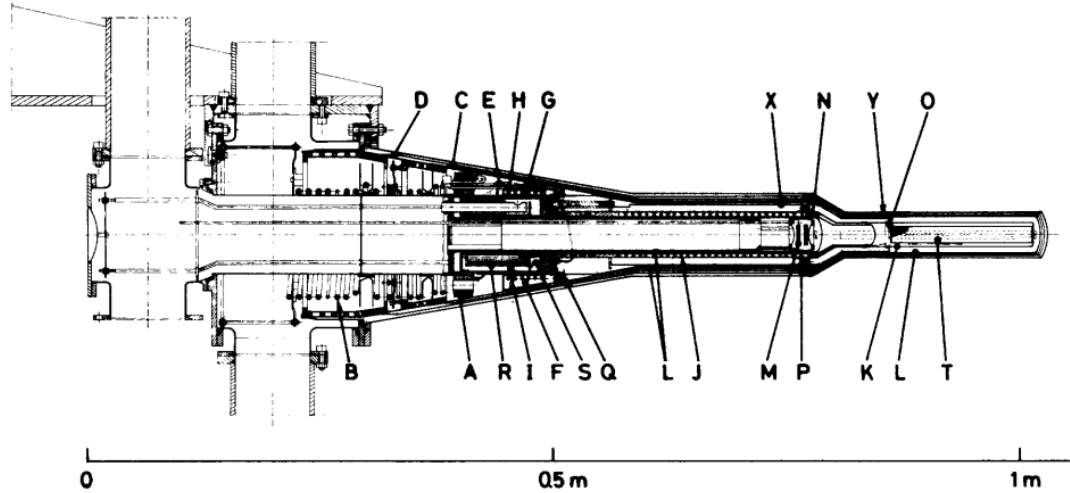


Fig. 5. Assembly drawing of the refrigerator: A—separator, B—tubular counter-current heat exchanger, C—radiation shield I, D—radiation shield II, E—evaporator needle valve, F—evaporator, G—condensing capillary, H—needle valve for precooling, I—still, J—heat exchanger between dilute and concentrated streams, K—mixing chamber, L—vacuum jacket, M—2 silicon surface barrier diodes in evacuated box, N—3 thermometers, O—end cap of mixing chamber, P—indium joint, Q—indium joint, R—boiling heater in still, S—still heat exchanger, T—target, Y—spring for thermal contact and centering, X—waveguide holder and thermal link.

In this diagram, we refer to the left side as the “upstream” end and the right as the “downstream” end of the dilution refrigerator. This terminology stems from the path taken by liquid helium in this refrigerator since the liquid helium from the supply dewar enters from the left (upstream) side and makes its way to the target (mixing) chamber on the downstream end. The liquid helium entering the refrigerator is controlled by two needle valves, which we refer to as the 1K and Bypass valves, labeled as E and H in Figure 16, respectively. The 1K valve is the main entrance of the liquid helium into the system, which guides the liquid into the evaporator, where the vapor is pumped until it is cooled from 4 to 1 Kelvin. The Bypass valve is the secondary route for the liquid, and channels the liquid directly to the downstream end. Its main function is to speed up the cooling process, so that any target material loaded into the target chamber does not warm up too much. The Bypass valve is not used in the dilution process and will be completely closed once the system is cold enough. From the upstream end, liquid helium is fed into a chamber called the separator (A in Figure 16) where the evaporating vapor is pumped through two different lines, called the Shield and the Counter-Current (D and B in Figure 16, respectively). The Shield functions as a barrier between the cryogenic insides of the refrigerator and the room temperature of the lab space. The Counter-Current line acts as a heat sink for recirculated ^3He , cooling the gas as it begins its journey to be condensed back into a liquid. These two lines are controlled by two valves on our pump stack and can be adjusted depending on what is needed during that particular step in the cooldown. During a cooldown, the two vacuum spaces are bounded by two metal barriers known as the Outer Vacuum Chamber (OVC) and the Inner Vacuum Chamber (IVC). The OVC (C) is made of two shells that when pumped down, provide a layer of insulation that prevents the heat from the outside world from coming into contact with the

function of the dilution refrigerator. The vacuum of the OVC is monitored during a cooldown to make sure that heat leaks from the ambient temperature are at a minimum and have a gauge attached to it. The inside layer of the OVC also forms the barrier of the ^4He vacuum space, whose primary function is cooling the helium bath (F in Figure 16) to 1K, and is pumped out to the outside world.

Figure 17: The OVC

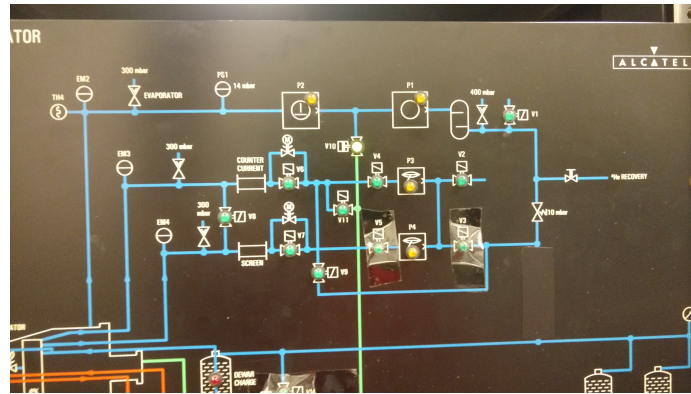


The IVC (L in Figure 16) is the physical barrier between the ^4He and ^3He vacuum space. Unlike the ^4He space, the ^3He space is not pumped out into the atmosphere and instead uses its pumps to recirculate the evaporated ^3He back into the upstream end of the refrigerator so it can be condensed once again. The holding coil for the target that is used during the frozen spin state is also coiled around the IVC. We use two different IVCs here, one with the coil for when we use the magnet, and one without a coil used for the cooldowns.

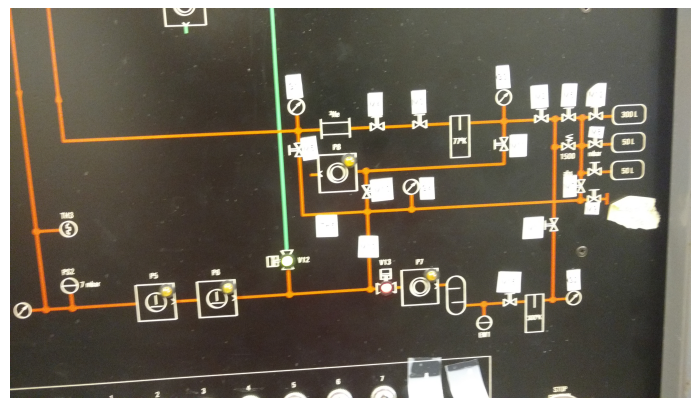
Figure 18: IVCs without (left) and with (right) the holding coils



(a) ^4He section pump schematic



(b) ^3He section pump schematic



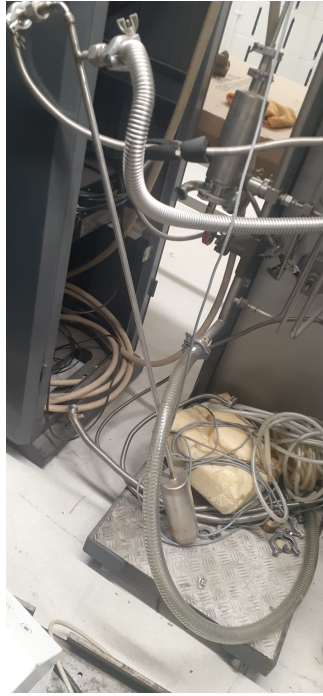
In the above figure, we have the panel where we control the pumps in our system. There are eight different pumps used in this setup, with four in each section. Pumps 1-4 are in the ^4He section, with pumps 1 and 2 connected in series to pump on the evaporator. P1 does most of the work and can be run at atmospheric pressure. P2 increases the pumping power, but cannot be run at atmosphere. If the pressure in the ^4He section rises above a certain threshold, the pump will overheat and shut off. Once it overheats, the pump must be reset by flipping its breaker behind the panel. Pumps 3 and 4 circulate the gas in the counter-current and shield lines, and are almost always run together. Pumps 5-7 help recirculate ^3He back into the upstream end of the refrigerator. P8 is not run during a cooldown, since its only function is to evacuate either the ^3He or the whole system of gas. Thus, it is always off and valved off from the rest of the ^3He system during a cooldown. It is primarily used for evacuating the system for leak checking or for pumping and purging the system right before a cooldown. Pumping and purging refer to the practice right before a cooldown where the system is cleaned of any contaminants (non-helium gases) inside. The system is evacuated using pumps 1,2, and 8. The pneumatic valves V10 and V12 are opened during this time to allow the pumps to work together to expel as many contaminants as possible.

Figure 20: Our pump stack used for cooldowns



Once the pressure is low enough, the pumps are turned off and the system is filled with ^4He gas back up to atmospheric pressure. Once that is done, the process is repeated 2-4 more times and left filled with helium in preparation for the start of the cooldown. Since it is impossible to eliminate all contaminants within the system, we also have liquid nitrogen traps on this system. The liquid nitrogen traps are a system of filters and pipes that use liquid nitrogen to condense any gas that is not helium. This apparatus is submerged in liquid nitrogen, and since the boiling point of helium is much lower, the helium gas flows through unimpeded. However, other gases in the system such as oxygen and water vapor will condense and/or freeze, effectively taking them out of the system.

Figure 21: One of our Nitrogen Traps



The trap itself is the metal cylinder at the end of the long tube in the picture above, and have steel mesh, sintered copper, and a steel disc inside to help trap the unwanted gases in our system.

3.2 Cooldowns

Since the dilution refrigerator is a complex system, it is necessary to practice for the experimental run. These practice runs are called cooldowns and have several practical uses outside of preparation for the experiment:

- Optimize the $^3\text{He}/^4\text{He}$ ratio for the target chamber
- Run diagnostics on the system
- Test new equipment at cryogenic temperatures

Depending on what our goal is, we will run one of two different types of cooldowns, an evaporation cooldown or a dilution cooldown. The evaporation cooldown is the simplest of the two, utilizing only the precooling evaporation system. Evaporation cooldowns are usually only used to test new equipment since it will not matter if the system is at 100 mK or 1K for the equipment to be properly tested in most cases. We usually only order about 100 liters of liquid helium for these types of cooldowns since it does not take long to fill the evaporator and get to 1K. Plus, whatever equipment we are testing can be adequately tested within the timeframe of the evaporation cooldown. Evaporation cooldowns can last from 12 to 24 hours, depending on the helium consumption. Dilution cooldowns utilize the entire system and usually require

the attention of everyone in our group. The process is also a lot more extensive, as detailed in the flowchart created by Ryan Duve [19]. These types of cooldowns go beyond the evaporation stage of the other type, and use our stock of ^3He gas in an attempt to get into the millikelvin range. These types of cooldowns usually require about 450 liters of liquid helium to run, and take place over several days. Once we have determined that we want to have a cooldown, there are a couple of steps to take to properly prepare. Once the liquid helium is ordered, we prepare the Liquid Transfer Line (LTL). The liquid transfer line is a metal tube used to move the liquid helium from the dewar into the refrigerator. To use it, it must first be pumped down using the leak checker. The leak checker has a coupling part that helps with this. One end is a KF flange while the other mates with the port on the LTL's bend. Once attached, the proper procedure to evacuate it is:

- Thread the black knob on the coupler to vacuum relief on the LTL
- Once threaded, pull on the knob
- Attach the KF end of the coupler to the leak checker and begin pumping
- After enough time has passed, push the knob back into place
- Unthread the knob completely and bring it back out
- Stop the leak checker and vent it

Figure 22: Several Liquid Transfer Lines in our lab



While the transfer line is being pumped on, we can start the pumping and purging process described in section 3.1. This process is usually started the day before the liquid helium is scheduled to arrive, with the system filled with ^4He gas overnight to minimize the amount of contaminants entering. Once the liquid helium dewar is in the lab, we replace the top with our custom-made one. This top has three different ports,

one for the LTL, one for the liquid level probe, and another for the other transfer line. The liquid level probe measures the amount of liquid left in the dewar, and the other transfer line is used to move liquid from other dewars into the dewar attached to the refrigerator. When the LTL is placed into the dewar, the exposed end is plugged (usually with a finger) so that the liquid stays in while we prepare the refrigerator. While this is happening, ^4He gas is backfilling the system, so that the entry point for the dewar is free of contaminants while the LTL is being inserted into the refrigerator. Once the LTL is secure, the backfill is turned off, and the dewar backfill is turned on. The backfill is controlled by a dedicated panel, with each valve on it going to a different system. The dewar is pressured to a few PSI above atmospheric pressure with ^4He gas to push the liquid from the dewar into the LTL and the refrigerator.

Figure 23: One of the valves on the backfill panel; there are four in total: ^3He , ^4He , dewar, and IVC backfill



Once the liquid is flowing, the 1K and Bypass valves are opened three turns each, and the shield and counter-current flows are set to their maximum setting for the first 30 minutes. Exchange gas is also introduced into the IVC during this time. The exchange gas is used to speed up the cooling of the internal parts of the refrigerator from room temperature. Since the pumps are being run, the inside of the IVC should be a vacuum, and therefore harder to cool. By adding the exchange gas, it loses the heat when coming into contact with the colder IVC shell, and steals a little bit of heat when coming into contact with the internal parts. Since the liquid helium coming into contact with the IVC acts like a 4K bath, the overall temperature of the internal parts will drop until it reaches about 30K, when the exchange gas is removed. After 30 minutes, the shield and counter-current flows will be reduced to 13 and 7 standard liters per minute (SLPM). Once the system is cold enough and the exchange gas is

removed, the Bypass valve will be closed and the 1K valve setting will be reduced (usually to 1/8 turns open). Once that is done and the evaporator is stable, ^3He will be added into the system and begin to be cooled. From then on, the system will be monitored by whoever is on shift and make adjustments when necessary.

3.3 Goals and Design

We regularly had cooldowns at UVA until late 2017. It was around that time that we discovered a leak coming from the still in our refrigerator. However, since it was an integral part of the dilution refrigerator, other important parts around it had to be removed with it. This included the heat exchanger and the vacuum layer can surrounding the still. After the painstaking process of removing it, we systemically disassembled and documented the innards of the entire unit. Given our situation, we took the opportunity to reflect on how the device was assembled and thought about how we could design our new unit to prevent our problem from happening in the future. Here are the two main goals of the design:

- Make the still unit easier to remove in case one of the components has a leak in the future
- Reduce the amount of solder used as much as possible

The first goal is self-explanatory, but the second goal arises partly from one of our theories on the origin of the leak: the solder might have had a different thermal coefficient of expansion from the stainless steel the rest of the unit is made of. Thus, over many cooldowns, the repeated cooling and heating of the dilution unit expanded and contracted at different rates, therefore creating a leak over time. Instead, we choose to replace any solder joints with indium seals, which are easier to undo, and something we already use in vacuum seals on other parts of our refrigerator. The other method used to seal would be to weld parts together, a more permanent option, but will not have the coefficient of expansion problem the solder had. During the disassembly, we also figured out a problem that had been plaguing our group for years. The one consistent issue we had was the inability to have microwaves travel to the target. It did not matter what the intensity was, we were always unable to perform DNP on the target to polarize it. We realized that the issue stemmed from the waveguide on the inside of the unit had snapped in half. This discovery came when we stuck an endoscopic camera on the inside of the old bellows. The new still unit will be assembled using a combination of those two methods. Despite these changes, the overall goal was to recreate the unit as closely as possible to the design used by Tapio Niinikoski to recreate the success he had with the refrigerator when he used it at CERN. The measurements taken during the disassembly process were then used to make three-dimensional models in SolidWorks. SolidWorks made the individual “parts” of the new dilution unit as they would be fabricated in our machine shop. The parts would then be used in an assembly file to visualize the final product. The use of the assembly file was paramount in helping our collaborators see what we were planning, as well as asking questions and making suggestions to improve its design.

Once the design was finalized, the fabrication and welding process was decided, going from the inside out. The main reason for this was so that we could leak check as we go, since some of the welds would be inaccessible once the unit was completed. For this purpose, leak check flanges were designed and made to make this possible. This process was initially done entirely at UVA until December 2020, when our head machinist retired. The rest of the welding was done by the machinists at Jefferson Lab.

Figure 24: The leaks were detected in the areas with the red circles



Figure 25: The Removed Still Unit



(a) Upstream end of Old Still (b) Downstream end of Old Still



(a) Upstream Face of Still Exposed (b) Inside of Still with Heater and Pumpout shown



(a) Still Exposed further;
 ^3He line prominent



(b) Old Unit featured two of these bypass tubes



(a) Shot of inside of Bellows with
Broken Waveguide shown



(b) Waveguide Half extracted from Bellows

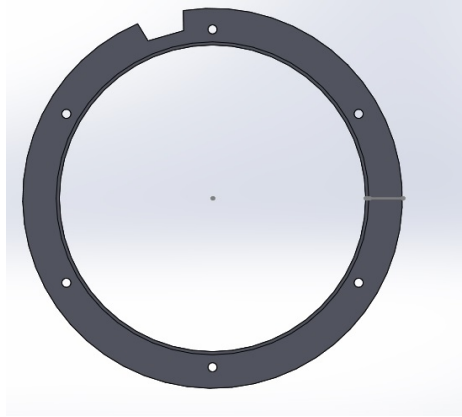


3.4 First Version

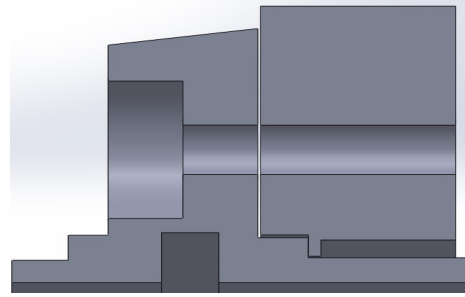
Indium Adapter Ring

The first part of this new unit is what we call the Indium Adapter Ring. This part has no functional purpose for cooldowns themselves but is rather a dock for the new unit to form a seal with the rest of the dilution refrigerator. The ring has been welded to the refrigerator and has a groove used to make an indium seal with the corresponding mating part on the back of the lip on the Vacuum Layer Can.

(a) CAD Drawing of Indium Adapter Ring



(b) Close-up of Indium Seal between Ring and VLC



Vacuum Layer Can

As the name implies, the Vacuum Layer Can (VLC) creates an insulating vacuum around the still. Its other function is to guide the wires from the back of the refrigerator to their ports at the mixing chamber through a tube-like thing on the backside of the VLC. The thick lip towards the front of the can has a double indium seal, with the back mating with the Indium Adapter Ring. The front mates with the Inner Vacuum Chamber (IVC), a part we already have, so the VLC was created with our IVC in mind. In the previous figure with the indium seal, you can see we made it so that the screws used would go into the lip of the VLC, so it would not interfere with the IVC seal on the other side. On the lip, there is a hole drilled into the side for the ^3He line exiting the evaporator. While the hole is sealed with solder, this does not go against one of the goals of the new dilution unit, because this hole will be able to be accessed by us in case of leakage. As long as the seal can be accessed without too much difficulty, the solder should be an acceptable sealant. Also attached to the VLC is a long sealed tube known collectively as the “Bellows”. The bellows reach upstream and form a seal towards the back of the refrigerator. The bellows’ main purpose is to form a separate vacuum layer around the waveguide since that part is inside of the ^4He vacuum space. The bellows also feature a cryogenic feedthrough, which is the medium that allows the sensor wires to cross from their source in the ^4He vacuum space to the ^3He vacuum space and the still. From the ^4He space, the wires are connected to plugs that lead to the readouts for the temperature sensors.

(a) CAD Drawing of Vacuum Layer Can



(b) Inside of VLC



The Still

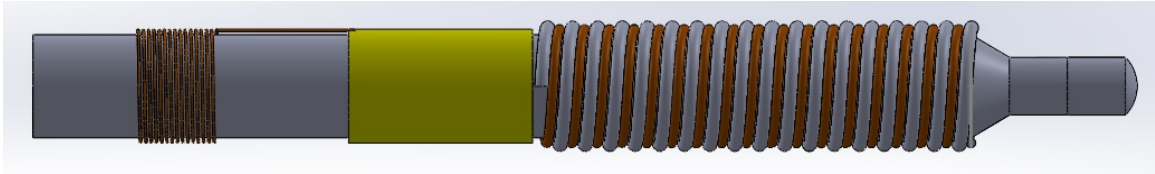
Inside the VLC is the still, where the liquid helium is stored and circulated. The still has two main parts inside of it, the pumpout flute and the waveguide tube. The pumpout flute's main purpose is to be an opening for the He-3/He-4 gas to be pulled out of and circulated through the He-3 piping. Four bundles of cryogenic wire from the VLC feedthrough also come through the still. These wires are attached to six different temperature sensors. Four of these sensors are CX-1030 Cernox sensors from Lakeshore Cryotronics. Their main purpose is to monitor the level of liquid inside the still. The idea is to have them at two different heights inside (two sensors per level), and based on the readings, we will be able to know whether the still is too empty, too full, or perfectly fine. The other two sensors are the ROx temperature sensors that are in the target chamber. The wires will be fed through the pumpout, to reduce the number of flanges on the still. This decision has two main advantages, simplicity and leak-tightness. By having a more simple design, it makes it easier to make and weld. As for leak-tightness, the fewer flanges there are, the fewer possible places there are for a leak to appear. The wire tube is the bypass area that allows the waveguide and NMR coil to pass through the still without encountering the liquid helium. A small hole has been drilled into the front face of the still. Its purpose is as an entrance for the ^3He line leaving the evaporator.

Heat Exchanger

The heat exchanger is a tube-in-tube style continuous heat exchanger. The inside tube is a simple cupronickel tube wrapped around the central tube in a helical path. The outside "tube" is sintered copper compressed around the inner tube. The sintered copper itself is copper powder compressed into a tube which is used to maximize the surface area to volume ratio which is used to maximize the heat transfer between the incoming and outgoing helium. The outgoing helium is forced to crawl along through the sintered copper with the use of a makeshift channel made from a nylon rope (also known as a parachute cord). The rope is wrapped between the gaps of the heat exchanger, forming the path the helium is forced to follow. A code was written to simulate the temperature drop from the still to the mixing chamber based on the

restrictions from the still geometry and measurements (more details on the code in section 5.2).

Figure 32: Heat Exchanger around central tube



Sleeve

The final part being designed is the metal sleeve, which slides over the heat exchanger and attaches to the still, separating that space from the vacuum in the IVC. The new sleeve has been designed with an indium seal to mate with the still, and a recreated version of the indium seal that mated with the mixing chamber. The sleeve has a slot that goes around the ^3He line entering the still as well as a hole for the waveguide to go through. The ID of the sleeve was carefully chosen to allow for just enough space for the heat exchanger and the rope channel. The reason for this is to compress the rope channel and prevent the liquid helium mixture from crawling over the rope instead of flowing through the sintered copper of the heat exchanger.

Figure 33: Sleeve



3.5 Second Version

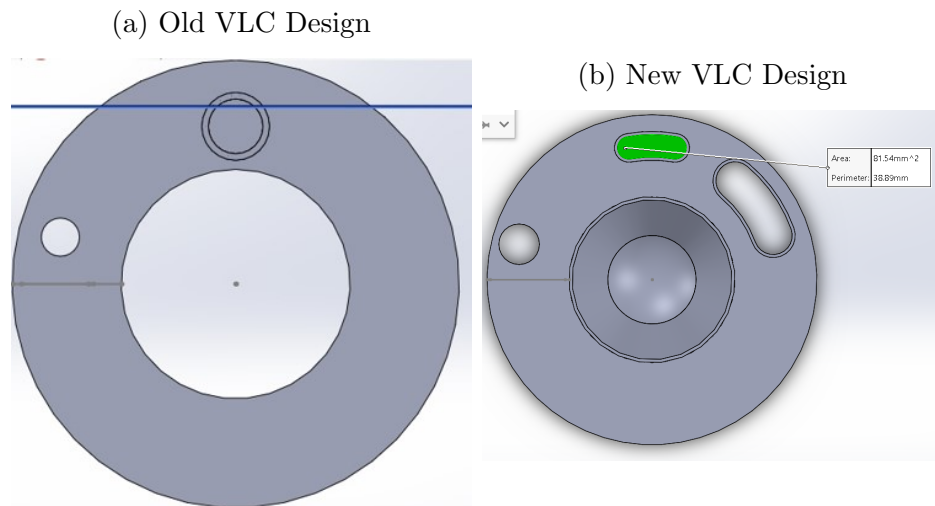
The first version of the new unit was in the process of reconstruction, but one of the indium seals was partially destroyed in the welding process. When this occurred, we had a meeting to discuss design changes that met our standards but eased the burden on the welders to avoid this problem again. We attempted to conserve as many parts as possible, as a method to shorten the process and save material. The second version was able to preserve the Indium Adapter Ring, most of the central tube, the final heat exchanger, and the downstream half of the VLC.

Vacuum Layer Can

After the redesign, the VLC was given two changes:

- Reduce pumpout OD
- Add feedthrough

Starting with the first bullet point on the list, the upstream face of VLC badly needed a redesign. Both the pumpout and the central tube were to be welded onto the VLC. However, the circumference of the pumpout and the central tube came very close to each other and made it extremely difficult to weld. It became necessary to reduce the diameter of the pumpout to give the welders more space to work with. The central tube could not be changed for several reasons, due to it accommodating the beam, the old sintered copper heat exchanger, and a tricky piece of welding that is unlikely to be duplicated. However, we needed to also maintain the high cooling power of our refrigerator, which is proportional to the cross-sectional area of the pumpout. Given this dilemma, we came up with a creative solution: Change the cross-sectional area of the pumpout from a circle to a bean-like shape.



The second change made was to add a port for the wire feedthrough. In the old design, the wires for the sensors and still heater would have been fed through the pumpout. However, the concern was raised that the very delicate wires could snap or otherwise break from the heat generated by welding. Thus, the decision was made to add a feedthrough flange for the sensor wires. However, due to the space constraints we are working with, it was extremely difficult to find a feedthrough that fit those constraints while also being able to accommodate the number of wires we needed. Fortunately, Chris Keith at Jefferson Lab gave us a guide on how to make our custom feedthrough. This allowed us to have even greater freedom in our designs, so we repeated the same design choice as the pumpout and went with a bean-shaped cross-section.

The Still

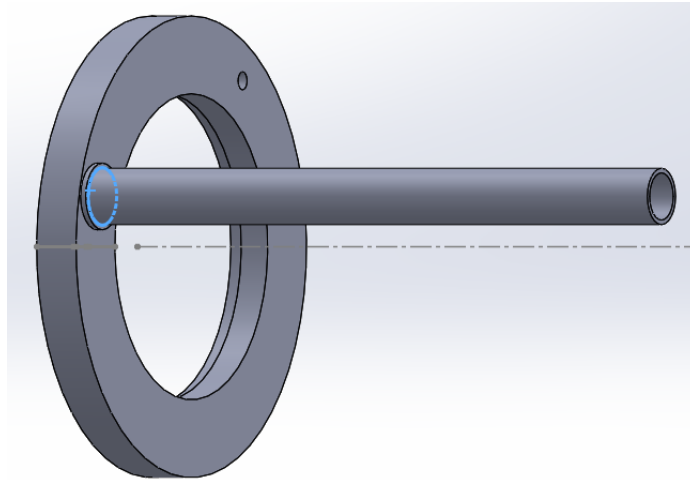
There are now fourteen screw holes for the indium seal with the sleeve. There were initially only six, but there were concerns about the integrity of the seal, so the

number of holes was increased to ensure that. Following the welding mishap, the still was given three additional changes:

- Move the weld between the downstream face of the still and the waveguide tube to the other side
- Add a beveled inlet for the ^3He line
- Reduce the number of sensors

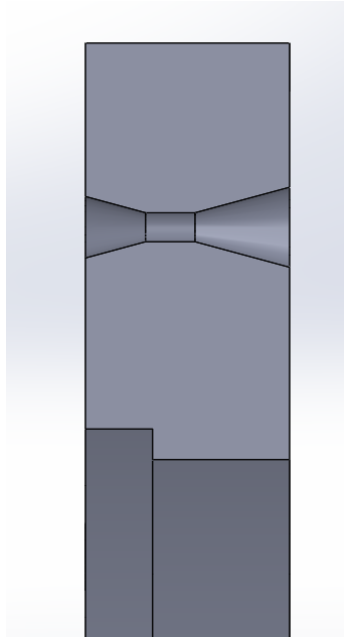
The first point was simple to implement, requiring less than five minutes in Solid-Works. The previous design had the weld prep for the two parts on the same side of the threaded holes and the indium seal. When the seal was destroyed, moving the prep to the other side was a common sense change.

Figure 35: Location of new weld prep



The second change made was to the inlet for the ^3He line. The original plan was to feed it through the hole on the downstream face of the still *before* welding it together. The concern with this plan was the same as with the wires being fed through the pumpout. The ^3He line in a small OD tube with thin walls, making it easy for it to snap from the heat of welding. So, both sides are to be given a conical cross-section. For the inside of the still, it is to help us feel for the hole and guide us to it. For the outside, it is to help the epoxy pool around the boundary for an easier seal. The third and final change was to the number of sensors. This change from the realization that the spare sensors for the liquid level were unnecessary. The Cernox sensors on the inside of the still are for convenience, and not integral to the operation of the dilution refrigerator. So, having spare sensors for that would be more trouble than they are worth, given the tight constraints on the dimensions of the still, and the difficulty involved with attaching them to the walls of the still. For more information on these sensors, refer to Section 4.3.

Figure 36: Beveled inlet



Sleeve

The sleeve was mostly preserved, except for the end that mates with the still. That end was removed and replaced with a design that fits the updated still.

4 Construction

The construction method of the dilution unit was optimized for speed. The basic principle was simple: Space the welds in a way that maximizes the number of parts fused, but still allows us to leak check critical components before they become inaccessible. Once the parts were ready, the drawings for the next parts were sent to our machine shop, and we would drive to Jefferson Lab in Newport News, Virginia for the welding. To perform the leak checking, flanges for that express purpose were fabricated.

4.1 Fabrication and Welding

The dilution unit was fabricated and assembled from the inside out. In this section, we will discuss the steps in detail. The steps are organized chronologically, and grouped in such a way that each step alternates with an official leak check. With that in mind, the unit was assembled from the inside out; starting from the still and going outward to the VLC and beyond. Some steps were welded on the same day, but ultimately, it took several trips to Jefferson Lab to completely assemble the dilution unit.

- Step 0: These welds were performed during the previous set of welds, and were one of the only sets we were able to reuse after the previous design failed. The

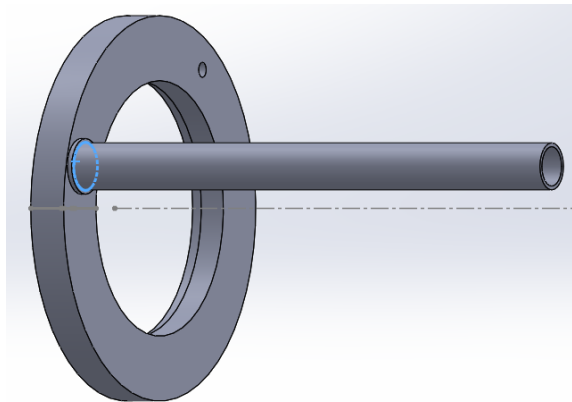
parts involved were the pieces of the central tube. The central tube extends along the axis of the beamline and provides the surface that the final heat exchanger follows along. The central tube initially came in three parts; the main shaft, the tip, and the coupler part that shifted the diameters between the two previous parts. The tip in particular is a real feat of skill since it has a “window” of about 0.01” of thickness on the end. This thin sheet of stainless steel allows our photon beam to go through while preventing the liquid helium in the target from crawling along the inside of the central tube. The baby bottle shape of the end also gives us the ability to use the tip to push the target beads into the target chamber without the fear of part of it hanging outside of that area. Given that these welds are easily accessible, we did not have to worry about leak checking them right away and could verify if they were leaking when checking future steps.

Figure 37: Central Tube



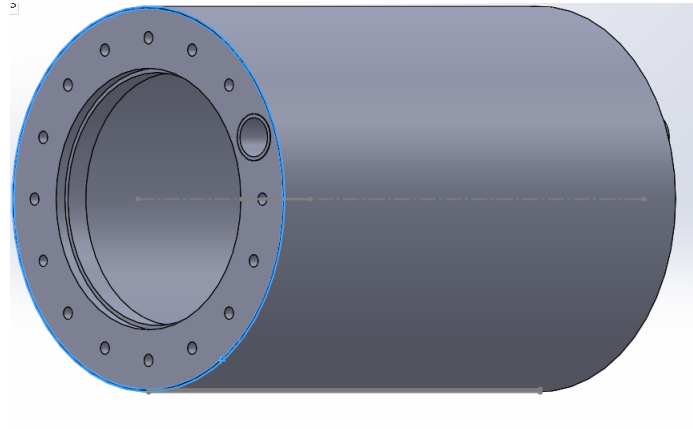
- Step 1A: Downstream face of still and waveguide tube- This was a simple weld, needing only one which was located on the backside of the still face. Leak checking was simple, needing only a rubber stopper on one end and a connection to a leak checker on the other.

Figure 38: Step 1A with weld highlighted



- Step 1B: Body of the still and the parts from step 1A- This weld needed a steady hand more than the previous step, due to the proximity of the weld to the screw holes on the still face. This weld did not need to be checked immediately, due to the ease of access, and would be checked once the still was completely together.

Figure 39: Step 1B with weld highlighted



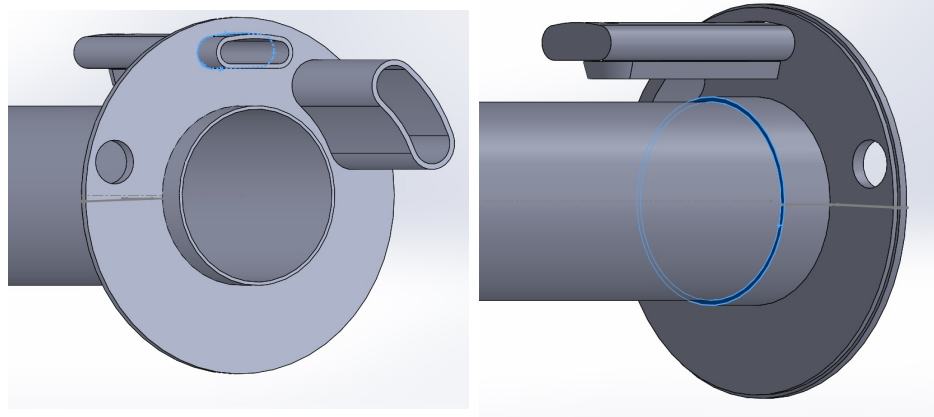
- Step 2: Upstream face of the still, the central tube, and the pumpout- Given how many parts are fused to the back of the still, it became important to stagger these joints on both sides to avoid any mishaps. Welding joints are usually not close together, but space constraints make that difficult. Staggering the joints on both sides of the face is the best compromise we have for this situation. On one side, we have the pumpout, and on the other, we have the central tube. Due to the unorthodox shape of its cross-section, the pumpout was fabricated into two halves, which were subsequently fused. Since the pumpout will also have to fuse to the upstream face of the VLC, it had to stick out a certain length to be fused to it. Another concern that was brought up was there was a possibility that liquid helium in the still could crawl up the pumpout and escape. To address both issues, a set of “fangs” were added to the underside of the pumpout. They had a sharp, triangular cross-section designed to impede liquid helium from crawling up, while also terminating where the pumpout would be exposed enough to reach the VLC for its future weld.

Figure 40: Underside of the pumpout



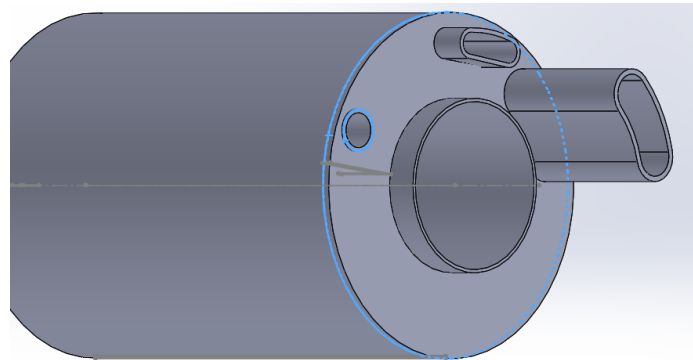
As for the weld joint on the central tube, the still face has an extrusion that functions as the weld prep for this joint. The extrusion is about half an inch long, to ensure the heat from the weld does not mess up the other joint.

(a) Step 2A with welds highlighted (b) Step 2B with weld highlighted

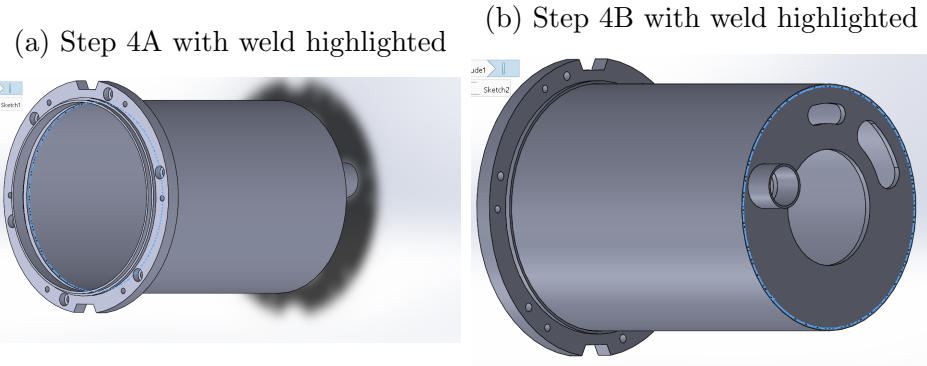


- Step 3: Welding the still together- With the two halves ready, we welded them together, with one seam along the circumference of the still, and the other at the waveguide tube on the upstream face of the still. To leak check it, we used the sleeve and a custom flange on the downstream end, and some plugs on the upstream end.

Figure 42: Step 3 with welds highlighted

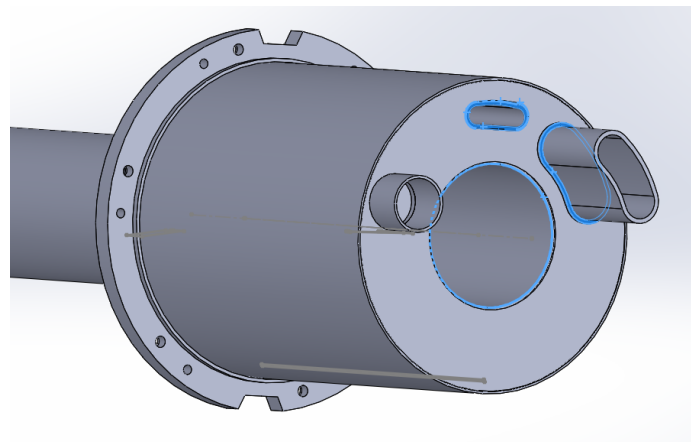


- Step 4: The Vacuum Layer Can- The VLC is sealed in two welds, but we had already assembled it during our previous attempt. So, we had to remove the upstream end of it and replace it so it would properly mate with the new design of the still. The first weld was made along the inner circumference of the body of the VLC, fusing it with the double seal. The second was made along the circumference of the upstream face of the VLC.



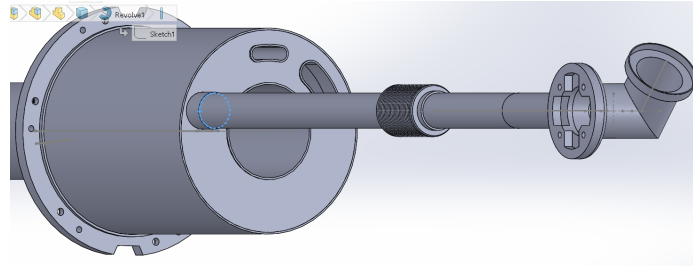
Step 5: Fusing the VLC and the still together- These two parts are fused on the same surface in three different places; the pumpout, the central tube, and the feedthrough port. The pumpout and the central tube are fused on the surface of the upstream face of the VLC, while the space for the feedthrough port had a weld prep, allowing it to extend past the face.

Figure 44: Step 5 with welds highlighted



- Step 6: The Bellows- The tube designed to hold the waveguide that extends from the back of the VLC to the upstream end of the refrigerator is collectively known as the Bellows. In the middle of the tube, there is a flexible stainless steel part designed to reduce strain. When the waveguide was placed inside, torlon rings were put on it to prevent the waveguide from touching the metal walls of its metal tube. When the microwave generator is turned on, it adds heat to the system, and by preventing it from touching the walls, it lowers the heat load added to the dilution unit. Once the parts were ready, they were fused along the weld preps on the flexible part and the Bellows assembly was then fused onto the port on the VLC.

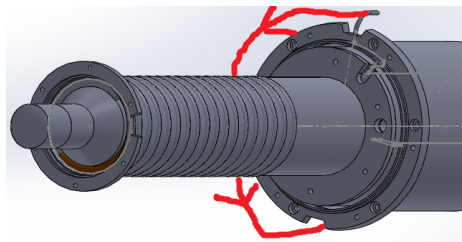
Figure 45: Step 6 with weld highlighted



4.2 The ^3He Line

With the body assembled, the next step was to add the systems that allow it to function. The first to be discussed will be the ^3He line. This line will attach to the existing line exiting the helium bath in the evaporator, and run to the target chamber on the dilution unit. The new line is made from a combination of cupronickel and nickel silver tubing, with the former having dimensions of 0.53mm ID/0.91mm OD and the latter having dimensions of 1.14mm ID/1.50mm OD. The reasoning for the two types is because that it is impossible to make this line in one piece. The smaller tubing makes up a majority of the new line, with the larger tubing acting as a coupler between sections of the line. Since the line has to go through different vacuum spaces, it was important to plot out its course beforehand. From the evaporator, it follows along the circumference of the VLC until it goes through a hole, bends into the downstream direction, and enters the still. Once inside the still, it goes to the back, wraps around the central tube a few times, and meets with the final heat exchanger. The final heat exchanger was reused from the old refrigerator and is wrapped around the central tube.

(a) From Outside to VLC



(b) From VLC to Still

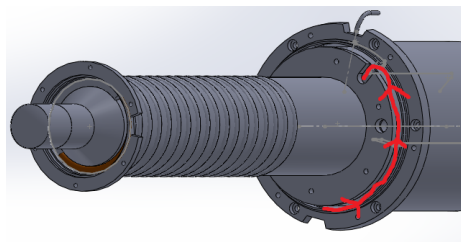
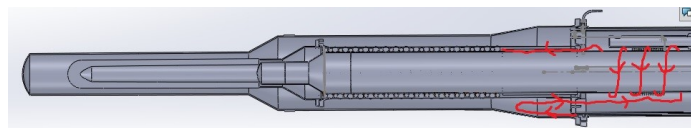


Figure 47: From Still to Final Heat Exchanger



Originally, we were going to just go directly into the VLC on the first part of the path, but there was an issue with getting the tube in there, so we had to make a

detour and go through the bottom divot on the VLC. Each section of the line was leak checked as it was assembled, using some homemade flanges made from our small tubing and some KF flanges.

Figure 48: Some example flanges for leak checking



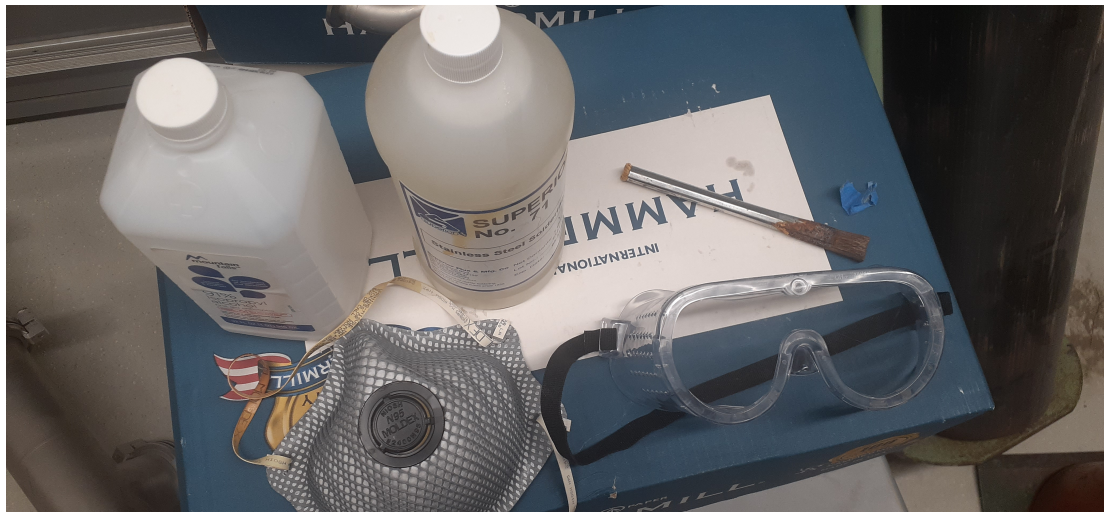
The flanges would be soldered onto the line and attached to our leak checker. The test itself was simple; with one end attached to the leak checker, the other end would be blanked off. If we sprayed helium around it and there was no spike in the leak rate, the test would be repeated without the blank off. If the leak checker spiked when the line was exposed to helium at this time, that proved that the line is working as intended. Each section of the He-3 line presented varying levels of difficulty when being leak checked, with the final heat exchanger presenting the most difficulty. It seemed to have clogs of unknown origin, which forced us to disassemble it and check each section of sintered copper tubing. The clogs were removed by using a soldering iron to heat it up and removing using a solder sucker. We would then verify that the line was cleared by putting one end of the line in some water and blowing helium through the other. If the line was clear, the water would bubble. Once each section was cleaned out, they were soldered back together. One section was removed entirely due to it not being completely leak-tight, but once the rest were reassembled, we were finally able to see it have flowing gas going through it while maintaining its leak-tightness. For the section inside of the still, a length of the 0.91mm OD tubing was shaped by our machinists in the shop. It follows along the central tube in a helical path, which then diverts outward in the radial direction, and turns toward the beveled inlet on the downstream face of the still. Given the tight space restrictions of the design, tweezers were used to maneuver the line into the inlet. However, we still had great difficulty in moving the line inside. To mitigate this, we hung a #75 drill bit in there to help guide the tube in there. The drill bit was held in place

with “wings” made from two pieces of tape stuck together to prevent it from falling through. We were then able to pull the line through the inlet with relative ease. For the remaining sections of the line, we bent those by hand. To ensure that the lines would not crimp, we placed wires inside the tubing before bending them and bent them little by little until they were in the correct form. For the part of the line that was going through the VLC, the thought process was the same, but we had a slight difference in the implementation. The tubing was bent by using a string to pull the tube in its desired direction while pushing it into the VLC, creating a smooth curve.

Soldering on Stainless Steel

Since solder was used to both seal and secure the ^3He line, it needed to stick to all surfaces involved, including the stainless steel of the dilution unit. However, solder does not stick to that material which means we have to find an alternative method. Silver solder can stick to it, but it requires much higher temperatures, and the heat causes the thin tubing to easily snap. Fortunately, there is a method to have solder stick to stainless steel with a specialized chemical. Known simply as Stainless Steel Flux or Superior No. 71, this chemical allows the solder to make a bond with stainless steel, but it is incredibly corrosive. Great care must be taken to use it, requiring the use of nitrile gloves, goggles, a mask, and a fume hood.

Figure 49: From Left to Right:
Back: Isopropyl Alcohol, Stainless Steel Flux, Brush
Front: Mask, Goggles



In addition to the supplies shown in the figure above, rosin-free solid core solder, kimwipes, soap, sandpaper, a soldering iron, and an old rag. Once these supplies and the proper precautions are taken, the steps to solder are as follows:

- Turn on the fume hood and put on the PPE
- Dab alcohol onto a kimwipe and clean the surface

- Use the sandpaper to scrape the surface
- Dab the brush in the stainless flux and apply it to the surface
- Insert the tubing and heat up the area where the solder will go
- Wait until the puddle of flux darkens a little and bubbles
- Once it is done, bring the solder over to the area and apply it
- When the solder is applied and solid, wet the rag using soap and water and wipe down the area

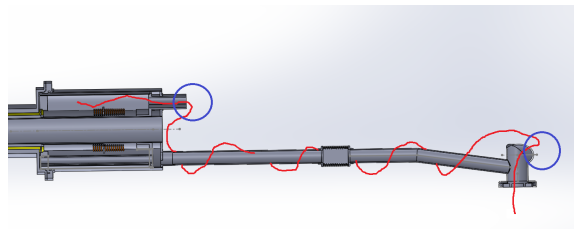
Cleaning the surface with alcohol eliminates any contaminants on the surface, while using the sandpaper scratches up the surface, making it easier for the solder to make a solid connection with the stainless steel surface. When the brush is dabbed in the flux, not a lot of flux is needed, so a quick dip in the bottle will be enough. As the surface is heated, the bubbling of the flux moves outward, and once the bubbling stops, that should be hot enough to apply the solder. As for the soap and water, that cleans off any remaining flux on the surface, and by cleaning it, prevents any corrosion from leftover flux. Once the process is done, turn off the fume hood and the soldering iron, and place the flux into a secure container. The flux is kept in a box with some of the other supplies and is placed somewhere where the chance of spill and/or exposure is minimized.

4.3 Electrical Connections

Electrical Feedthroughs

To effectively operate the refrigerator, it is necessary to have sensors and other devices on the inside. To make that a reality, it is necessary to plot out the paths of proposed electrical wires and provide leak-tight methods of transporting them through different vacuum spaces.

Figure 50: Proposed path from upstream port to still



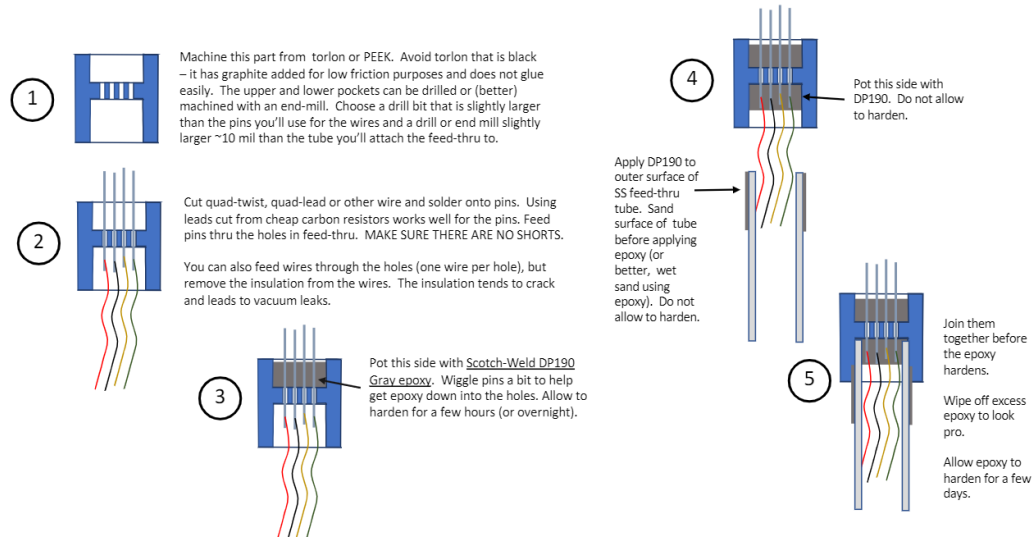
Above, we have a picture showing the proposed path of the wiring, shown in red. The places where it enters a vacuum space are shown with blue circles. On the upstream end of the refrigerator, there is a port with spots for vacuum-sealed electrical connections that serve as the starting point for our wires. The big issue then becomes how to get these wires, which start in our ^4He vacuum space, to the inside of the still,

which is part of the ^3He vacuum space. To prevent cross-contamination between these spaces, we used feedthroughs, one that was made in the lab, and another that was given to us by Christopher Keith at Jefferson Lab. Starting from the upstream end, we used the feedthrough that was given to us. It is a circular 19-pin connector from CeramTec with a weld prep. When the bellows were first being fabricated, we took the time to solder the wires into place on one end of the connector. Once the wires were on, the connector was then welded onto the upstream end of the bellows. This sequence of events was due to the permanence of welds, as well as the inaccessibility of the connector in its current orientation. With the first feedthrough done, it then became time to start work on the second. Due to the space constraints of our setup, we were unable to find a commercially available feedthrough that satisfied those restraints while also accommodating the necessary number of wires. However, Chris Keith was able to provide a solution to our dilemma once again. He gave us a step-by-step guide on how to build our vacuum tight feedthrough, as well as a list of the necessary materials. The feedthrough body was made with Torlon 4203, the contacts were made from resistor leads, the wires used were Lakeshore 32 AWG Quad Lead Cryogenic wire, and everything was sealed with DP 190 epoxy. The manufacturing is a simple five-step process:

- Machine the body of the feedthrough
- Solder the wires onto one end of the resistor leads and place the leads into their corresponding holes in the body
- Add epoxy into the end of the body that will be on the outside. The solder joints from the previous step should be on the other side. Let the epoxy harden.
- Add epoxy into the other end and wipe some epoxy onto the outer surface of the mating flange
- Join the two together and let the epoxy harden

Figure 51: Chris Keith's feedthrough manual [20]

Miniature feed-thru for low temperature



One thing that was suggested to us was to make the feedthrough body 5-10 mm larger in diameter than the flange it would be attached to. The reasoning for this is that torlon has a larger coefficient of expansion than stainless steel, meaning that as the temperature drops, the torlon shrinks more, making an even better seal as it tightens around the steel flange. With all of this information, we began making our own. The machine shop made two feedthroughs, and about half a dozen practice ones to get used to the process. The practice feedthroughs were circular, and featured four holes in a diamond pattern in the center. The stainless steel flanges were KF-40 straight tubes purchased from McMaster-Carr. Once the practice feedthrough was made, we leak checked it. Since this feedthrough would have to deal with fluctuating temperatures, the procedure for it was a simple one: Dunk the feedthrough in liquid nitrogen, heat it back to room temperature with a heat gun, and repeat it four more times. After the fifth reheating, the flange was attached to the leak checker, and the test was performed.

Figure 52: Test Feedthrough used in cold test



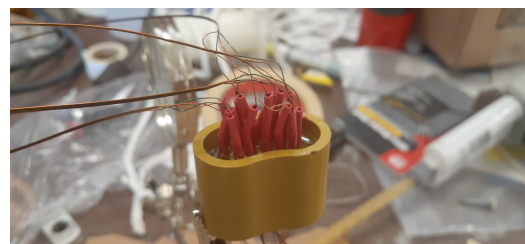
We initially found some leaks, but they would disappear within 5 minutes of the start of the leak check. This was not a problem for a couple of reasons. First, the temperature fluctuations during an actual cooldown would not be as rapid or drastic, going down to 77 K at a slower rate than being directly submerged in liquid nitrogen. The feedthrough would then stay at that temperature for several hours or days and would return to room temperature in a couple of hours, as opposed to one or two minutes when subjected to the heat gun. Second, if this feedthrough leaks gas for a couple of minutes, it is of no consequence. The lab-made feedthrough is attached to a flange on the back of the still, meaning it acts as a wall between the still and the ^3He vacuum space on the upstream end of the refrigerator. So, it acts less like a trap for the gas, and more as a wall to keep the liquid mixture inside of the still in this instance. With the leak checking a success, we began soldering the wires onto the resistor leads. The resistors were supplied by the department stockroom and cut off with wire cutters. The quad lead wire was also prepared at this time. Depending on what bundle of wires would be attached to, they were cut to specific lengths. For the bundles traveling between the feedthroughs, they were cut to be three feet in length. For the bundles connecting the target chamber sensors, they were cut to about seven feet, considering they would wrap around the central tube on their way to the target chamber. The still heater wires were cut to be one foot in length. Once the wires were cut, we had to expose the conductors on both ends and separate the four wires. This was done using 2000-grit sandpaper, which was rough enough to strip off the

insulation, but not rough enough to potentially break the delicate wires. Once both ends were done, the connection was checked using a multimeter. We started soldering one end of the connectors and slid them inside the body of the feedthrough. Because of their proximity to each other, we had our department electronics expert, Larry St. John do the other side since none of us trusted our skill enough to attempt it. Once both sides were done, we dabbed some nail polish onto the solder joints to provide some insulation and prevent cross-talk. This was done and left to dry overnight. However, we observed that the joints had started to come undone after a few days. With this unfortunate development, we had to step back and discuss the next steps. Considering that one side of this feedthrough would be inaccessible after epoxying, the undoing of the solder joints was unacceptable. After some discussion, we decided to consult a local electronics firm, WWW Electronics. After looking over Chris Keith's manual and hearing our process, they made one major change to it: Replace the resistor leads used as the conductors with a pair of terminal pins (Digi-Key Part number ED1323-ND) and pin receptacles (Digi-Key Part number ED1366-ND). This new setup had the key advantages of being much easier to make and having a stronger bond between the wire and the terminal. The new process starts with placing the exposed wire into the pin or receptacle. Solder is fed through the hole on the side of the pin/receptacle until it is full, and then the electrical connection is checked with a voltmeter. This process was repeated 31 more times, (16 pin connector times 2 sides) and the wires were then ready for the body. One warning we were given regarding this method is that there was a very low chance that some epoxy could seep into the holes with the contacts, and could potentially get in between them and cut off the connection between the two halves when the epoxy hardened. The solution that was provided to us was to drill the holes in the feedthrough to be slightly larger than the receptacles. When the receptacles are placed inside, they would act as a plug to keep the epoxy from flowing through the holes. We cut sixteen pieces of heat shrink to prevent touches between pins and slid them on. The heat gun was used to activate the heat shrink, and the receptacles were pushed into place. That side of the feedthrough was then filled with epoxy and left overnight.

(a) Feedthrough Body



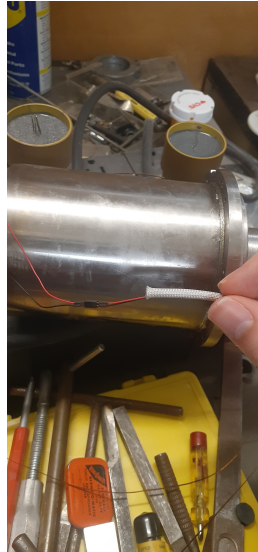
(b) Adding the epoxy



Once that was done, we could prepare for the other side. Given the permanent nature of the feedthrough, we approached this step with caution and were methodical in the setup. To prevent any mishaps, we fed the wires that would be attached through

the heat shield we got from the welders at Jefferson Lab. We could then get the wires through without the chance of it catching on something inside the still. Once all of the wires were in place, the unit was then held vertically and the epoxy was added to the feedthrough. It was then slowly guided onto its flange and held in place using zip ties. Once it was secure, it was then left overnight to harden.

(a) Wires with Heat Shield



(b) Attaching the feedthrough to the unit



With the feedthrough in place, the next thing to address was the wires from the back of the vacuum layer. Since the feedthrough is located close to where the beam would be, we had to secure the wires out of the way. This was done by wrapping the wires around the bellows and holding them in place with duct tape. Then, pin receptacles were soldered onto the wires to connect to the feedthrough welded onto the end of the bellows. Heat shrink was then cut and added to each receptacle and guided to the appropriate pin on the feedthrough. The idea was to keep bundles of four wires together across both feedthroughs to make it easier to keep track of each wire's path. Once the paths were constructed, we were then able to place the unit into the refrigerator for the test cooldown. However, once that test had finished, we were alarmed to see that some of the wires had snapped in the process. The working theory is that the flat plate used to seal the bellows at the point where the wires come out bend and frayed the wires enough for them to snap.

Figure 55: A hand with the broken wires for scale



Given the inconvenient proximity to the bellows and the permanence of the feedthrough the wires were attached to, our next moves were to find a way to repair them as well as make guidelines to prevent this from happening again. Despite the difficulty of the situation, we were able to reconnect the broken wires. Due to this, we decided to use 80-grit sandpaper to remove the insulation on the part of the wires inside the bellows and soldered on the pin terminals/receptacles to each half. They were plugged together, and heat shrink was added to prevent touches on the metal walls and other pin pairs. The guidelines added to protect these wires are as follows:

- Never use the flat plate to seal the bellows port on the refrigerator when the dilution unit is inside
- Only insert/remove the unit from the refrigerator when it is absolutely necessary.

The second point was added when more broken wires were discovered after a period when we were moving the unit in and out of the refrigerator multiple times in a short time frame.

The Electronics

Two necessary things needed on the inside of the dilution unit are the target chamber sensors and the still heater. The target chamber sensors are used to monitor the temperature of the Helium mixture, which we can adjust based on the reading, or verify that a specific mixture gives us the desired results. The target chamber sensors are Ultra-Low Temperature Ruthenium-Oxide (ROx) sensors from Lakeshore Cryotronics, designed to read down to about 10 mK. The still heater, on the other hand, which sounds counter-intuitive, plays an important role. The circulation of ^3He in the system is supplied by the vapor pumped out of the still after returning from the target chamber. If the liquid in the still is too cold and not enough helium is being boiled off, the still heater is turned on to help do so. The still heater is made with resistive wire secured to an aluminum chassis. Due to space constraints, we had to use wire with higher resistivity. We settled on 30 AWG wire made from Nichrome 60 alloy from Pelican Wire, which had a resistance of about 6.75Ω per foot. The still heater in the old system had a resistance of about 90Ω , so to match its impedance and fit it inside the still, the wire was wrapped around teflon rods and threaded through holes in the aluminum chassis. The wire was also cut in half and set up onto the two halves of the chassis. The wires were then secured in place by tying some small plastic tubing where the wire was threading the holes in the chassis. The wires extend past the chassis, which are also placed inside the plastic tubing as an extra layer of insulation. Some contact pins were soldered onto the ends of the wires to reconnect the two halves and eventually connect them to the wires that will supply the power to it.

Figure 56: Still Heater



When we were getting ready to connect it inside the refrigerator, we added some heat shrink to the pins connecting the two halves, to prevent metal-on-metal contact with the heater and the stainless steel body of the dilution unit. Once the two halves were on the central tube, more of the small plastic tubing was used to tie it in place. Small holes were drilled onto the ends of the teflon rods, so the tubing was threaded through those all along the circumference of the chassis, and tied together to hold it

Table 2: Still Sensor Logic Table

Low Sensor	High Sensor	Meaning	Action
High Temp (4K)	High Temp (4K)	Liquid level low	Add more liquid
Low Temp (1K)	4K	Liquid level good	No action needed
1K	1K	Liquid level high	Boil off excess liquid

in place. This was done twice, one for each end of the still heater. The heater was then pushed into place inside the still. In addition to these necessary systems, we added sensors inside the still. These two sensors were epoxied onto the inside walls of the still and will be used to monitor the liquid level of the still. Since we know that the liquid will be colder than the vapor, we can use this simple logic to interpret the data:

Once everything was connected and set up, we documented every wire path, organizing it based on wire color, the bundle number, and the system it was connected to. The bundle number was determined arbitrarily and is labeled with a piece of tape located on the wires coming out of the bellows. The resistance values were recorded for each wire or resistor in the case of the still sensors. When this list was first compiled, it was discovered that there was a touch between two wires. There were a few attempts to fix it, but it soon became apparent that the touch was most likely located on the torlon feedthrough on the side inside of the still. Luckily, the touch was between two wires on the bundle supplying power to the still sensors, the one non-essential bundle in the setup. Given this discovery, we determined that it would not be worth it to remove the feedthrough to fix this touch. Instead, we recorded the resistance values for every possible wire combination in that bundle for reference.

Figure 57: Tabulated Resistance Values

	Bundle 1				Bundle 2				Bundle 3				Bundle 4			
	Red	Green	Black	Gold	Red	Green	Black	Gold	Red	Green	Black	Gold	Red	Green	B	A
SH Red	5.6	∅	∅	∅	∅	∅	∅	∅	∅	∅	∅	∅	∅	∅	∅	∅
Green	∅	6.0	∅	∅	∅	∅	∅	∅	∅	∅	∅	∅	∅	∅	∅	∅
Black	∅	∅	6.1	∅	∅	∅	∅	∅	∅	∅	∅	∅	∅	∅	∅	∅
White	∅	∅	∅	5.7	∅	∅	∅	∅	∅	∅	∅	∅	∅	∅	∅	∅
R Sensor 1					N/A	5.1	48.2	55.7	∅	∅	∅?	∅	∅	∅	∅	∅
G Sensor 2					5.1	N/A	47.7	55.4	∅	∅	∅?	∅	∅	∅	∅	∅
B Sensor 1					48.2	47.7	N/A	98.1	∅	∅	∅?	∅	∅	∅	∅	∅
A Sensor 2					55.7	55.4	98.1	N/A	∅	∅	∅?	∅	∅	∅	∅	∅
Rox 1 Gray									12	∅	∅?	∅	∅	∅	∅	∅
Rox 1 Red										12.3	∅	∅	∅	∅	∅	∅
Rox 1 Black											12.3	∅	∅	∅	∅	∅
Rox 1 Orange												11.3	∅	∅	∅	∅
Rox 2 Red													11	∅	∅	∅
Rox 2 Gray														12.6	∅	∅
Rox 2 Orange															12.3	∅
Rox 2 Black																11.8

* without Still Heater or Rox sensors attached

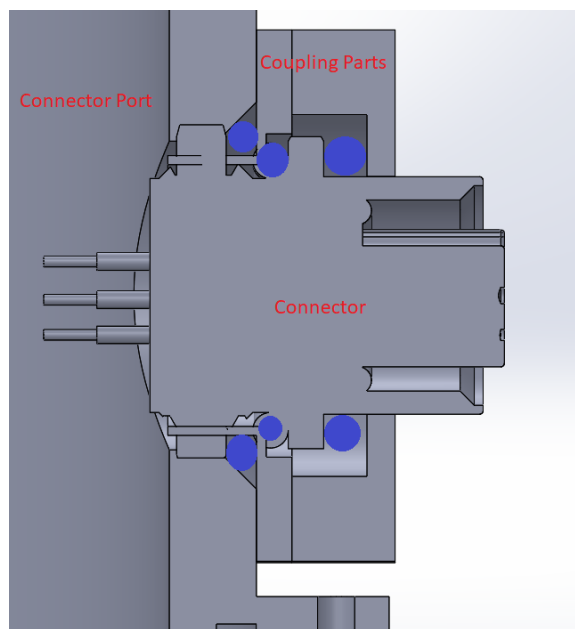
The process used to record these values was a simple one, needing only a multi-meter, one electrode on the exposed wire coming out of the bellows, and the other

in the appropriate port. But we added the necessary additional step of checking the adjacent ports to look for touches. For the still sensors, since they were attached to the inside walls before we recorded these values, we just used the bellows-end wires since the other ends were inaccessible. After adding the still heater, the resistance across the red and green wires in bundle number one should read between $100 - 110\Omega$. With the wiring on the inside of the dilution unit complete, it was time to shift focus to getting them connected to our equipment on the outside.

External Connections

On the old refrigerator, there were two 12-pin connectors with vacuum seals that fed power to the sensors inside. When we took the refrigerator apart for the first time, we discovered that one of the connectors was now unable to form a vacuum seal, and while the other could, it would be inadvisable to connect our new wires to it. This is due to the previous setup's wires and insulation still being present, and not having an easy way to remove them and install the new wires. With these two hurdles, we decided to purchase new connectors for our set-up. After some research, we settled on the pair of connectors (Digi-Key part numbers A142125-ND and A133900-ND) and began planning how to adapt them to our system. These connectors have 8 pins, giving us the exact number needed. Stainless steel coupling parts were designed in SolidWorks and manufactured by our machine shop. The coupling parts came in two pieces, one for adapting the connector port for the connector, and the other to hold it in place and make a leak-tight seal. To make that seal, three different O-rings were used.

Figure 58: Cross-sectional Shot of Connector Port assembly;
O-ring locations indicated by blue circles



We initially struggled to get the assembly to seal properly, but we soon discovered

that the connector pair is only sealed when they are connected. When we realized this, the leak rate dropped but did not completely disappear. Although this was not ideal, we accepted it due to a few factors. First, the leak was incredibly small, since the leak checker was able to make it down to the low 10^{-8} /high 10^{-9} range. Second, it was located in the ^4He vacuum space, meaning that it would be pumped out and not interfere with any ^3He , and finally, it was located right next to the port reserved for a turbopump, meaning it would be pumped out as soon as it leaked in. With that done, we could now focus on the other connector and get that attached to a cable. Since the mating connector was just an end, we had to splice it onto a cable. Since we got rid of the previous connector, its corresponding cables were the perfect candidates. We started by removing the old connector heads with an Exacto knife and a pair of wire cutters. Then, the connections were mapped, and old documentation on the wiring was consulted to determine which wires would be plugged into the connector. The cables contained 12 wires wrapped together in pairs with some shielding. The foils were unwrapped, and the insulation on each wire was trimmed. The wires we planned to use had their conducting cores twisted with pliers and placed inside a terminal corresponding to a pin. Then, the screw that held them in place was tightened. Heat shrink was added as an extra measure to prevent touches. Once they were in place, the connector was assembled and the process was repeated for the other cable.

Figure 59: Pin Labels with cable ends facing user

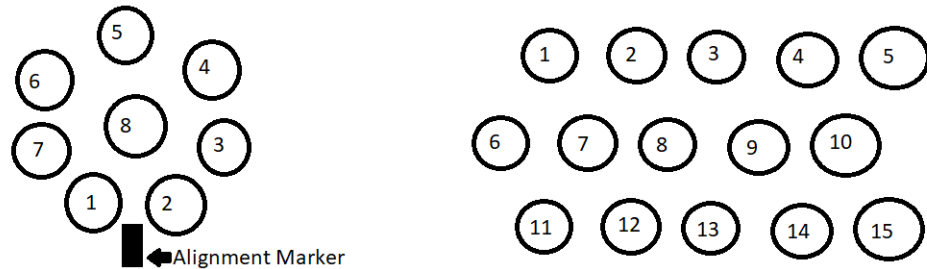


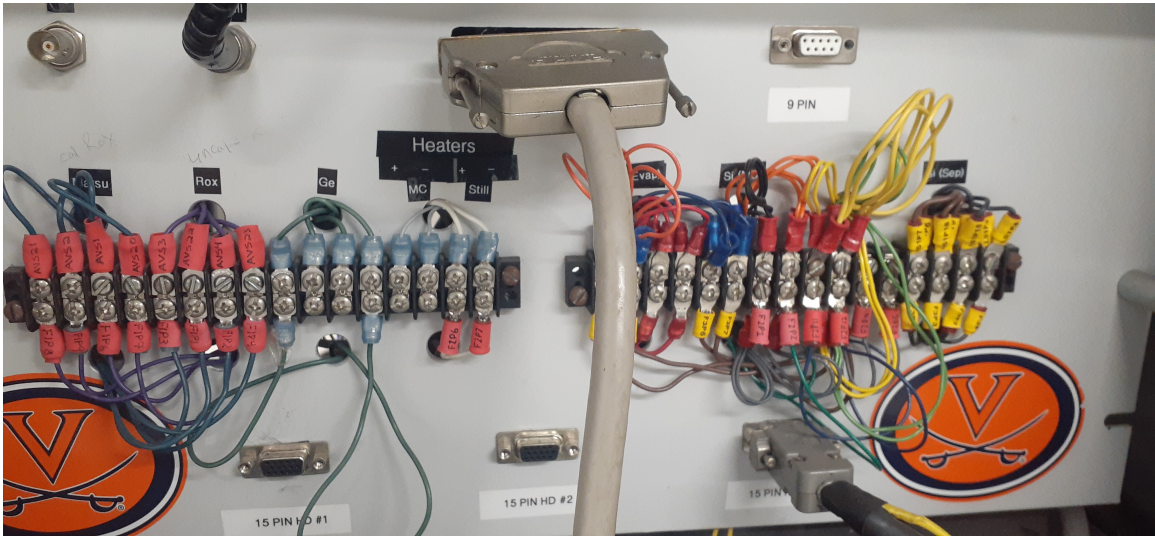
Table 3: Cable Pinouts

Connector 1(No Heat Shrink)			Connector 2(Heat Shrink)		
Pin on 8-pin	Pin on 15-pin	Sensor	Pin on 8-pin	Pin on 15-pin	Sensor
1	4	I- Uncal. ROx	1	4	Still Low
2	9	V- Cal. ROx	2	15	Spare
3	7	V+ Cal. ROx	3	14	Spare
4	6	I+ Cal. ROx	4	1	Still High
5	8	I- Cal. ROx	5	7	Still Heater-
6	1	V+ Uncal. ROx	6	5	Still Low
7	2	V- Uncal. ROx	7	2	Still High
8	3	I+ Uncal. ROx	8	6	Still Heater +

Table 4: Wiring Map on Bridge

HD 1		HD 2	
Label	Sensor	Label	Sensor
AVS 3	I+ Uncal. ROx	F2P1	Still High
AVS 4	V- Uncal. ROx	F2P2	Still High
AVS 23	I- Uncal. ROx	F2P4	Still Low
AVS 22	V+ Uncal. ROx	F2P5	Still Low
AVS 21	I- Cal. ROx	F2P6	Still Heater +
AVS 1	I+ Cal. ROx	F2P7	Still Heater -
AVS 20	V+ Cal. ROx	F2P14	Spare
AVS 2	V- Cal. ROx	F2P15	Spare

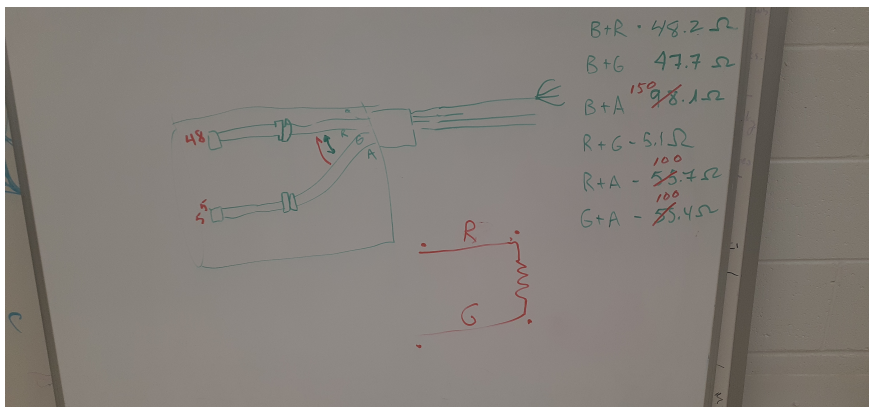
Figure 60: Wiring Bridge on Setup



One thing that we noticed with these cables is that we have to be careful when twisting them. The end with the 8-pin mating end has two separate rotation mecha-

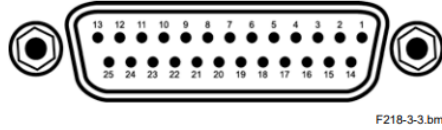
nisms. When screwing it on the corresponding port, it is important to make sure the cable is not rotating with it, since it will be very likely that the wires will either break free of the port on the inside of the cable or just break. When attaching it, only the part with the threads should rotate, with the cable itself staying relatively still. With the cables done, we could begin the process of setting up the readout for the newly made cables. After consulting our documentation on our connections, we rearranged the connections for the terminals that were formerly for the wires that were part of the 12-pin connectors on the upstream end of the refrigerator. The focus of the rearrangement was primarily on the still sensors. Our Lakeshore 218S readout was room for eight sensors, the wires for which are fed into two different 25-pin terminals on the back of the readout. Two of the channels were already occupied by the high and low separator sensors. Channels three and four will be dedicated to the still sensors, also designated as high and low. With the discovery of the touch between these sensors, channels 5-8 have been designated for the four remaining combinations of wire pairs for these sensors.

Figure 61: Diagram of the Still Sensors



The sensors occupy all four wires on a single wire bundle, with one taking the black and red wires, and the other taking the green and gold ones. The purpose of having the other four channels occupied will serve as a diagnostic tool to observe the sensors during a cooldown. Having these extra channels active may provide extra information in case of something goes wrong during a cooldown. With this goal in mind, we got some color-coded wire from the stockroom and began cutting lengths of wire. Using the diagram below, we used this as a guide to how we soldered the wires.

Figure 62: Infographic of Pins for Lakeshore Readout[21]



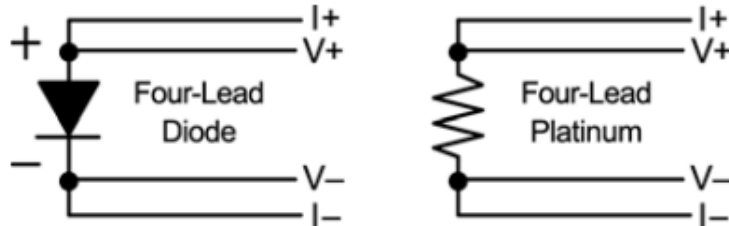
F218-3-3.bmp

Input Connector (Inputs 1-4)				Input Connector (Inputs 5-8)			
PIN	DESC.	PIN	DESC.	PIN	DESC.	PIN	DESC.
1	NC			1	NC		
2	S	14	S	2	S	14	S
3	1I+	15	1I-	3	5I+	15	5I-
4	1V+	16	1V-	4	5V+	16	5V-
5	S	17	S	5	S	17	S
6	2I+	18	2I-	6	6I+	18	6I-
7	2V+	19	2V-	7	6V+	19	6V-
8	S	20	S	8	S	20	S
9	3I+	21	3I-	9	7I+	21	7I-
10	3V+	22	3V-	10	7V+	22	7V-
11	S	23	S	11	S	23	S
12	4I+	24	4I-	12	8I+	24	8I-
13	4V+	25	4V-	13	8V+	25	8V-

Figure 3-3. Model 218 Input Connector Pinouts (S = Shield, NC = No Connect)

The cable from the 25-pin connector on the readout connects to another 25-pin connector that is attached to our electronics setup. In preparation for this, the connector on our setup was removed and held with alligator clips for the soldering. This connector has solder cup pins, making it simple to make a sturdy connection. Each wire had a length of heat shrink on it to ensure that there were no touches between pins. An important thing to note is that the pins for the readout are configured for 4-pin sensors, while the Cernox 1030s used in the still have only two. This can be fixed by having two inputs of the same sign (V+, I+ and V-, I-) go to the same pin, as shown in the diagram below.

Figure 63: How to adapt two-pin resistors to the readout



Given that two inputs must be paired, once one end of the wire was soldered into its corresponding terminal, the other end was twisted together with the other wire in the pair, placed into a spade terminal, and crimped. The spade terminals fit into the corresponding port on our front panel and are held in place with a screw. Once all of the wires for channels 5-8 were set up, the 25-pin connector was put back and the spade terminal ends were put in their corresponding spots on the front panel. To test the connections, we got a variable resistor that had a range of around 100 Ω . Two short segments of wires were stripped of their insulation and connected to the two ends of the resistor. The other ends of the wires would touch two different spade terminals on the same channel to see if there was a response. If it was working, the channel would either read resistance or some temperature value, depending on what the settings of the readout are. When we first set this up, we had issues with the readout. Even without any of the terminals connected to a resistor, we had display values for some of the channels read something other than “S.Over” which corresponds to an open circuit. When the resistor was connected to a pair of terminals, the corresponding channel would read out as expected, but we would notice adjacent channels change as well, as if the signal was being picked up by the other channels. We consulted a representative at Lakeshore, and we were told that the channels do not have a universal ground. With this information, we had our department electronics head try to connect it. While it was less reactive, there was still some cross-talk between the channels. Given that these channels are for diagnostics, not having these four channels connected during a cooldown will not be an issue, plus there may be different behavior once the system is cold.

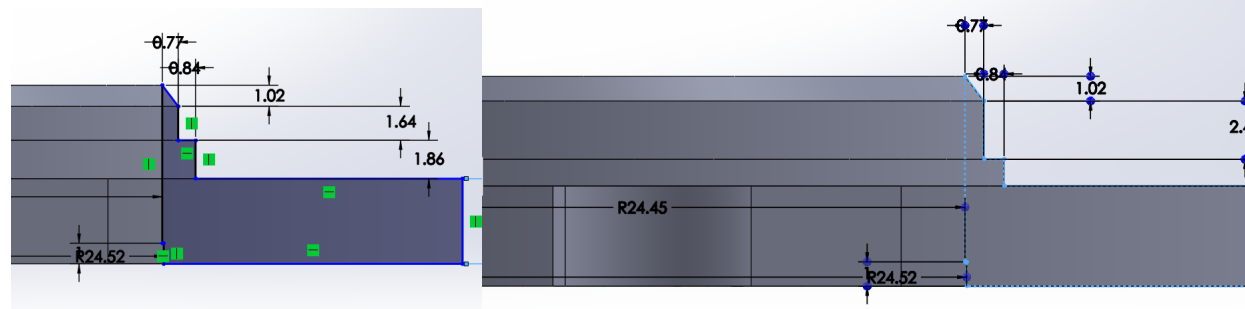
4.4 Sealing up the assembly

With the plumbing and electrical wiring on the dilution unit done, it was time to get the unit into place. To get the unit inside, two people are necessary. The first person stands at the downstream end and guides the unit inside. It is usually their job to prepare some indium on the back lip of the VLC to prepare it to seal with the refrigerator. There is some resistance between the unit and the rest of the refrigerator. To slide it inside, the person holding the unit up must grip the central tube and slowly rotate the unit around the axis. The unit’s motion should be similar to that of a top precessing about its axis. Once the unit is in far enough, the resistance should disappear and the unit should easily slide in. The second person should be at the upstream end of the refrigerator. Their job is to support the bellows as the unit is being put in, with extra attention paid to the wires leaving the bellows head. Since these wires have been broken in the past due to accidental crushing, the second person carefully feeds the wires through the port once the bellows get close enough. The O-ring that ensures the seal between the bellows and the connector port has the wires fed through it and is put into its groove. The bellows are then secured into place with 4 screws and then tightened. While this is happening the first person can begin adding the screws into the VLC attaching it to the corresponding holes on the Indium Adapter Ring. Once they are tightened, the sleeve can slide on the central tube. The indium seal between the sleeve and the still is unique within this system.

There was a mishap during the fabrication of the new seal on the sleeve with the indium shelf. The shelf was accidentally made too small, with no room for indium to sit on. The decision was made to machine a new shelf lower down on the piece to save time and resources since it would require making the piece again otherwise. Because of this, there is more space between the indium shelves on the sleeve and the still. This space is larger than the diameter of the indium used to make the seal, leading to a dilemma. After some discussion, this dilemma was solved by adding a second length of indium to the space. When one strip of indium is placed along the circumference of the metal surface, the second strip is placed on top.

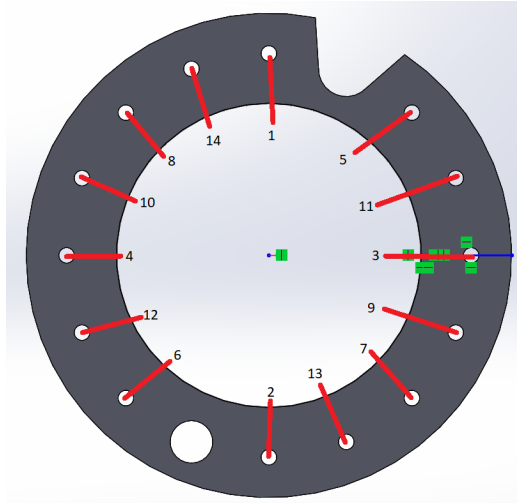
(a) Planned Dimensions of Sleeve to Still Seal

(b) Actual Dimensions



While this does consume more indium, it initially seemed to work. With the heat exchanger and the rope channel in place, there is resistance to putting it on. A simple method to get it in place is to hold the rope channel and rotate the sleeve counterclockwise as the sleeve is being pushed in. This method works until the mating end reaches the waveguide, then that method is adapted within the confines of the port for the waveguide in the sleeve. The sleeve is twisted counterclockwise when pushed in, and then “reset” by twisting clockwise until it hits the other end. This process is repeated until the sleeve reaches another bout of resistance a couple of millimeters from the face of the still. When it reaches this stage, it is not a good idea to force the sleeve into place, since there is a risk of breaking something delicate and/or on the inside of the still. Instead, four M2.5×10 mm screws are placed inside. The screws should be long enough to be able to reach the threads on the inside of the still. These screws should be placed in a square pattern, with opposite corners being directly across from each other on the sleeve. In addition to bringing the sleeve closer, these screws also help align the sleeve for the final approach on the still. Once close enough, the rest of the screws are added, using a modified version of the star pattern. To understand how it works, view the figure below:

Figure 65: Screw tightening sequence for the sleeve



The sequence is a modified version of the star pattern for 16-hole bolt flanges, but since we have the gaps for the ^3He line and the waveguide, those spaces are skipped over when doing the tightening. The starting point was picked due to a suggestion from our machinists when we consulted them after discovering we had difficulty getting some of the screws in all the way. They suggested that we cut some screws down by a millimeter and that the holes marked numbers 8 and 14 in Figure 65 were some of the last holes tightened in the sequence. Due to this, it is suggested that when the alignment screws are used, the four holes they should be placed in are the ones marked 11-14 in Figure 65. As for the actual screws used in forming this indium seal, they are a mixture of $\text{M}2.5 \times 8\text{mm}$ and $\text{M}2.5 \times 7\text{mm}$ screws. The 7mm screws are not commercially available and were cut from the 8mm ones. The 7mm screws are placed in screw holes 3, 8, 11, and 14. Once there is significant resistance in tightening all of the screws, it is suggested to wait about an hour to let the indium “settle” before going around the sequence once again to ensure that the screws are as tight as possible. Once that is done, a leak check flange is added to the other end of the sleeve. This flange forms an indium seal with the sleeve, while the other end is a KF-40 flange. This allows the system to be either blanked off or attached to a leak checker/turbopump. The back flange on the upstream end of the refrigerator is secured, and that end can also be blanked off or attached to a pump. For this leak-checking step, it is suggested to have a turbopump on one end, and the leak checker on the other. This is because the volume is slightly too big for the leak checker to pump it down alone, making it work harder than usual. Once the pressure is low enough, the leak checking can begin.

The Problem

With the volume pumped down, helium was waved in front of every flange to find evidence of a leak. Unfortunately, we found evidence of leaks every time we attached the leak checker, no matter how many times we remade the indium seal. The leak

rate seemed to have a minimum in the high 10^{-8} mbar/s range, with spikes always seeming to appear when waving the helium around the indium seal between the still and the sleeve. At first, we believed that it was due to the indium and began to wonder if we needed the indium shelf on the sleeve to be like our initial drawings (see Figure 64a). We attempted multiple methods of changing this result, the first of which involved the application of the indium. Initially, we applied the two strips of indium on different flanges, with one going on the still and the other going onto the sleeve. We noticed that after we undid the seal after an unsuccessful leak test that the indium seemed to “spill” over on the sleeve in the same location over different tests.

Figure 66: Indium on Sleeve after Leak Check



In the figure above, we have a picture of the sleeve with the indium spillover. While difficult to see, the indium seems to have stuck on the flange for about half a circumference. If we were to use the labels from Figure 65, this indium was stuck by hole number six, then goes past the hole for the waveguide, all the way to the slot for the ^3He line. While there is some variation, the worst of the spillover always seems to be by the waveguide port, holes six, two, thirteen, seven, and nine. We started by varying how we applied the indium, starting with having both strips of indium on the sleeve, and then both on the still. We observed that when both strips were applied to the still, there was no spillover of the indium. We had hoped that the leak was due to the indium spilling over and preventing the sleeve and still from touching, therefore making the indium unable to seal, but that was not the case. We even tried making the seal without using vacuum grease on the indium, but that also did nothing. In response, we tried using some plumber’s putty on the crease of that seal, but that also did nothing. We used more putty to block the gap between the VLC and the still. It was not until we blocked the port for the waveguide that we got a change in the leak rate. However, it did not drop as we expected but instead rose from the 10^{-8} - 10^{-7} range to 10^{-5} mbar/s. This was concerning, not just because of the rise in the leak rate, but also because we had no idea what would cause such a change in the leak rate. We even tried plugging the waveguide itself with a rubber stopper and sealing the crack with the putty, but that did not improve the leak rate. Our first reaction was to test the putty since we thought that the only way the leak rate would respond the way it did is if the putty was somehow outgassing. We tested this with a simple setup: We attached a flange to the leak checker and plugged the other end with a rubber stopper. The leak checker was turned on and pumped down the space. The leak rate was able to reach the 10^{-7} mbar/s range, with leak spikes happening whenever

helium was sprayed at the space between the stopper and the metal flange. With the leak checker running, the putty was applied to the space between the stopper and the metal flange. As soon as the putty was completely covering that space, the leak rate plummeted to the 10^{-10} mbar/s range. A quick spray of helium confirmed that the putty was leak-tight, and confirmed our initial thoughts on the putty’s performance. This putty was first given to us by the machinists at Jefferson Lab and was used in the initial leak check on the welds performed in Step 3 (see Section 4.1). With any doubts about the putty’s performance erased, we were once again unsure about the origins. We decided to build a leak check flange that perfectly imitated the still to check if it was the indium seal, but due to circumstances beyond our control, there was a delay. During that time, we made an interesting observation. We saw that there was a change in the leak rate depending on what end the leak checker was pumping on. Given this observation, we also made observations with the presence and absence of the rope channel on the final heat exchanger. The results are tabulated below: This

Table 5: Note the 2 orders of magnitude difference in the leak rate in red

		Leak Checker Position	
		Upstream	Downstream
Rope Channel	Present	$1.0 \times 10^{-5} \text{mbar/s}$	$1.0 \times 10^{-7} \text{mbar/s}$
	Absent	$2.4 \times 10^{-7} \text{mbar/s}$	$1.0 \times 10^{-7} \text{mbar/s}$

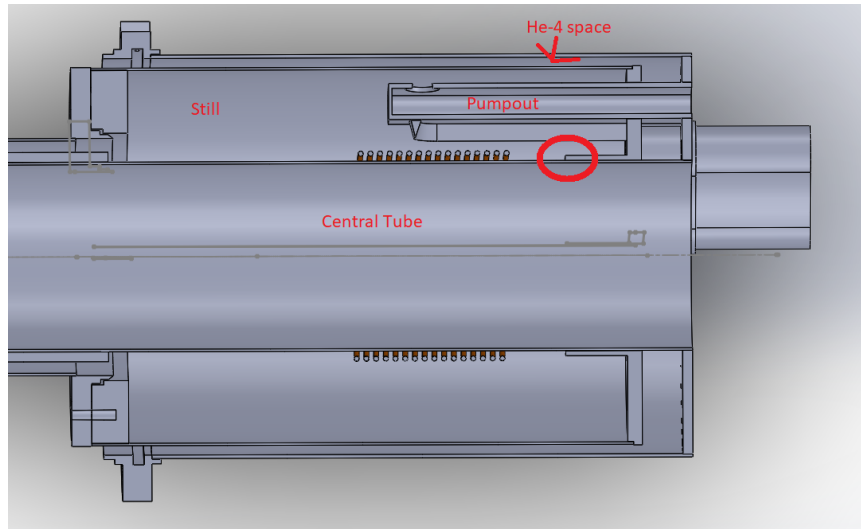
difference led to two different theories: The first is that the rope channel creates such an impedance for the air in the vacuum space that it becomes a sort of “pseudo-leak” and air molecules from the other side are consistently trickling through. The second theory stems from an observation of the central tube. It was noted that the distance from the central tube to the indium shelf on the still was inconsistent. Looking toward the still from the downstream end, the distance between those two points was about 2 mm smaller on the bottom right quadrant than on the opposite end. Due to this difference, it is theorized that due to a small error in the machining, the central tube was not perfectly perpendicular to the still. Because of this, when the central tube is put on, it forces the central tube into a more perpendicular position. When the rope channel is in place, this push is more forceful, and after a few leak tests, a crack in the weld between the central tube and the still has formed. This theory would support the observations with the leak rate since the rope channel would force the central tube to move more than with just the sleeve alone, and in doing so, forces the crack to open more, and by extension, let more air in. Two welds that could give us this result are:

- The weld between the central tube and the VLC
- The weld between the central tube and the still

Starting with the first point, if the leak was located here, it would be a relatively simple fix, requiring us to simply pinpoint the location of the crack and have a machinist touch it up with the welding torch. This weld joint is out in the open, so we tested

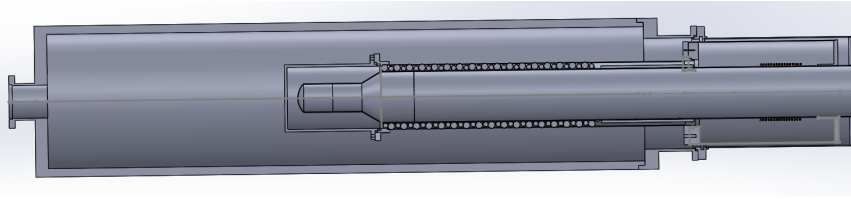
it by applying epoxy to the weld. As an added measure, we also applied the putty onto the inside of the central tube, specifically where the other weld was made. We did not know the crack connected the two vacuum spaces, but if the crack exited into the inside of the central tube, the putty would cover it and we would be able to see it. However, when we tested it, there was no change in the leak rate, meaning that the most probable location where it could be is at the second point, which is circled in the figure below:

Figure 67: Visual Aid for the Possible Leak Location



While we were confident about its location, we had trouble coming up with a method to verify it. The only ways into the still are through the downstream face, which is closed when the sleeve is on, and through the pumpout, which is inaccessible when the unit is in the refrigerator. After discussing this, we realized that we could run the leak check without having a vacuum on both sides of the window on the end of the central tube. We initially performed leak checks in the refrigerator to minimize the risk of the window being destroyed by a pressure differential. While this does allow us to leak check the unit without being inside the refrigerator, it still does not allow us to probe the inside of the still, since we are pumping on the ^3He space. To get around this, we designed and constructed a leak check flange that allowed us to pump on the ^4He space instead. If this crack in the weld does exist, we would be able to detect it, while having the advantage of being able to send a probe inside of the still. This flange covers the downstream half of the dilution unit, attaching to the lip of the VLC on the downstream side. It leaves the pumpout, still feedthrough, and the upstream entrance of the central tube exposed. There is also a companion piece that seals the head of the bellows since that is part of the ^4He space. As for probing the inside of the still, the needle on the end of the helium bottle is too big to fit inside, so instead a length of small plastic tubing would be attached to the needle and fed through. When the flange is attached and the leak checker is pumping, helium will be sprayed at various joints and the spikes and delays will be noted.

Figure 68: SolidWorks model of He-4 space leak check assembly



In addition to the large cylinder and the cap on the bellows, we also had a cap made as a substitute for the target chamber (located around the center of Figure 68), since the chamber itself is fragile and extremely valuable to us, and a blank off for the large cylinder to test it before we used it on the dilution unit. Once we verified that the cylinder was leak-tight, we attached both caps to their respective areas on the dilution unit and sealed it with the large cylinder. However, when we attached the assembly to the leak checker, we were unable to get the pressure low enough for the leak checking to begin. It was only when we plugged the pumpout with a rubber plug and some putty that were we able to get the pressure low enough. This was extremely troubling since was definitive proof that there was a large leak between the ^3He and ^4He sections of the dilution unit. We eliminated the possibility of the indium seal between the target chamber cap and the sleeve being responsible for what we were seeing for two reasons:

- A faulty indium seal would not be enough to explain the magnitude of the leak
- We remembered that the tests on the ^3He section required two different turbopumps to pump on the assembly

With this unfortunate development, we concluded that this leak made the unit irredeemably broken, and decided to take it apart to see inside and perform a sort of “autopsy” on it.

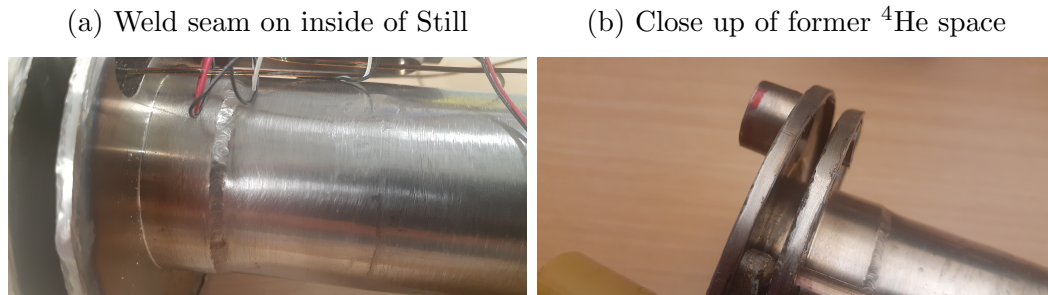
4.5 Diagnosing the Problem

We gave the unit to the shop for disassembly and got the unit back in four different pieces; the bellows, the still, the vacuum layer can, and the central tube. We searched around the area of what used to be the inside of the still, but we could not see any evidence of a large crack in the assembly. While this was incredibly frustrating, we organized the evidence that we compiled over the last few months to find the aspect of the design that we need to address:

- The leak rate is spiking around the indium seal between the still and the sleeve
- The leak rate is spiking dramatically after blocking off the port for the waveguide
- The presence of the rope channel and the location of the leak checker affecting the leak rate

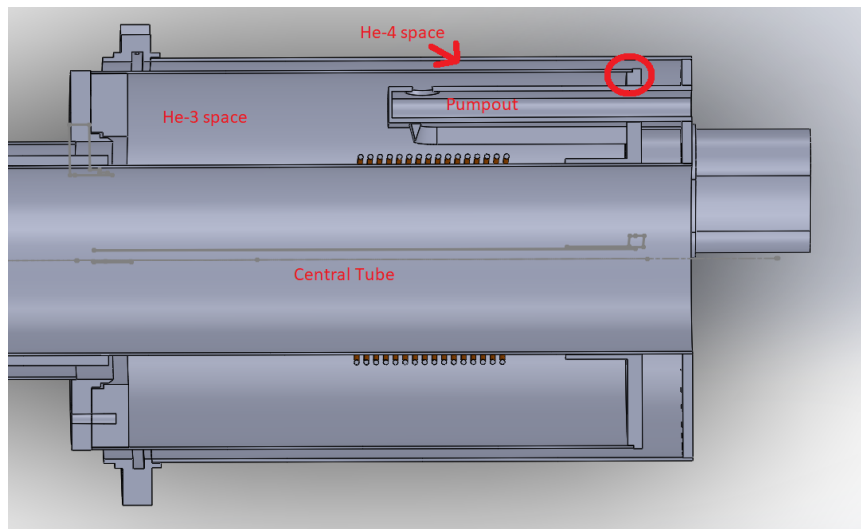
- The noticeable asymmetry in the spacing between the central tube and the opening of the still
- We were able to successfully make the indium seal between the still and the sleeve on at least two separate occasions in the past.
- Using more than one turbopump to pump it down is necessary

This information seems to suggest that the asymmetry first mentioned in section 4.4 is most likely the root cause for how the leak formed, even if we could not find the exact location. This leak most likely formed over time, and would not have been noticed during the leak checks performed during the assembly.



Sometime after the unit was disassembled, we realized where the leak most likely was. While we were focused on the central tube, we failed to consider a third location for our leak, shown in the figure below.

Figure 70: Likely location of the leak circled in red



When the indium seal between the sleeve is made, it would not only add a torque on the central tube but also on the still. The weld between the upstream face of the still and the still body fuses a lot less material than either of the welds on the central tube, making it the most likely candidate. But we cannot verify this hypothesis since

this realization came after the disassembly of the unit. Given the likely location of the leak, we had to be careful in our efforts of redesigning and rebuilding it.

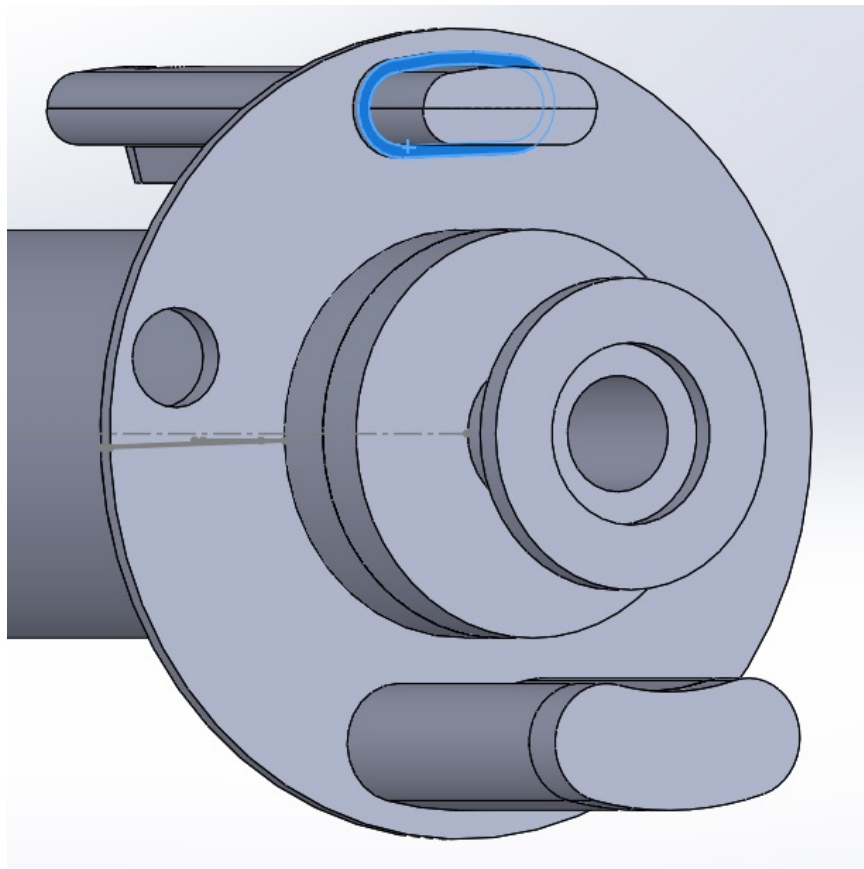
4.6 Third Version

The main focus of this third design was to make it easier for parts to be as perpendicular or parallel as possible. Most deviations from these conditions are either due to human error or manifest during welding. While this was the main focus, the design was not changed too much from the previous iteration. These changes can be summarized in the following points:

- Extending certain parts and closing them off with blank-offs

This idea was brought up by one of the machinists at Jefferson Lab as a way to make the leak checking a bit more simple. We would weld the part into place, leak check it, and when we were done, we would simply remove the blank off by cutting it. This will be primarily done with the parts with irregular cross-sections like the pumpout and the feedthrough flange.

Figure 71: Weld Step 2 with blanked off parts



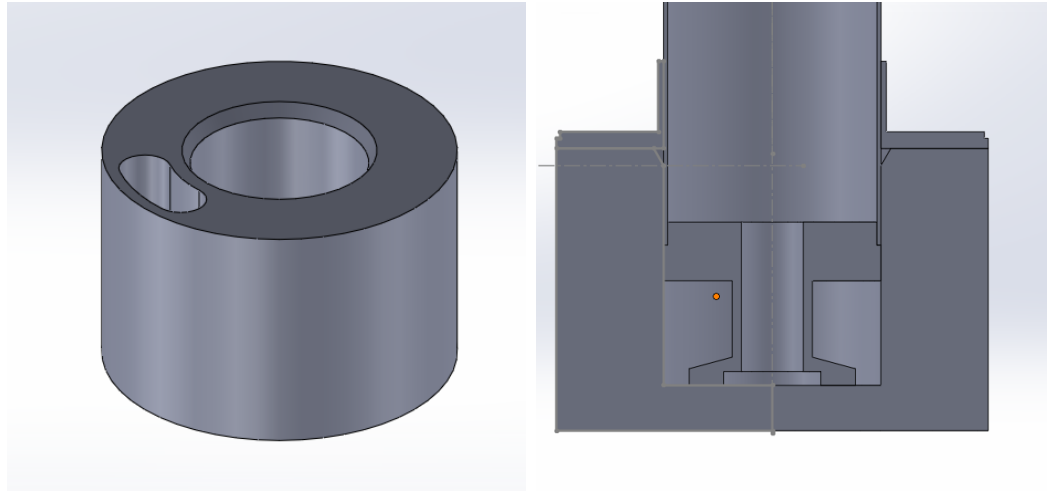
As seen in Figure 71, the central tube also has a KF flange on it. This flange would indirectly leak check the weld between the central tube and the upstream face

of the still. This flange would also be cut off once the preliminary leak checks were finished.

- Designing pieces in SolidWorks that will help maintain alignment during welding

Given that the alignment is our main focus for the next iteration, we are in the process of making a procedure that will ensure that everything is as aligned as possible, while still making it relatively simple to weld.

(a) Proposed piece to help alignment (b) Cross-section of alignment assembly



During the second step of the welding, the upstream face of the still would be placed on top of the piece shown in Figure 72a, and the central tube would be slid into the hole at the center of the piece. The depth is picked so that it is deep enough for the central tube to stick out at the exact length that it needs to for the future weld between it and the Vacuum Layer Can. Clamps are added to hold the assembly together and prevent it from moving during the weld. It is important to note that this is a rough draft, and we are discussing the possibility of adding something to hold the central tube steady at a higher point along the shaft. We are also working on something that will help maintain the alignment for the welding of the still together during Step 3 (see section 4.1). Since the walls of the still are relatively thin, it is likely that different ends of the still have different degrees of melting and shift the alignment slightly. The piece that we design will address this and will minimize if not eliminate any misalignment that results from the welding.

- Make the upstream face of the still a little bigger and thicker

Even the greatest welder cannot avoid any mismatches due to differential heating. As a way to correct this, one of our machinists suggested milling the upstream face of the still as a way to correct for any microscopic shifts in the alignment. We would make the upstream face a little bigger, and after it is welded to the central tube, we would measure the angle between the two parts and shave off parts of the still face to make the angle closer to 90° . The extra material would allow us to make this correction

without sacrificing the structural integrity of the still. As of writing this, (June 2023) we currently do not have a model with exact dimensions on this, because we are also considering how this piece will fit with the body of the still. Since the body of the still is just as relevant to the alignment as the central tube and is also made with a relatively thin wall of stainless steel, it is just as vulnerable to getting misaligned. Thankfully, once we can work out the details of how we can ensure its alignment, it should be a simple task to make a model in SolidWorks.

- Move the feedthrough flange

As seen in Figure 71, the current model of the upstream face of the still has the feedthrough flange moved to the bottom, opposite the pumpout. There is no operational advantage to moving it there but instead allows machinists to have more room to cut off the ends of the pumpout and the central tube and reduce the risk of accidentally cutting the feedthrough flange too short.

5 Other Systems

5.1 The Residual Gas Analyzer

After a cooldown is finished, some important processes must take place, one of those being gas recovery. If ^3He was used, we do our best to preserve as much of the gas as we can. The gas is directed from the ^3He section of the refrigerator to an outside tank using the pump in that section. Once that is done, the tank is sealed off, and the pressure on the tank is recorded. Once the cooldown is over, we can check the composition of the gas using a Residual Gas Analyzer, or RGA. We originally had a Halo 201 model from Hiden Analytical, but we found that it was not working. We were in contact with specialists from Hiden to fix it and spent a lot of time troubleshooting it. We tried both software and hardware fixes to solve this problem, but it was challenging. It was difficult to find someone well-versed in this particular model due to its age. Because of this, a lot of the fixes, especially the hardware fixes, were mostly improvisations. This was due to a lot of the components being replaced now obsolete. Modern equivalents were found in a lot of cases, but eventually concluded that this RGA was not going to work and we had to find a replacement. However, our time with the Halo 201 was still helpful in our understanding of the workings of RGAs and was the foundation of developing a system used for feeding gas to the RGA and helped inform us on what to look for in our new RGA. RGAs have a maximum pressure that they can handle, so we had to provide some way to keep that pressure well below the maximum. Our initial plan was to use a circulating pump, that way we could pump down the line as well as pump the gas back into its tank, but there was no feasible method to do that, as well as our own circulating pump having a minimum pressure above the maximum pressure of even the most robust RGAs available. Eventually, we settled on using our turbopumps to pump on the line. We would lose whatever ^3He gas used in the test, but if done right, we could minimize those losses. The way we did that was to make the system as compact as

possible, and have several valves to bleed the gas in. With this in mind, we started researching different RGAs to use and had to decide between two models. The first was the HPQ2 model from MKS. The HPQ series boasted a higher pressure threshold than most RGAs available (maximum pressure around 10^{-3} mbar), but because it was an obsolete model, we would have to get one used, and the current model at the time was extremely expensive. The second was the e-Vision 2, a readily available model with a lower (10^{-4} mbar) maximum pressure. We picked the HPQ2 model due to the lower cost and higher pressure ceiling, but there was a lot of work to do to get it working. When we initially bought it, it only came with the RGA unit, and none of the software, cables, or other parts needed to run it. We almost immediately bought the power cable and RGA software needed to run it. However, when we plugged it in for the first time, we did not realize it would automatically turn on, and accidentally burned a circuit board on the inside of the unit. Once we had that repaired, we learned how the unit worked and made some creative improvisations to replace the auxiliary systems we did not get from the people we bought the unit from. The head of the unit uses a pneumatic valve to expose the filaments of the RGA to the sample gas being tested. We were able to get that working with the addition of two things; a tank of nitrogen gas and a simple switch to open and close the valve. To protect the delicate filaments used to identify the gas, the valve stays closed by default. To work the valve, the head is filled with around 70 PSI of pure nitrogen gas, which gives the valve the ability to open once the button on the switch is pressed. With that done, we began to plan out the plumbing of the RGA system. We had two key desires for the plumbing; minimize the amount of tubing used to make it easier to pump down, and have some sort of valve to bleed gas into the chamber with. For the tubing, we used a cross to directly connect three ends of the setup, the RGA, the turbopump, and the pressure gauge. The pressure gauge used was a Balzers PKR 250 gauge with a TPG 252 readout. The last end of the cross piping went to the inlet of the gas tank being tested. A needle valve was attached right next to the inlet valve of that gas tank. Between the needle valve and the cross was a long, thin KF tube.

Figure 73: RGA Setup in our lab



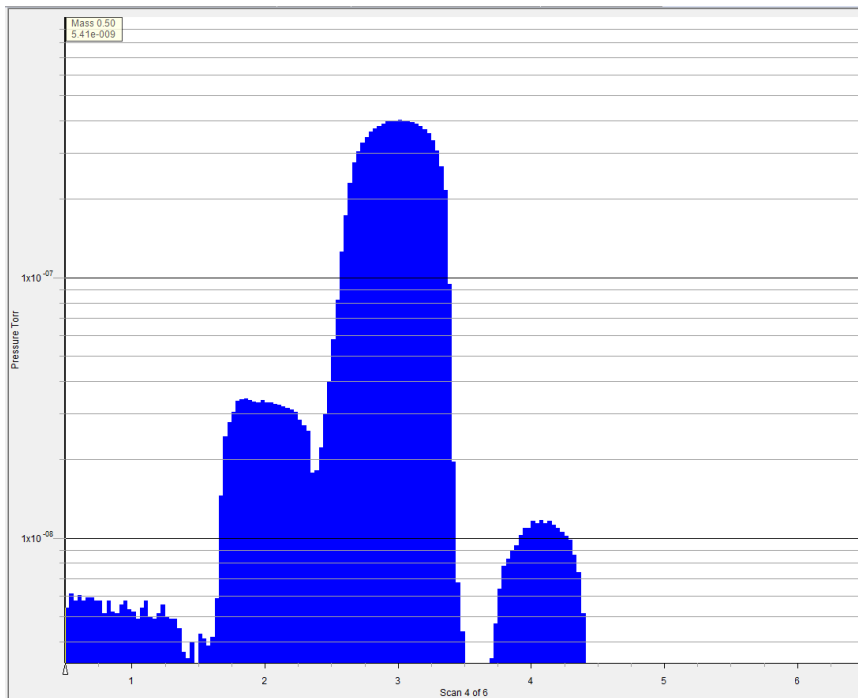
To keep all of these pieces close together, a stool and some styrofoam padding were used to hold up the RGA unit and the turbopump in a way that minimized the strain on the plumbing setup (see the figure above). Once that was done, we began to test our RGA and calibrate it. After a few weeks of attempting to understand it, we were unable to get rid of some background noise on the scans. The noise took the form of peaks at amu values of 18(water vapor), 28(nitrogen gas), 32 (oxygen), and 44 (carbon dioxide). We were well aware that this was the normal composition of air, but what made us believe it was noise was because in scans the partial pressures of some of the peaks were registering higher than the measured pressure on the readout for the pressure gauge. After some discussion, we decided to not try too hard to get rid of it since the main purpose of the RGA was to measure the ratios of ^3He and ^4He in a tank. Any of the gases mentioned before are unimportant and can easily be filtered out through the use of a nitrogen trap. Due to that fact, we usually display only masses 1-6 on our scans not only to get rid of the distracting background peaks but also to speed up the scan. We normally use the analog scan since it gives the full profile of the calculated masses instead of automatically binning them in assigned values. It can sometimes skew the results, and since the accuracy of the ratio is paramount, the analog scan is our go-to setting. Once our setup was up and running, we took the time to create a write-up to detail how to operate the RGA to prevent any future mishaps. The setup must have the RGA unit, the turbopump, the pressure gauge, and the tank being tested attached. The needle valve between the tank and the unit should be open all the way to pump out the entire line. On the RGA unit, a tube supplying nitrogen to the valve should be securely attached to the small elbow with the red end near the head of the unit. The wires on the switch should be connected to the plug on the cylinder attached to the head of the unit. The process to turn on the RGA is as follows:

- Open up the nitrogen and set it to 70 PSI
- Press the button on the switch to open the valves it should make a low plop or a thud
- Start up the turbo pump
- Once the turbopump is at full rotation and the pressure gauge reads below 10^{-3} mbar, plug in the RGA unit
- Plug the other cable on the unit into the computer

Once all of these steps are done, we can start up the software that plots the data, Process Eye Professional. The software has a bunch of features, but for our purposes, we only need the bare minimum. Once the RGA is connected to the software, we can turn on the filaments by clicking the blue zigzag line on the interface. While the filaments are warming up, we usually take the time to close the needle valve. Once that is done, we open the tank and let the gas fill the space between there and the needle valve. The tank is then promptly closed to minimize the amount of gas lost. Once the gas is inside, we start an analog scan by clicking the button with the blue

hill on it. With the scan started and recording data, we very slowly open the needle valve while watching the pressure readout. We open the valve until it rises to the 10^{-4} or 10^{-3} range. We allow a few sweeps of the analog scan to finish, and then fully close the needle valve. While the suggested maximum operating pressure of the unit is 10^{-3} mbar, it is perfectly OK for the pressure to spike to that range for short periods. However, the pressure must never pass the 10^{-2} mark, or risk breaking the delicate electronics inside. Once done, we can save our scans to the computer to analyze later. To shut everything down, we just follow the start-up steps in reverse: Turn off the filaments, close the program, unplug the RGA, turn off the turbopump, close the valve, and shut off the nitrogen. One important thing to remember is that the valve should be closed after the turbopump has come to a complete stop, and when the valve closes, the valve emits a hissing noise. The main reason we also shut off the nitrogen is because the tubing we have that supplies the nitrogen is not perfectly leak-tight, and closing the valve after we are done prevents the unnecessary loss of any more nitrogen.

Figure 74: Actual scan testing a bottle in our inventory;
Y-axis on log scale with units of pressure, X-axis is mass in amu



5.2 Simulations

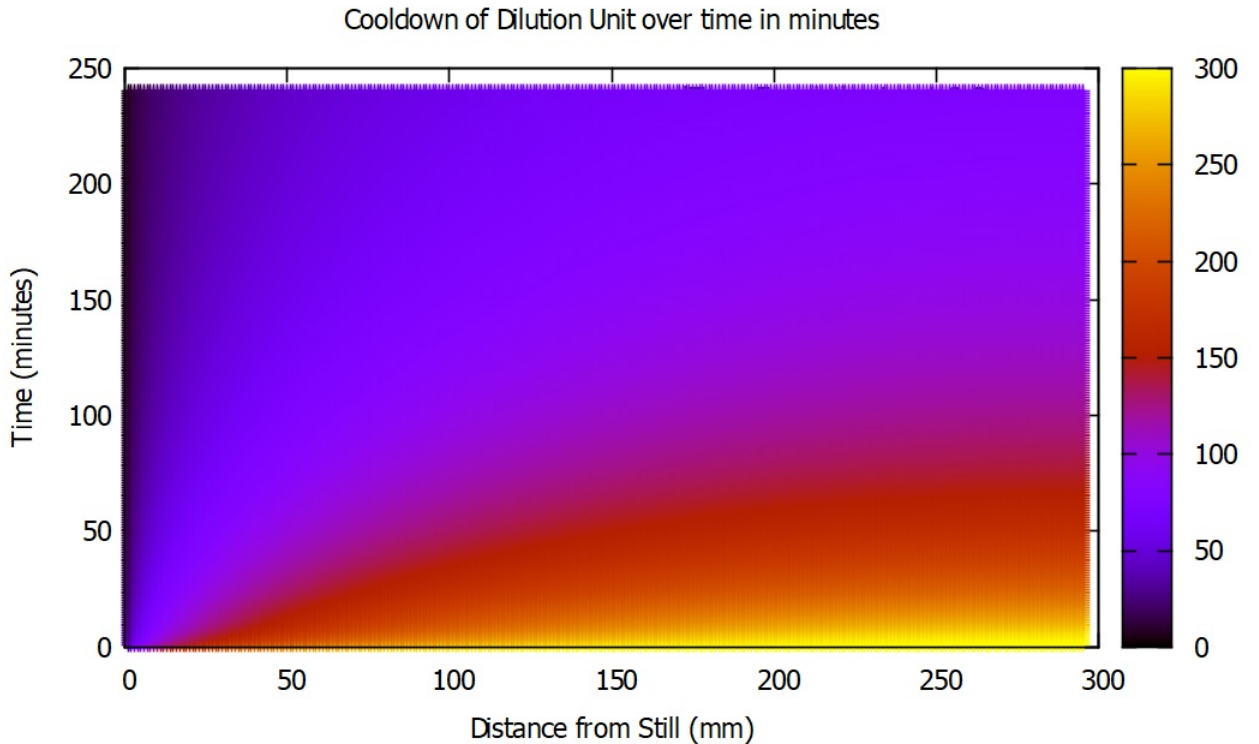
With the new dilution unit being rebuilt, it was prudent to simulate its performance before everything was put into place so that we can have an appropriate length of heat exchanger that achieves a suitable temperature without too much difficulty. In this simulation, we tried to account for everything that can contribute to the minimum temperature, such as possible heat leaks, the impedance of the tube, and the flow rate

of the ^3He . In addition to finding the theoretical minimum temperature in the mixing chamber, another important question to answer is the question of how long it takes after the start of a cooldown until we can start dilution. This simulation will be taken in several steps, with each subsequent step adding a layer of complexity and bringing it closer to what happens in the lab. The primary goal of this simulation is to use it as a sort of guide for those running cooldowns to know when specific temperatures will be reached. The timescale chosen for these simulations is 4 hours, around the time that we believe that it takes to get cold enough to start dilution.

Phase 1: Setting up the cooldown simulation

Here is the initial setup of the simulation: The evaporator is full and operating optimally, with the still at 1 Kelvin. We make the case that the central tube and the surrounding sleeve start at room temperature (300 Kelvin). For simplicity, we imagine the central tube and sleeve as a one-dimensional bar, with one end at 1K. From there, we use the 1D heat equation to predict the time evolution of the temperature throughout the bar. The primary value we want from these simulations is the temperature at the other end of this bar after 4 hours since that end simulates the temperature of the mixing chamber. We can ignore any angular dependence due to symmetry, and we can ignore any radial dependence when we make two assumptions. 1) The temperature distribution is uniform across the face of the still and 2) There is a perfect vacuum around both of these pieces, leading to zero radial thermal dependence. The result is the figure below, a heatmap created with time and position axes.

Figure 75: Phase 1 Heatmap



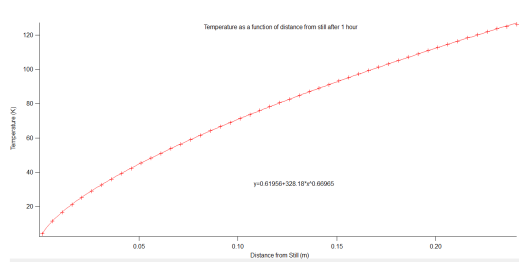
After 4 hours, the simulation predicts that the temperature of the mixing chamber will be about 100 Kelvin. For a simple case scenario, this is an excellent result, however, like most simple scenarios, neglects a lot of factors present in the real thing. The next phase in the simulation introduces the exchange gas, about 30 mbar of Helium gas in between the central tube and the sleeve.

Phase 2: The Exchange Gas

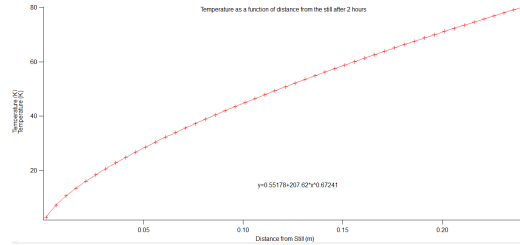
The exchange gas is introduced into the system towards the start of the cooldown to help cool the system faster. To code it, we had to update it to two dimensions since we lost the vacuum and now have a radial thermal dependence. The setup is now thought of as a rectangle formed by the axial and radial components, with a “stripe” of helium parallel to the axial sides. The parameters for helium like thermal conductivity, density, heat capacity, etc. were added to the code. Another change from the previous phase is the reduced axial length. The axial length is now 241 millimeters, which is the length from the face of the still to the edge of the sleeve where the mixing chamber is attached. The main reason for this change is mostly for ease of coding. Since the code works using an array of 1mm^2 sections, the conical shape of the tip of the central tube and the mixing chamber would make this difficult to code. However, since it goes up to the mixing chamber, it is safe to assume that the temperature values the code will spit out will be fairly close to the actual temperature of the mixing chamber. When the code was finished, the temperature at the mixing

chamber was found to be about 50 Kelvin, about half the result from the previous phase. One thing to note about this code is that it takes a long time to run (about 5 hours), so it was best to use the results it output to extrapolate the temperature at times later than 4 hours, or when a point reaches a certain temperature. To do that, we plotted the temperatures as functions of distance from the still at different times and found equations for each of the fits:

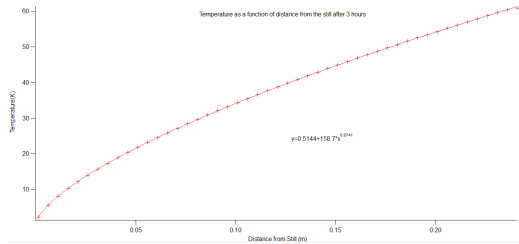
(a) Temperature vs. Distance after 1 hour



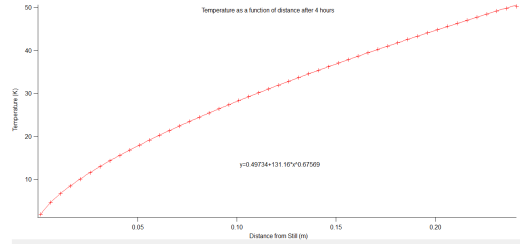
(b) 2 hours



(a) 3 hours



(b) 4 hours



An important thing to mention is that all of these points were taken from the central tube. We did not include any radial dependence in our extrapolation due to it being a small effect at later times and at positions close to the mixing chamber (the area we are most concerned with). As shown in the graphs above, the temperature seems to be proportional to the distance from the still raised to some power. However, each of the offsets, constants, and powers are different due to an unknown time dependence. That dependence can be found using the same method as before, and the full extrapolation equation comes out to be:

$$T(x, t) = 0.30484 + 0.31496t^{-0.35988} + (-1.3673 + 329.55t^{-0.65717})x^{0.65819+0.01147t^{0.3029}} \quad (30)$$

Where x is the distance from the still in meters and t is the time after the start of the simulated cooldown in minutes. To test this equation, a random number generator was used to pick different x and t values, and the number that came out was compared to the value in the data file generated by the simulation. In most cases, the extrapolation equation and the data file were found to be within about 1 percent of each other. The only time the equation failed was at higher x -values (close to 241) and low t -values. However, this is rectified after t reaches 20 or 30 minutes. Using this extrapolation equation, we began to ask ourselves how long it would take the

mixing chamber to reach certain temperatures. This is relevant because, during an actual cooldown, we would remove the exchange gas once the system reached about 30 Kelvin. According to this equation, it would take 8 hours and 45 minutes to reach 30 Kelvin, and almost 2 days to reach 10 Kelvin. We know that this is not true due to all of our prior experience in previous cooldowns. Therefore, this simulation is also insufficient. So, in the next simulation phase, the next thing to be added will be movement in the exchange gas.

Gas Movement

Due to limitations in computing and coding ability, it was inadvisable to code particle movement and pressures in each $1mm^2$ area, so using some creativity, a substitute was used: a secondary heat transfer step. In the second phase of the simulation, all of the heat transfer was done in two major steps. 1) The differential temperature was calculated for every value in the array based on its surroundings at that moment in time and 2) updating all of those temperatures all at once. So, to simulate gas movement, we repeated that step with two big differences: 1) Only the temperature values in the exchange gas area were updated and 2) everything outside that space was ignored, meaning the only heat transfer happening was between the Helium atoms. Given that it made sense that the more energetic, higher temperature atoms would want to leave their hotter, higher pressure areas for the colder, lower pressure areas, we added this next step and ran this new simulation. After four simulation hours, we found that the mixing chamber was about 33K. We then repeated the same process as the previous phase to find the extrapolation equation:

$$T(x, t) = 10.43 + 43.548e^{-0.014701t} + (46.46 + 26251t^{-1.2759})x^{0.98722 - 0.0027103t + 8.1097 \cdot 10^{-6}t^2} \quad (31)$$

Using this equation, we found that 30K can be achieved in just under 5 hours, and 10.43K (the lowest this equation can go) in a little over 16 hours. Like the previous extrapolation equation, the error between the actual simulation values and the calculated ones was non-negligible at low values of time, but fall within one percent after an hour. More variables affect this simulation, with one of the biggest being the liquid helium supplied by the bypass line. However, implementing that into the simulations would add another layer of complexity into the simulations, since the bypass line runs along the top side of the IVC, therefore adding an angular dependence to the initial conditions of the simulation. Undertaking that into the simulation would require a lot more time and dedication than we had available.

Heat Exchanger Analysis

The code that was written to simulate the temperature gradient in the heat exchanger was based heavily on the one described in the paper written by Jacob Higgins[22]. We used the same assumptions he did, namely that almost all the heat exchanged was due to the Kapitza conductance and that the heat exchanger was ideal. This means that any heat flow must be between the concentrated and dilute phases. The code starts from the temperature of the mixture in the still (for our refrigerator that's

about 0.78K) and works its way down to the mixing chamber. The code works in two main steps. The first is to evaluate the value of T_b in the following equation:

$$\frac{d\sigma_c}{dx} \int_{T_b}^{T_c} \frac{dT}{\rho_c} = \frac{d\sigma_d}{dx} \int_{T_d}^{T_b} \frac{dT}{\rho_d} \quad (32)$$

The indices stand for “concentrated”, “body” (the heat exchanger itself), and “dilute”. This equation assumes that all of the heat transfer is between the two phases. $\frac{d\sigma_i}{dx}$ is just a geometry term depending on the phase being looked at, which is simply $2\pi r_i$. r_c is the inner radius of the cupronickel tubing, and r_d is the outer radius. ρ_i is a temperature-dependent term known as the Kapitza resistivity. Based on what form ρ_i takes, this equation must solve for T_b , which is needed for the next step of the code:

$$dT_c = -\frac{2\pi r_c}{\dot{n}_3 c_c} \int_{T_b}^{T_c} \frac{dT}{\rho_c} dx \quad (33)$$

When this is evaluated, it is subtracted from the starting temperature and the process is repeated along the entire length of the heat exchanger. The length of the heat exchanger is based on the length of the tube it’s going to be wrapped around, the diameter of the sintered copper surrounding the heat exchanger, and an arbitrary spacing between each coil. Other parameters We can adjust in this code include the heat load on the mixing chamber, the flow rate of the He-3, and the radii of the inner and outer tubes of the heat exchanger. The heat load on the mixing chamber is due to contact with the stainless steel of the refrigerator and the photon beam on the target. The beam can be turned on or off in the code when the prompt appears when the program is executed. The flow rate of the He-3 is determined primarily by the pumping power of the pump stack. Currently, we have three pumps that circulate He-3, labeled P5, P6, and P7 in diagrams. Based on the specifications from the manufacturer, the flow rate (in m^3/s) can be converted into mol/s for the code. Another important aspect to simulate in the heat exchanger is theoretical pressure drop. It’s important because the pressure of the incoming concentrated phase must counteract the dilute phase in the mixing chamber and the phase boundary between them is stationary. Using a flow rate of 0.7 mmol/s, a target mixing chamber temperature of 50mK, and a heat load of 22.3 μW , we have simulated the length of the heat exchanger and the pressure drop at various radii:

Table 6: Theoretical Lengths needed for 50mK

Heat Exchanger (Inner/Outer)radius (mm)	Length needed (m)	Pressure Drop (milliTorr)
0.32/0.40	13.8263	7.37
0.45/0.53	9.95493	1.36
0.53/0.63	8.43611	0.598
0.63/0.74	7.11532	0.253
0.70/0.82	6.40768	0.149
0.91/1.05	4.94539	0.040
1.08/1.20	4.20193	0.017

These numbers are not believed to be exact, since the code that produced them has an unknown error. This error would produce lengths that would be an order of magnitude higher than what we would believe to be true. So, to rectify this, a factor of ten was introduced to the temperature drop. At present, we would not be able to justify its existence in a way other than the fact it gives us more believable numbers. Therefore, the length estimates are most likely wrong. Due to the difficulty of attempting to get the accurate length of the heat exchanger required, any attempts to get this code working was deemed a low priority compared to designing and rebuilding the dilution unit. We decided to use about one meter of cupronickel tubing in addition to reusing the final heat exchanger with the sintered copper in our new unit, given that this was around the same length of tubing used in the old unit. Several years after abandoning this code, a conversation with Mr. Higgins revealed that the errors created in our code could be due to how the heat equations were implemented. He revealed the existence of programs specifically made for heat transfer equations, and since the heat transfer steps in our code were handwritten by us, this could likely be the cause.

5.3 The DAQ

During a cooldown, our Data Acquisition Program, or DAQ for short is essential for recording the relevant data for 24 hours a day. The code is written in Python and has three main variables that it measures; temperature, flow rate, and pressure. For temperature, it records the data for the evaporator (3 sensors), the separator (2 sensors), and the target chamber (2 sensors). The still sensors are not included for two main reasons. First, the exact temperature of the still itself is not the highest priority, plus we had an idea of the temperature of the still based on the evaporator, due to their proximity to each other. Second, this code was written years ago, well before the discovery of the leak in the still back in November 2017. For the flow rates, we have the Shield and the Separator, which are monitored to ensure proper circulation of helium in the system. We have target values of flow rate that we aim for when we are diluting and attempting to maintain a steady state operation, mainly 13 SLPM for the Shield and 7 SLPM for the Separator. Lastly, we have the pressure readings for the OVC, the IVC, and the evaporator. The OVC requires a layer of insulation, which is provided by a vacuum. The inside of the IVC is part of the ^3He vacuum space, hence the need to monitor that. As for the evaporator, it is not to make sure that it is at vacuum, it is to monitor the vapor pressure. The vapor pressure coming from the evaporator gives us an additional look at its status since the vapor pressure will be at a minimum when the temperature of the liquid helium bath is also at its minimum. To access the DAQ, the program must be started on the computer above the bridge (Username: uva Password: uva1). This computer is a Linux device, so to start the program the command window must be opened. Below is a manual of how to start the programs for each of the three main types of measurements, with each line break separated by hitting the enter key:

- Temperature

```
cd code
cd serial
./python lakeshore218s-read.py
```

- Flows

```
cd code
```

```
cd MCCDAQ-1608G-backend$
```

```
./mysql-usb1608G
```

- Pressure

```
cd code
```

```
cd serial
```

```
cd pfeiffertpg262
```

```
./tpg262.py
```

Since all three are usually run together, it is important to note that a new command window must be opened for each system. Once the programs are running, the real-time values for each measurement can be monitored from anywhere, but can only change their display from the Linux machine in the lab. Different measurements can be hidden from view, as well as the range displayed on the axes. The data recorded is automatically stored and can be accessed anytime for analysis once a cooldown is over.

Figure 78: Data Request Form

Slow Control Data Request Form

Device: evapSi sepSiLo sepSiHi

mcSi OVCPressure

IVCPressure he3Pressure

evapPressureCm330

evapPressureMv110 sepFlow

shieldFlow he3Flow evapFlow

100klevel alcateIASM120H

avs47 sepSi

Beginning Time:

End Time:

For more detailed information on the DAQ and how it works, refer to [23]. This data is invaluable since it can be used to discuss how a cooldown went as well as pinpoint the results of actions recorded in the logbook. When things do go wrong during a cooldown, we may not necessarily know how to fix them at the time, so the data also serves as a guide to help us figure out what went wrong, why it happened, and possibly how to fix it.

5.4 The Stepper Motor

With a lot of attention usually on the issues with the refrigerator and the effort that went into optimizing its performance, we decided to spend some time to start a side project that could help us during our actual experimental run. When the refrigerator has achieved dilution and has the beam firing on the target, the space will be closed off from all personnel, due to obvious safety concerns regarding the radiation coming off of the target. If the beam is on and we need to make adjustments to the helium flow rate in the refrigerator, we would have no way to do so. This is when we had the idea to program a small motor to do this job since we could, in theory, control it from outside of the room. The motor we chose was the STM17Q-1AE model from Applied Motion Products. It was chosen for its small size and its programming compatibility. It is configured to run using the STConfigurator software, a software created by Applied Motion Products.

Figure 79: Stepper Motor on platform



This software comes with a list of simple commands, which range from setting the motor to a certain position, adjusting the rotational velocity, and stopping all current motion. As we only needed it to open and close the 1K valve on the refrigerator, we did not need many of them outside of the basic ones. With the motor secured, there were two main things to secure before we can attempt to run it: Something to hold

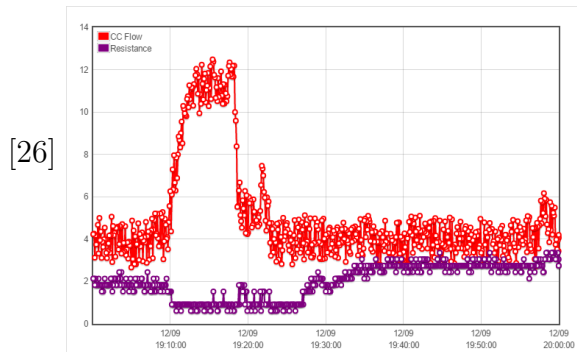
it up, and something to couple it to the 1K valve. To hold it up, we had a simple rig made in the machine shop. It was a length of steel with a simple platform on the end. The platform had a groove for the motor to sit in that made sure it was aligned with the 1K valve. The rig was secured to the refrigerator using two C-clamps to hold it on the side. Once in place, the motor would be placed on the platform and the coupler attached. This coupler for the valve and the motor was not as simple as locking them together since there was always the danger of the motor going haywire and accidentally breaking the delicate needle valve. So, with that danger being present, we decided on an adjustable clutch. We got a 4mm bore adjustable clutch from Ondrives.us, part number 311.16.1818. The clutch is two concentric cylinders that can rotate independently from each other. The torque can be adjusted, so that the motor can turn the valve, up until it reaches enough resistance. Once it meets that resistance, the cylinder attached to the motor shaft can keep turning, while the other cylinder stays still. There is a screw inside of the cylinders, which allows the clutch to grip the shaft when tightened. Once we were able to secure the motor in place, we shifted our focus to programming it. The motor came with an RS-232 cable that was attached to its top. We got an RS-232 to USB cable and used that to send the commands. We first verified that we could use the STConfigurator software to issue basic commands, and when we were able to achieve that, we moved on to writing code. For the code, we used Labview, and most of the code was written by an undergraduate student, Paul Cordova. During his time with us, he was able to write two separate codes that controlled the motor[24]. The first, which he dubbed 'main.vi' was the first code that was thought to be good enough for use during a cooldown. It featured two modes, manual and automatic. Manual mode has only two functions and was only there as a precaution in case the automatic mode was not working properly. The two functions manual mode has is the ability to set the position of the motor and a crush ice feature. During a cooldown, it is not uncommon for ice to form around the end of the needle valve. The crush ice function simply opens and closes the valve several times to destroy that build-up. Automatic mode was able to read the flows from the DAQ and controlled the motor using a PID feedback loop. The PID values chosen to run the code are $P=5$, $I=0.001$, and $D=0.1$. The user picks a target flow rate for the program to aim for and will adjust the 1K valve accordingly. This program was tested using another program that simulates the flows during a cooldown, with random fluctuations added in. Automatic mode also has a crush ice button added in. The second code that was created, 'mainAutomaticIce.vi' is a more advanced version of the previous code that has the added ability to "detect" the presence of ice buildup on the 1K valve. It does this by writing the most recent data on the flows in an array. If the maximum value of this array is below a certain threshold, the program interprets this as the system having ice buildup and begins opening and closing the valve to combat it. With the code functional, we first tested it during a cooldown in early November 2017, and we had promising results on its performance but were unable to proceed further due to the detection of the leak in the still soon afterward. Thus, we were unable to properly run this program due to the much more pressing matter of replacing the dilution unit.

6 Notable Cooldowns

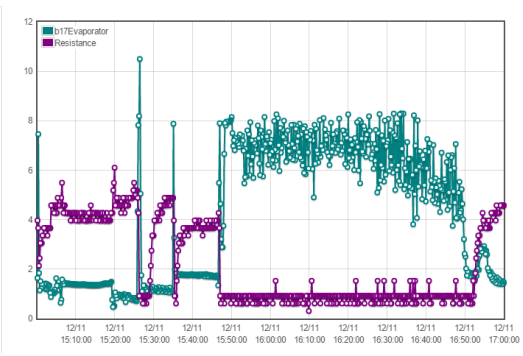
6.1 December 9th, 2016

One of the goals of this cooldown revolved around the monitoring of the superconducting coil[25]. At this point, we had trouble keeping the coil in this state, so we documented every time the coil went superconducting, as well as the actions that were taken that could have affected it. The coil stayed superconducting for a maximum of about four hours. The coil usually entered the superconducting state when the system was running at higher flows.

(a) Superconducting Coil in Purple

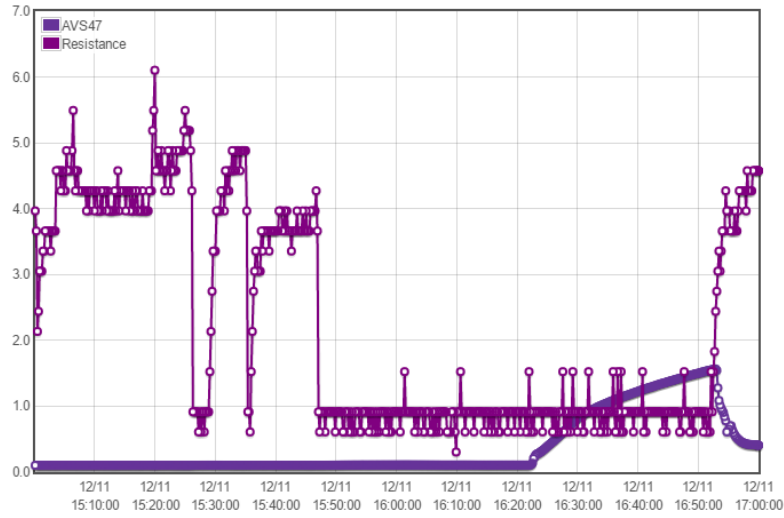


(b) Evaporator flow going high



We were able to dilute during this cooldown, with the target chamber reaching about 100 mK at one point, but we were unable to maintain it without the bypass valve being open. On top of that, any additional heat load seemed to affect the target chamber temperature and the superconducting coil. One example of this was when a routine trap cleaning saw a drastic rise in the temperature in the target chamber rose from 100mK to about 1.5 K. This subsequently led to the coil leaving the superconducting state about 30 minutes later, when the trap cleaning was completed and was placed back in liquid nitrogen.

Figure 81: Trap cleaning began at 16:23, finished at 16:50



After the cooldown was done, several leaks needed to be addressed, one being between the evaporator and the counter-current line, one in the IVC, and a leak in the water line for one of the pumps.

6.2 November 7th, 2017

This was a less involved cooldown due to the absence of ^3He use. The purpose of this ^4He cooldown can be narrowed down to two main goals:

- Test the OVC vacuum
- Test the stepper motor

The reason we were not having a full cooldown was due to the issues we had been having with our vacuum. Given our issues with the OVC, we had been running higher flows than usual, and in the aftermath of those cooldowns we had made some attempts to address them. Teflon tape was applied to the nose of the OVC to help with the issue of touches between the two layers. We also had a lot of ice build-up in the liquid helium leading to an irregular flow in a previous cooldown. We were able to get down to 1K in the evaporator within four hours and was running stable, but we had to have the valve open more than usual, needing the higher flows to maintain operation. This was also a good cooldown to test the stepper motor in a basic capacity. We attached its platform to the refrigerator and secured the motor to the 1K valve. The motor showed promising results in regulating the flows, but we had some issues with it overtightening the valve. Given that the needle valve is delicate, it had a real risk of breaking off. After the cooldown was finished, we decided on purchasing the adjustable slip clutch. The high flows necessary to run the cooldown led us to believe that there was a leak in the system. After a careful search, we eventually found it a week later in the still. This led to a meeting with everyone

involved in attendance, and the decision was made to remove the dilution unit from the rest of the refrigerator and rebuild it completely.

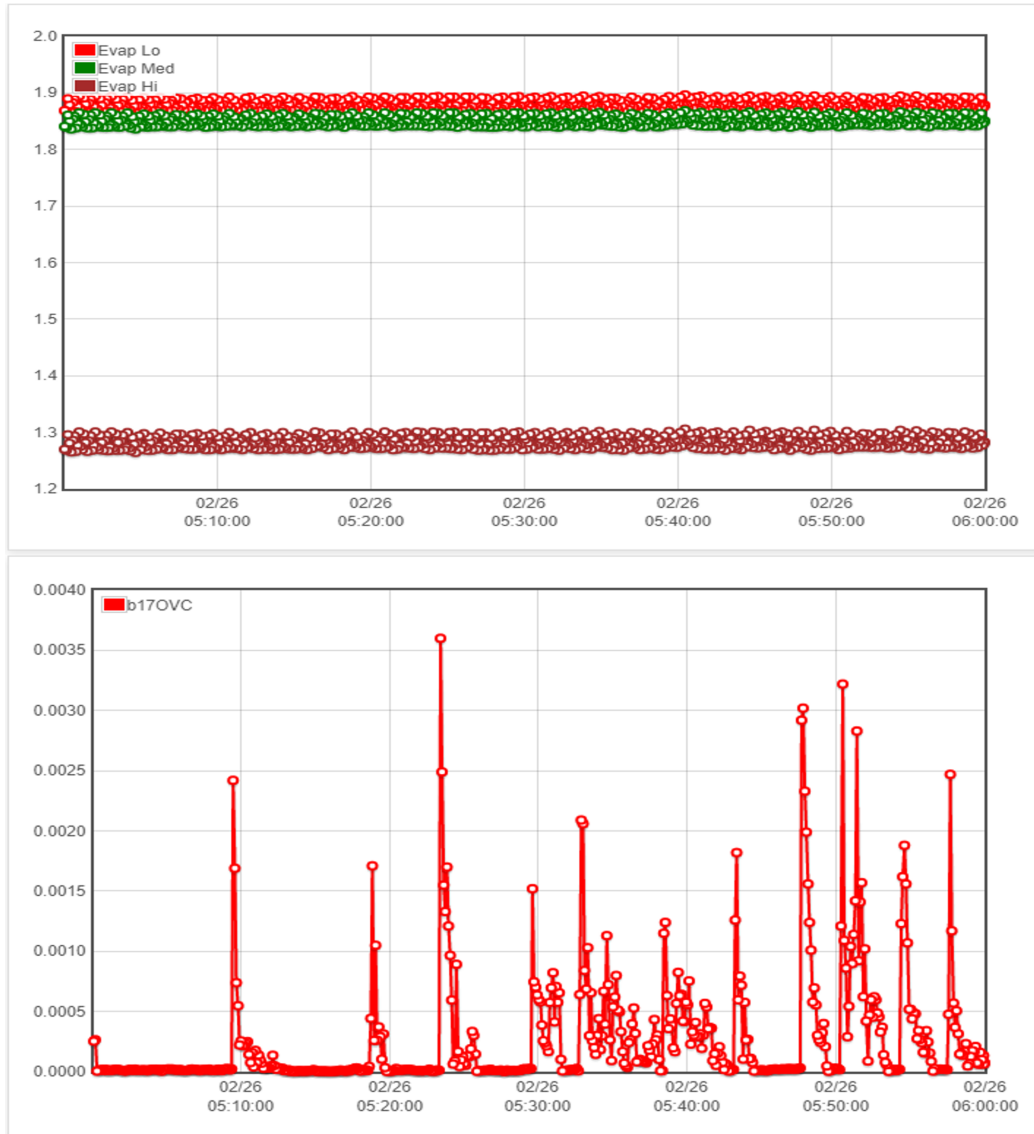
6.3 February 25th, 2019

In the aftermath of the discovery of the leak in the still, cooldowns were stopped for over a year, since there was no point in practicing without being able to dilute. However, in early 2019, it was determined that a cooldown was necessary with three goals in mind:

- Get down to 1K in the evaporator
- Maintain 1K in the evaporator with just the 1K valve
- Determine the effect of the leak in the shield

Without the dilution unit, this was a much more simple cooldown, and we were able to get the dilution unit down to 1K in a little less than five hours. During a large percentage of that time, the separator was struggling to get lower than 50K, which was alleviated by running the shield and counter-current at higher flows. They were first raised to 15.5 and 10 SLPM, and then to 18 and 12 SLPM, respectively. This second jump in the flow rate was what allowed used to finally reach the target temperatures in both the separator and evaporator. When the temperature in the evaporator was stable, we closed the 1K and Bypass valves in an attempt to see how long it would take the evaporator to empty. Based on our observations, it took about half an hour to do so, starting from the time both valves were closed, to when the Evap Low sensor starts to spike in temperature. After that, we attempted to get the system stable with just the 1K valve open. We were ultimately successful, with the 1K open half a turn and the shield and counter-current flows at 15 and 8 SLPM, respectively. The system then remained stable for the rest of the night, until around 10:30 AM, when we determined that we had run out of liquid helium. Given this result, we determined that because of the leak in the shield, we now have to run at higher flows than usual. We decided that due to the nature of the leak, we would not attempt to plug it. One thing that was strange during this cooldown was the presence of pressure spikes in the OVC.

Figure 82: OVC Pressure compared to Evaporator Temperature



One thing to note was that a leak was spotted in the OVC almost two months before this cooldown, but we found where it was, and had our machinists fix it. Given that the pressure spikes resolved themselves rather quickly, we believed there was always the possibility that the OVC was not pumped on enough before the cooldown, and it was still outgassing where we had plugged the leak. The origins of these spikes were investigated afterward, and eventually, we found that the spikes were in fact due to a faulty gauge attached to the OVC.

6.4 July 2nd, 2019

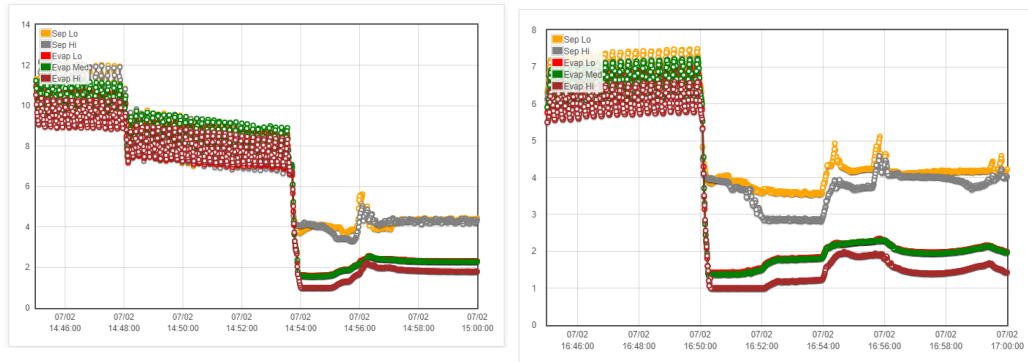
With the OVC pressure spike issue resolved, we had another ^4He cooldown with two goals in mind:

- See if the OVC pressure spikes were gone
- Get some practice leading a cooldown

This cooldown was met with many challenges, the first of which stemmed from being unable to record the OVC pressure using the DAQ. While this was inconvenient, we were able to monitor the gauge and record the values by hand. It soon became apparent that the pressure spikes had disappeared from the OVC, given that the OVC pressure remained stable and slowly dropped over time. Some other challenges stemmed from human error, but thankfully they were easily resolved. We initially had trouble getting the evaporator cold, but we then realized we had forgotten to close valves V10 and V12, the valves that connected the ^3He and ^4He sections. The second human error was due to the shield and counter-current lines being disconnected from the refrigerator. They were reconnected quickly after that discovery, and the cooldown proceeded.

Figure 83: Fixing Human errors

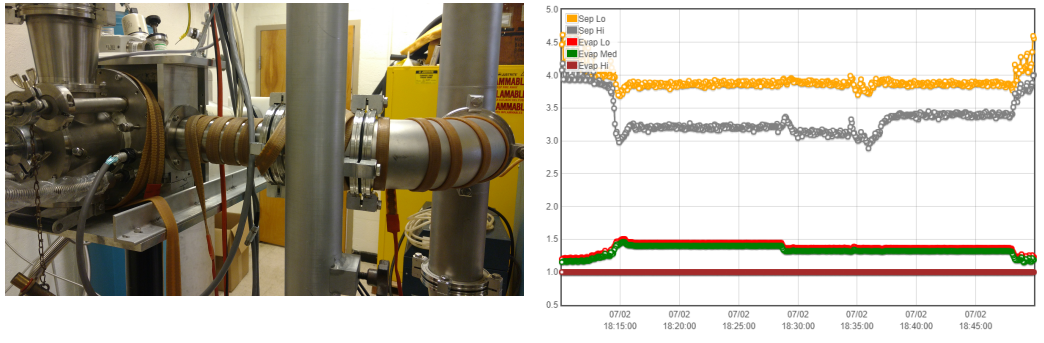
(a) V10 and V12 were closed at 14:54 (b) Shield and CC lines were reconnected around 16:50



However, the biggest challenge faced during this cooldown was from the pump P2, which overheated several times during this cooldown. Whenever there was a spike in the evaporator pressure, it would trip that pump, requiring us to reset it. This was due to poor circulation in the ^4He section, which was resolved by applying the heating tape onto the pipes leading from the refrigerator to the ^4He pump stack. This eventually led us to be able to run the evaporator at 1K, and we attempted to find where we could find the lowest number of turns on the 1K valve that would keep the temperature stable. This continued until we ran out of liquid helium around 20:30.

Figure 84: Fixing Human errors

(a) Heating Tape setup on refrigerator
(b) Fine tuning the 1K valve with stable evaporator temperatures



Similar to the cooldown five months prior, we found that we had to have the 1K valve open half a turn to maintain the temperature in the evaporator.

6.5 February 12th, 2022

Once the second iteration of the dilution unit was welded together, one of the first things that we wanted to test was this unit's ability to circulate helium in a cooldown. To do so, we had to begin installing the ^3He line into the unit. We also wished to install the feedthrough and the wires for the sensors, so long as we could get those done before the deadline to evacuate our lab space on February 15th, 2022. So, our goals for this cooldown were:

- Install the ^3He line to see if the unit could circulate
- Install the feedthrough and test the function of the still sensors
- Check the integrity of the welds on the new unit

Given the pressing time constraints, we wanted to have the basic setups for the ^3He line and the electronics done before this cooldown, but we were, unfortunately, unable to do so. For the full details on our troubles regarding these systems, refer to sections 4.2 and 4.3. At a bare minimum, we were able to at least get the ^3He line installed, albeit without the ideal conditions. We had to secure the line to the stainless steel of the unit using epoxy, which was far from ideal due to the epoxy's coefficient of expansion being higher than stainless steel, meaning those interfaces were at a higher risk of leaking. Plus, we had the misfortune of having part of the tubing snap off during the installation of the unit into the refrigerator. Since we were unable to install the feedthrough on the back of the still/VLC, we had our machinists weld a stainless steel cap there to take its place. Once we received the liquid helium to start the cooldown, we had even more problems. When we went to seal one of the pipes on the ^4He system, we were unable to, due to one of the screws necessary to seal it being missing, necessitating a trip to the local hardware store to replace it. When

we tried to start up the Linux machine where the DAQ was run, we were unable to turn it on, forcing us to record the necessary measurements by hand. We were also impeded by the flow of room-temperature helium gas into the evaporator. This was rectified once we realized that both the ^3He and ^4He backfill lines were open, and promptly closed their valves. We were running the 1K and Bypass valves (1 3/4-2 1/4 and 1 turn respectively) to get the evaporator to run at 1K. Eventually, we were able to circulate gas throughout the system, which is the bare minimum of what we wanted from this cooldown. In our post-cooldown investigation, we found that there were leaks between the ^3He and ^4He sections, but we found no indication that it was due to the welds on the unit but was most likely due to the haphazard soldering attempt on the ^3He line to the rest of the refrigerator. So despite all of the hurdles that came before and during this cooldown, it was ultimately rated as a success.

7 Conclusions

While the discovery of the leaking unit in November of 2017 was a setback, we have made substantial progress on rebuilding it. Replacing this unit has presented us with the rare opportunity to make this dilution refrigerator more suited for our purposes. It has been a valuable learning experience that has also answered some questions that have been plaguing the group for years. We have also worked on some support systems that are necessary for our work, as well as some that have the potential to make running this experiment easier. There is still a lot of work to be done, starting with making a procedure for maintaining the alignment of the third iteration of the dilution unit. Once we have a working unit, we can run a cooldown to measure its performance. When these results are promising enough, we can plan a cooldown at TUNL, and possibly schedule beam time to run the experiment.

Bibliography

- [1] Helbing, Klaus (2006). “The Gerasimov-Drell-Hearn Sum Rule”. arXiv:nucl-ex/0603021v3
- [2] S. Hoblit, et al., *Measurements of $\vec{H}\vec{D}(\vec{\gamma}, \pi)$ and Implications for the Convergence of the Gerasimov-Drell-Hearn Integral*, LEGS-Spin Collaboration, Physical Review Letters 102 (2009) 172002.
- [3] “Search for supernarrow dibaryons in pd interactions,” L.V. Fil’kov et al., Phys. Rev. C61, 044004 (2000).
- [4] “Search for Super Narrow Dibaryons,” A. Cichocki, PhD Dissertation (unpublished), University of Virginia, May 2003.
- [5] Tamii, A., Hatanaka, K., Hatano, M., Hirooka, D., Kamiya, J., Kato, H., Maeda, Y., Saito, T., Sakai, H., Sakoda, S., Sekiguchi, K., Uchigashima, N., Uesaka, T., Wakasa, T., & Yako, K. (2002). Search for narrow dibaryon resonances by the $pd \rightarrow pdX$ and $pd \rightarrow ppX$ reactions. Physical Review C , 65. <https://doi.org/10.1103/PhysRevC.65.047001>
- [6] B. Norum, R.Pywell, B.Sawatzky, and H.Weller, Measurements of the Drell-Hearn-Gerasimov Integrand for the Deuteron, Proposal to HIGS PAC, 2009.
- [7] Khrykin, A. S., Boreiko, V. F., Budyashov, Y. G., Gerasimov, S. B., Khomutov, N. V., Sobolev, Y. G., & Zorin, V. P. (2001). Search for NN-decoupled dibaryons using the process $pp \rightarrow \gamma\gamma X$ below the pion production threshold. Physical Review C, 64. <https://doi.org/10.1103/PhysRevC.64.034002>
- [8] “Differential polarization of photoneutrons from deuterium,” R. Nath, F.W.K. Firk, and H.L. Schultz, Nucl. Phys. A194, 49 (1972).
- [9] H. Arenhovel, W. Leidemann, and E. Tomusiak, Few-Body Syst. 28 (2000) 147.
- [10] M. Borghini, Mechanisms of nuclear dynamic polarization by electron-nucleus dipolar coupling in solids, Conf. Proc. C710830 (1971), 1–32.
- [11] D. G. Crabb and W. Meyer, Solid polarized targets for nuclear and particle physics experiments, Annual Reviews Nuclear and Particle Physics 47 (1997), no. 1, 67–109.

- [12] Pobell, F. (2007). In *Matter and methods at low temperatures: With ... 28 tables ...* (pp. 81–137). essay, Springer.
- [13] *Dilution Refrigerator*, https://en.wikipedia.org/wiki/Dilution_refrigerator
- [14] V.N. Litvinenko et al., “Gamma-ray production in a storage ring free-electron laser,” *Phys. Rev. Lett.* 78 (1997) 4569.
- [15] M.W. Ahmed et al., “Background reduction in FEL-generated gamma-ray beam experiments using giant high-peak power pulses,” *Nucl. Instrum. Meth. in Phys. Res.* 516 (2004) 440.
- [16] *Triangle Universities National Laboratory* www.tunl.duke.edu
- [17] Sawatsky, B. D. (2005). *A Measurement of the Neutron Asymmetry in $d(\vec{\gamma}, n)p$ Near Threshold* (dissertation).
- [18] T.O.Niinikoski and F.Udo, “Frozen Spin” Polarized Target, *Nuclear Instruments and Methods* 134 (1976) 219.
- [19] Duve, R. (n.d.). Cooldown Runplan.
- [20] Keith, C. (2021). *Miniature feed-thru for low temperature* [Photograph].
- [21] *User’s Manual Model 218 Temperature Monitor*. (2017, July 25). Retrieved March 10, 2023, from https://www.lakeshore.com/docs/default-source/product-downloads/manuals/218_ma
- [22] Higgins, J. (2017). *Design and Analysis of a Compact Dilution Refrigerator* (thesis).
- [23] Duve, R. (2016). *A Nuclear Frozen Spin Target For Deuteron Photodisintegration Experiments At The High Intensity Gamma Source* (thesis).
- [24] Cordova, P. (2017, September 25). *Stepper Motor*(email).
- [25] Duve, R. (2016, December 14). *Hifrost December 2016 post cooldown work*.
- [26] Roberts, M. (n.d.). December Cooldown.